# The Behavior of DASPMI in Living Cells:
# Spectrally and Spatially Resolved Fluorescence Lifetime Imaging

Dissertation

zur Erlangung des Doktorgrades

der Naturwissenschaften

vorgelegt beim Fachbereich

Biochemie, Chemie und Pharmazie

der Goethe-Universität

in Frankfurt am Main

von Radhan Ramadass

aus Chingleputt, Indien

Frankfurt am Main 2008

(D30)

vom Fachbereich Biochemie, Chemie und Pharmazie
der Goethe-Universität als Dissertation angenommen.


Dekan:            Prof. Dr. Harald Schwalbe

1. Gutachter:     Prof. Dr. Jürgen Bereiter-Hahn

2. Gutachter:     Prof. Dr. Josef Wachtveitl


Datum der Disputation:

**TABLE OF CONTENTS**

## SUMMARY

Cellular metabolism can be envisaged by fluorescence lifetime imaging of fluorophores sensitive to specific intracellular factors such as $[H^+]$, $[Ca^{2+}]$, $[O_2]$, membrane potential, temperature, polarity of the probe environment, and alterations in the conformation and interactions of macromolecules. Lifetime measurements of the probes allow the quantitative determination of the intracellular factors. Fluorescence microscopy taking advantage of time-correlated single photon counting is a novel method that outperforms all other techniques with its single photon sensitivity and picosecond time resolution.

In cell biology, fluorescence lifetime imaging has been widely used as a spectroscopic ruler to determine the interaction between suitably tagged specific proteins (eg. oligomerization of epidermal growth factors), lipids, enzymes and nucleic acids, as well as cleavage of a macromolecule or protein conformational change. The availability of fluorescence proteins has increased the use of such applications, due to their minimally invasive nature and possibility of direct tagging by genetic means. Fluorescence lifetime imaging of auto-fluorescent proteins such as NAD(P)H has provided an quantitative measure of their pools and has enabled enhancement of contrast in complex biological tissues. Fluorescence lifetime determinations for imaging interactions or determination of intracellular factors are more reliable than intensity based measurements. Fluorescence lifetimes are in general independent of variations of illumination intensity, fluorophore concentration or photobleaching. Time-dependent fluorescence anisotropy decays are dependent on the rotational mobility of the macromolecule to which the fluorophore has been attached. Anisotropy decays are affected by the viscosity of its environment, or by binding and conformational changes that affect the rotational mobility. For instance, correlation times obtained from tryptophan anisotropy decays can been used to understand the internal dynamics of a protein. The energy transfer between same type of fluorescent molecules i.e. homotransfer, affects the anisotropy decay by depolarization.

In this work, a time- and space-correlated single photon counting system was established to obtain spectrally and spatially resolved picosecond fluorescence decays of 2-(4-

I

(dimethylamino)styryl)-1-methylpyridinium iodide (DASPMI) in living cells. This was achieved by optically coupling an inverted fluorescence microscope with a tuneable infrared femtosecond pulsed laser excitation after frequency doubling and pulse-picking. Spatial filter system had to be used to get a uniform illumination at the sample. Spatially resolved fluorescence decays were obtained from the projection of the magnified two-dimensional area of the sample in focus, onto a time- and space-correlated single-photon counting detector (quadrant-anode (QA) detector). Spectrally resolved fluorescence decays were obtained by introducing a Czerny-Turner spectrograph between the detection port of the microscope and time- and space-correlated single-photon counting detector (delay-line (DL) detector).

The potential of the established picosecond fluorescence decay microscope was demonstrated by obtaining spectrally and spatially resolved fluorescence decays of cyan and yellow fluorescent protein. Such detailed study proved the interactions of cation channel "transient receptor potential vanilloid 4" (TRPV4) and microfilaments. Living cells co-expressing TRPV4-CFP and actin-YFP, when excited for the donor molecules (CFP) exhibited an emission peak at 527 nm and decrease of the lifetime in the wavelength band 460-490 nm; corresponding to resonance energy transfer to YFP. CFP fluorescence decay was fitted best by a dual mode decay model. Considering the average lifetime of the donor, both in the presence and absence of acceptor yielded an apparent FRET efficiency of ~ 20 %. This is rather high placing the minimum distance of chromophores in the two fluorescent proteins in the range of 4 nm. Thus, this study shows for the first time that TRPV4 and actin intimately associate within living cells. The significance of this finding for cell volume regulation is highlighted.

The picosecond fluorescence decay microscope was further used to investigate the behavior of DASPMI in living cells. DASPMI is known to selectively stain mitochondria in living cells. The uptake and fluorescence intensity of DASPMI in mitochondria is a dynamic measure of membrane potential. Hence, an endeavour was made to elucidate the mechanism of DASPMI fluorescence by obtaining spectrally resolved fluorescence decays in different solvents. A bi-exponential decay model was sufficient to globally

describe the wavelength dependent fluorescence in ethanol and chloroform. While in glycerol, a three-exponential decay model was necessary for global analysis. In the polar low-viscous solvent water, a mono-exponential decay model fitted the decay data. The sensitivity of DASPMI fluorescence to solvent viscosity was analysed using various proportions of glycerol/ethanol mixtures. The lifetimes were found to increase with increasing solvent viscosity. The negative amplitudes of the short lifetime component found in chloroform and glycerol at the longer wavelengths validated the formation of new excited state species from the initially excited state. Time-resolved emission spectra in chloroform and glycerol showed a biphasic increase of spectral width and emission maxima. The spectral width had an initial fast increase within 150 ps and a near constant thereafter. A two-state model based on solvation of the initially excited state and further formation of TICT state has been proposed to explain the excited state kinetics and has been substantiated by the de-composition of time-resolved emission spectra in chloroform, glycerol and glycerol/ethanol mixtures. The knowledge of DASPMI photophysics in a variety of solvents now provides the means of deducing complex physiological parameters of mitochondria from its behavior in living cells.

Spatially-resolved fluorescence decays from single mitochondria or only very few organelles of XTH2 cells signified distinctive three-exponential decay kinetics of viscous environment. Based on DASPMI photophysics in a variety of solvents, these lifetimes have been attributed to the fluorescence from locally excited state (LE), intramolecular charge transfer state (ICT) and twisted intramolecular charge transfer (TICT) state. A considerable variation in lifetime among mitochondria of different morphology and within single cell was evident corresponding to the high physiological variations within single cells. Considerable shortening of the short lifetime component ($\tau_1$) under high membrane potential condition, such as in the presence of ATP and/or substrate, was similar to quenching and dramatic decrease of lifetime in polar solvents. Under these conditions $\tau_2$ and $\tau_3$ increased with decreasing contribution. Upon treatment with ionophore nigericin, hyperpolarization of mitochondria resulted in remarkable shortening of $\tau_1$ from 159 ps to 38 ps. Inhibiting respiration by cyanide resulted in notable increase of mean lifetime and decrease of mitochondrial fluorescence. Increase of DASPMI

fluorescence on conditions elevating mitochondrial membrane potential has been attributed to uptake according Nernst distributions, to de-localisation of $\pi$ electrons, quenching processes of the methyl pyridinium moiety and restricted torsional dynamics at the mitochondrial inner membrane. Accordingly, determination of anisotropy in DASPMI stained mitochondria in living XTH2 cells, revealed dependence of anisotropy on membrane potential. Such changes in anisotropy attributed to restriction of the torsional dynamics about the flexible single bonds neighboring the olefinic double bond revealed the previously known sub-mitochondrial zones with higher membrane potential along its length. The direct influence of the local electric field on the transition dipole moment of the probe and its torsional dynamics monitor changes in mitochondrial energy status within living cells. Membrane-potential-dependent changes in anisotropy have further been demonstrated in senescent chick embryo fibroblasts. An attempt has been made to discern the polarity and viscosities based influences of the fluorescence of DASPMI in mitochondrial inner membrane and hence determine the relative differences.

In conclusion, a single photon counting system capable of obtaining spectrally and spatially resolved fluorescence decays with picoseond time resolution was established to investigate the various photochemical, photobiological and photophysical process in living cells. Spectroscopic observations of excited-state kinetics of DASPMI in solvents and its behavior in living cells had revealed for the first time its localisation, mechanism of voltage sensitive fluorescence and its membrane-potential-dependent anisotropy in living cells. The systematic approach using various steady-state methods and novel time- and space-correlated single photon counting has revealed the simultaneous dependence of DASPMI fluorescence characteristics on mitochondrial membrane potential and inner membrane viscosity. The simultaneous dependence of DASPMI photophysics on mitochondrial inner membrane viscosity and transmembrane potential has been highlighted and its importance in the scenario of investigation of cellular ageing and dynamic processes such as mitochondrial fission-fusion events has been discussed.

## ZUSAMMENFASSUNG

Der Zellstoffwechsel kann durch die räumliche Messung der Fluoreszenz-Abklingzeit von Fluorophoren, die auf spezifische Änderungen intrazellulärer Bedingungen reagieren, wie z.B. $[H^+]$, $[Ca^{2+}]$, $[O_2]$, Membranpotential, Temperatur, lokale Polarität und Konformationsänderungen oder Interaktion von Makromolekülen ins Auge gefasst werden. Die Messung der Abklingzeit spezifischer Sonden erlaubt dabei die quantitative Bestimmung der intrazellulären Bedingungen. Die Kombination von Fluoreszenzmikroskopie und zeitkorrelierter Einzelphotonenregistrierung stellt eine neue, leistungsfähige Methode zur Verfügung die in ihrer Empfindlichkeit und zeitlichen Auflösung anderen Techniken überlegen ist.

Auf dem Gebiet der Zellbiologie wird die Fluoreszenz-Abklingzeit-Mikroskopie (fluorescence lifetime imaging, FLIM) zur Bestimmung des Abstands spezifisch markierter Proteine (z. B. Oligomerisierung von Wachsumsfaktoren), Lipide und Nukleinsäuren, sowie von Konformationsänderungen oder Spaltungen von Makromolekülen genutzt. Die Verfügbarkeit unterschiedlicher fluoreszierender Proteine hat zu einer weiteren Verbreitung dieser Methode geführt, da die direkte Markierung von Proteinen auf genetischer Ebene erfolgen kann und daher nur wenig invasiv ist. Weiterhin konnte die Autofluoreszenz zellulärer Komponenten wie z. B. NAD(P)H zur Mengenbestimmung und zur Kontrastverbesserung bei der Abbildung komplexer Gewebe genutzt werden. Bei der Bestimmung von Interaktionen oder Stoffmengen hat sich das Verfahren zudem als deutlich verlässlicher als Intensitäts-basierte Methoden erwiesen, da es unabhängig von Konzentration und Ausbleichen des Farbstoffs, sowie Änderungen der Beleuchtungsintensität ist. Die zeitabhängige Fluoreszenz-Anisotropie eines Fluoreszenz-markierten Makromoleküls hängt von dessen Rotationsbeweglichkeit ab. Die Viskosität der unmittelbaren Umgebung und Interaktion bzw. Konformitätsänderungen beeinflussen diese Beweglichkeit. So kann die Korrelation der Anisotropie von Tryptophan zur Aufklärung der innen Dynamik von Proteinen genutzt werden. Der Energietransfer zwischen gleichartigen Fluorophoren (Homotransfer) beeinflusst deren Anisotropie durch Depolarisation.

Im Rahmen dieser Arbeit wurde ein Versuchsstand zur Zeit- und Orts-korrelierten Einzelphotonenregistrierung aufgebaut und spektral und ortsaufgelöste Messungen der Fluoreszenz-Abklingzeit von 2-(4-(dimethylamino)styryl)-1-methylpyridinium iodide (DASPMI) in lebenden Zellen durchgeführt. Hierfür wurde ein Femtosekunden-gepulster, spektral durchstimmbarer Infrarotlaser über einen Frequenzverdoppler optisch an ein inverses Fluoreszenzmikroskop gekoppelt. Die homogene Ausleuchtung der Probe wurde durch einen räumlichen Kollimator gewährleistet. Die ortsaufgelöste Fluoreszenz-Abklingzeit des fokussierten Probenbereichs wurde mit einem Zeit- und Orts-korrelierten Einzelphotonen-Detektor (Quadrant-Anoden (QA) Detektor) bestimmt. Für die Bestimmung der spektral aufgelösten Fluoreszenz-Abklingzeit wurde ein Zeit- und Orts-korrelierter Einzelphotonen-Detektor (delay-line (DL) Detektor) mit vorgeschaltetem Czerny-Turner Polychromator genutzt.

Die erste Validierung des Aufbaus erfolgte durch die Messung der zweidimensionalen, spektral aufgelösten Fluoreszenz-Abklingzeit des cyan bzw. gelb fluoreszierenden Proteins (CFP und YFP). Dadurch gelang der Nachweis einer Interaktion von Mikrofilamenten und dem Ionenkanal TRPV4 (transient receptor potential vanilloid 4). In Zellen, die die Fusionsproteine TRPV4-CFP und Aktin-YFP exprimieren, liefert die Anregung des Donors (CFP) ein Emissionsmaximum von 527 nm bei gleichzeitiger Verringerung der Fluoreszenz-Abklingzeit im Bereich von 460 - 490 nm, entsprechend einem Resonanz-Energietransfer von CFP zu YFP. Der Fluoreszenzabfall von CFP konnte am besten durch ein bimodales Modell beschrieben werden, wobei die mittlere Fluoreszenz-Abklingzeit von CFP allein, sowie in Anwesenheit des Akzeptors (YFP) eine FRET Effizienz von 20 % liefert. Dieser hohe Wert deutet auf eine geringe Distanz zwischen den Chromophoren der beiden fluoreszierenden Proteine (4 nm) hin. Somit konnte im Rahmen dieser Arbeit erstmals gezeigt werden, dass TRPV4 und Aktin in lebenden Zellen in engem Kontakt stehen. Die Bedeutung dieses Befundes für die Volumenregulation von Zellen wird hervorgehoben.

Der Aufbau wurde weiterhin zur Untersuchung des Verhaltens von DASPMI in lebenden Zellen eingesetzt. DASPMI reichert sich in lebenden Zellen in den Mitochondrien an, wobei sowohl der Grad der Anreicherung als auch die Fluoreszenzintensität vom mitochondrialen Membranpotential abhängen. Um den Mechanismus der Fluoreszenz von DASPMI aufzuklären wurden zunächst zeitaufgelöste Spektren in unterschiedlich polaren Lösungsmitteln aufgenommen: In Ethanol und Chloroform konnte der Fluoreszenzabfall global durch ein bi-exponentielles Modell beschrieben werden, wogegen in Glycerin ein tri-exponentielles Modell notwendig war. In Wasser, das stark polar und niedrig viskös ist war ein mono-exponentielles Modell hinreichend. Der Einfluss der Lösungsmittelviskosität wurde in Ethanol/g-Mischungelyzerinn unterschiedlicher Verhältnisse untersucht. Mit zunehmender Viskosität des Lösungsmittels stieg auch die Fluoreszenz-Abklingzeit. Das Auftreten einer negativen Amplitude der kurzen Abklingzeit in Chloroform und Glycerol bei größeren Wellenlängen belegt die Entstehung eines weiteren angeregten Zustandes aus dem anfänglichen angeregten Zustand. Die zeitaufgelösten Emissionsspektren in Chloroform und Glycerol zeigten einen biphasischen Anstieg des Emissionsmaximums und der spektralen Breite. Die spektrale Breite stieg anfänglich stark an und blieb nach 150 ps nahezu konstant. Um die Kinetik des angeregten Zustands zu erklären, wurde ein zweistufiges Modell entwickelt, das auf der Solvation des initialen angeregten Zustands und des TICT Zustands basiert. Die Zerlegung der zeitaufgelösten Emissionsspektren in Chloroform, Glycerin und Ethanol/Glycerin Mischungen unterstützt dieses Modell. Die Kenntnis der photophysikalischen Eigenschaften von DASPMI in unterschiedlichen Lösungsmitteln erlaubt nun auch die Ableitung komplexer physiologischer Parameter aus dem Farbstoffverhalten in den Mitochondrien lebender Zellen.

Die Untersuchung von einzelnen Mitochondrien bzw. wenigen Organellen von XTH2-Zellen zeigte die für eine hoch visköse Umgebung typische tri-exponentielle Kinetik des Fluoreszenzabfalls. Auf Basis der photophysikalischen Eigenschaften von DASPMI in verschiedenen Lösungsmitteln wurden die gefundenen Fluoreszenz-Abklingzeiten drei unterschiedlichen angeregten Zuständen zugeordnet locally excited (LE), intramolecular charge transfer (ICT) und twisted intramolecular charge transfer (TICT) state. Eine

bemerkenswerte Variation in der Abklingzeit von Mitochondrien unterschiedlicher Form innerhalb einer Zelle war offensichtlich, was den hohen Variabilitaten der Zellphysiologie entspricht. Die starke Verringerung der kurzen Abklingzeit ($\tau_1$) unter Bedingungen hohen Membranpotentials, wie z. B. in Anwesenheit von ATP oder Substrat entsprach dem Quenching und der dramatischen Abnahme der Abklingzeit in polarem Lösungsmittel. Unter diesen Bedingungen nahmen $\tau_2$ und $\tau_3$ mit abnehmendem Beitrag zu. Nach Behandlung mit dem Ionophor Nigericin, führte die Hyperpolarisation der Mitochondrien zu einer bemerkenswerten Verkürzung von $\tau_1$ von 159 ps auf 38 ps. Die Hemmung der Zellatmung mit Cyanid führte zu einer beachtlichen Zunahme der Abklingzeit und einer Abnahme der mitochondrialen Fluoreszenz. Die Zunahme der DASPMI Fluoreszenz unter Bedingungen eines erhöhten mitochondrialen Membranpotentials ist einer Aufnahme entsprechend einer Nernst-Verteilung, der Delokalisation von $\pi$-Elektronen, Quenching der Methylpyridinium-Gruppe und der eingeschränkten Torsionsdynamik an der inneren Mitochondrienmembran zugeschrieben worden. Dementsprechend enthüllte die Bestimmung der Anisotropie von DASPMI-markierten Mitochondrien in lebenden XTH2-Zellen, die Abhängigkeit der Anisotropie vom Membranpotential. Solche Änderungen in der Anisotropie, die der Beschränkung der Torsionsdynamik um die flexiblen Einzelbindungen in Nachbarschaft der olefinischen Doppelbindung zugeschrieben werden, erwiesen die bereits vorher bekannten submitochondrialen Zonen erhöhten Membranpotentials entlang des Mitochondriums. Der direkte Einfluss des lokalen elektrischen Feldes auf das Übergangsdipolmoment des Farbstoffs und seiner Torsionsdynamik spiegelt Veränderungen des mitochondrialen Energiestatus in lebenden Zellen wieder. Membranpotential-abhängige Veränderungen der Anisotropie wurden darüber hinaus in seneszenten Hühnerembryo-Fibroblasten nachgewiesen. Es wurde versucht, die Einflüsse der DASPMI Fluoreszenz in der inneren Mitochondrienmembran, die auf der Viskosität und Polarität beruhen zu unterscheiden und somit die relativen Unterschiede zu bestimmen.

Zusammenfassend wurde ein Aufbau zur Einzelphotonenregistrierung etabliert, mit dem spektral- und ortsaufgelöste Fluoreszenzabfälle in einer zeitlichen Auflösung im

Pikosekunden-Bereich erreicht werden kann. Somit lassen sich photochemische, photobiologische und photophysikalische Prozesse in lebenden Zellen untersuchen. Spektroskopische Beobachtungen der Kinetik des angeregten Zustands von DASPMI in verschiedenen Lösungsmitteln sowie in lebenden Zellen zeigten zum ersten Mal seine genaue Lokalisierung, den Mechanismus spannungssensitiver Fluoreszenz und seine Memranpotential-abhängige Anisotropie in lebenden Zellen. Ein systematischer Ansatz, der verschiedene Gleichgewichts-Methoden verwendet und neuartige Zeit- und Orts-korrelierte Einzelphotonenregistrierung verwendet, hat die gleichzeitige Abhängigkeit der DASPMI-Fluoreszenz-Eigenschaften von mitochondrialem Membranpotential und der Viskosität der inneren Mitochondrienmembran gezeigt. Diese gleichzeitige Abhängigkeit der photophysikalischen Eigenschaften von der Viskosität der inneren Mitochondrienmembran und dem Transmembranpotential wurde ausgearbeitet und seine Bedeutung für ein Modell zellulären Alterns sowie dynamischer Prozesse, wie etwa mitochondriale Fusion und Teilung wurde diskutiert.

## 1. INTRODUCTION

### 1.1 Fluorescence Microscopy

Fluorescence microscopy provides a sensitive means of visualizing the organization and dynamics of complex cellular structures using endogenous and exogenous optical probes. Recent rapid state of evolution of fluorescence microscopy now permits quantitative measurement of three-dimensional intensity distribution and acquisition of spectroscopic information with unsurpassed detection sensitivity and ultra-high spatial-temporal resolution (Egner & Hell, 2005; Klar et al., 2001; Petty, 2007; Axelrod, 2001; Cappello et al., 2003; Lewis et al., 2003; Suhling et al., 2005; Wallrabe & Periasamy, 2005). A diverse range of advanced techniques in fluorescence spectroscopy including fluorescence lifetime imaging, has been implemented allowing real-time microscopic examination of biochemical processes of molecular binding, association, conformational change and diffusion in living cells.

Additionally, development of fluorescent probes that change there intrinsic fluorescent properties, as a function of physiological parameter or chemical reaction state, due to spatial proximity or direct protein interactions make fluorescence microscopy a prominent tool for investigating the biological machinery of living cells and tissues. Endogeneous probes in biological tissues, like aromatic amino acids (tryptophan, tyrosine and phenylalanine), NADH, flavins, chlorophyll, structural proteins (collagen and elastin) or lipopigments (e.g. ceroids and lipofuscin) are noninvasive in nature. Intrinsic fluorescence protein (fluorescent proteins such as variants of GFP's), fluorescent markers bound to immunoglobulins or any other proteins or metabolites and extrinsic associated probes (DASPMI, JC-1, TRITC, Hoechst 33342) are minimally invasive. Observations inside a living cell are important and necessary to understand the behavior and biochemistry in its natural environment wherein specific environments like complex organization and compartmentalization are made probable.

Fluorescence microscopy is minimally invasive and takes advantage of various fluorescence characteristics, such as, emission intensity, polarization, wavelength, and lifetime to map their spatio-temporal distribution in living cells and tissues. Fluorescence microscopes with sub-nanosecond temporal resolution can report on various environmental factors influencing the fluorophore in the excited state and hence, determine the relative differences in various regions of a living specimen.

## 1.2 Fluorescence Lifetime Imaging Microscopy

Fluorescence lifetime imaging microscopy (FLIM) takes advantage of the differences in excited-state lifetime of fluorescent probes as a contrast mechanism for imaging the biochemistry inside a living cell. Excited-state lifetime is a molecular property and is usually independent of variations in fluorophore concentration, illumination intensity, light path length, scatter, or photobleaching. Several fluorescent probes change their characteristic lifetimes in response to local viscosity, pH, or refractive index, as well as interactions with other molecules (Figure 1.1).

FLIM offers complementary information on local physical parameters (eg. microviscosity, polarity) and chemical parameters (e.g. pH, ion concentrations), in addition to the information acquired from the steady-state characteristics (fluorescence spectra, excitation spectra and polarization). The necessity of only very small excitation volumes, its single photon detection sensitivity and the possibility of combining multi-parameter spectral imaging of cellular structures with FLIM, makes it an outstanding biological tool.

The distinct lifetime of fluorophores allows the discrimination of fluorescence signals from background autofluorescence in living specimens. The sensitivity of fluorophores excited-state lifetime to its microenvironment allows distinction of co-localized spectrally similar probes. Numerous applications taking advantage of FLIM have been reported – calcium imaging; membrane fluidity, transport and fusion; protein-protein interactions; DNA sequencing; clinical imaging for quantitative measurements of disease markers.
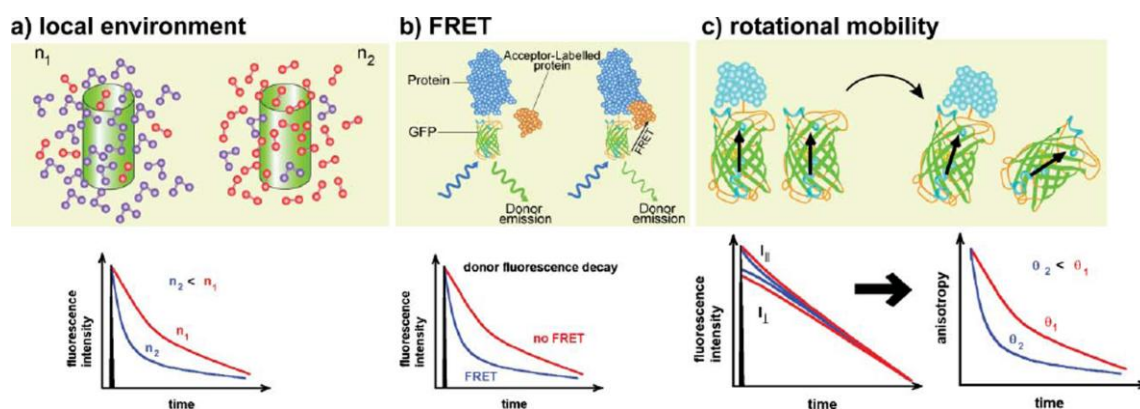
**Figure 1.1** *Photophysical phenomena commonly investigated by FLIM and there influence on fluorescence lifetime of a fluorescent protein.* **(a)** *The decay of fluorescence depends on the local environment of the fluorophore. For example, a high refractive index causes shortening of the GFP lifetime.* **(b)** *FRET is a non-radiative form of energy transfer between two fluorochromes in the distance of $10 - 100 \overset{0}{A}$. This long-range dipole-dipole interaction requires the emission spectra of the donor molecule overlap with the absorption spectra of the acceptor molecule and can be used as a spectroscopic ruler to measure the distance between fluorophore tagged proteins in living cells. The quenching of fluorescence due to such interactions leads to a shortening of the lifetime.* **(c)** *The rotational mobility of a fluorophore can be investigated by time-resolved fluorescence anisotropy imaging. The rotational mobility of a fluorophore can be hindered by the viscosity of the fluorophore surroundings, or by its binding affinity and conformational changes. The rate of depolarization of fluorescence is characterized by the rotational correlation time and can be calculated from the differences between the polarization-resolved parallel and perpendicular decays. (Suhling et al., 2005)*

Fluorescence lifetime imaging using time-correlated single photon counting can provide valuable and accurate information on the dynamic processes. However, the power of correctly applied FLIM is in obtaining good quality data and reliable parameter estimates. Distortions of the fluorescence response due to artifacts may have disastrous consequences. The requirement of expertise in photophysical properties of probes, complexity in interpreting the lifetime differences in terms of the underlying cell biochemistry and the complex expensive equipment for data acquisition makes it a complicated tool.

## 1.3 Molecular Fluorescence

The Perrin-Jablonski diagram (Figure 1.2) is an important scheme to visualize the various photophysical process, such as, photon absorption, internal conversion, fluorescence, intersystem crossing, phosphorescence, delayed fluorescence and triplet transitions involved in the phenomenon of luminescence. Molecular fluorescence depends on the interactions with other molecules (energy transfer, electron transfer, proton transfer, excimer formation, etc.) and local environment (polarity, hydrogen bonds, pH, pressure, viscosity, temperature, quenchers, electric potential, ions). Fluorescence characteristics, such as, excited-state lifetime and quantum yield change in a measurable manner and are influenced by the changes imposed by the local environment on the electronic configuration.

The fluorescence lifetime $\tau$ is the average time a molecule remains in an "excited-state" after absorbing a photon and is defined as

$$\tau = \frac{1}{k_r + k_{nr}}$$

where $k_r$ is rate constant for radiative deactivation, and $k_{nr}$ is the rate constant for non-radiative deactivation. The fluorescence quantum yield $\Phi_f$ is the fraction of excited molecules that return to the ground state with the emission of a photon and are related to lifetime as

$$\Phi_f = \frac{\tau}{\tau_0} = \frac{k_r}{k_r + k_{nr}}$$

However, the above relation may not be valid if de-excitation pathways are such as due to interaction with other molecules or formation of non-fluorescent ground-state complex.
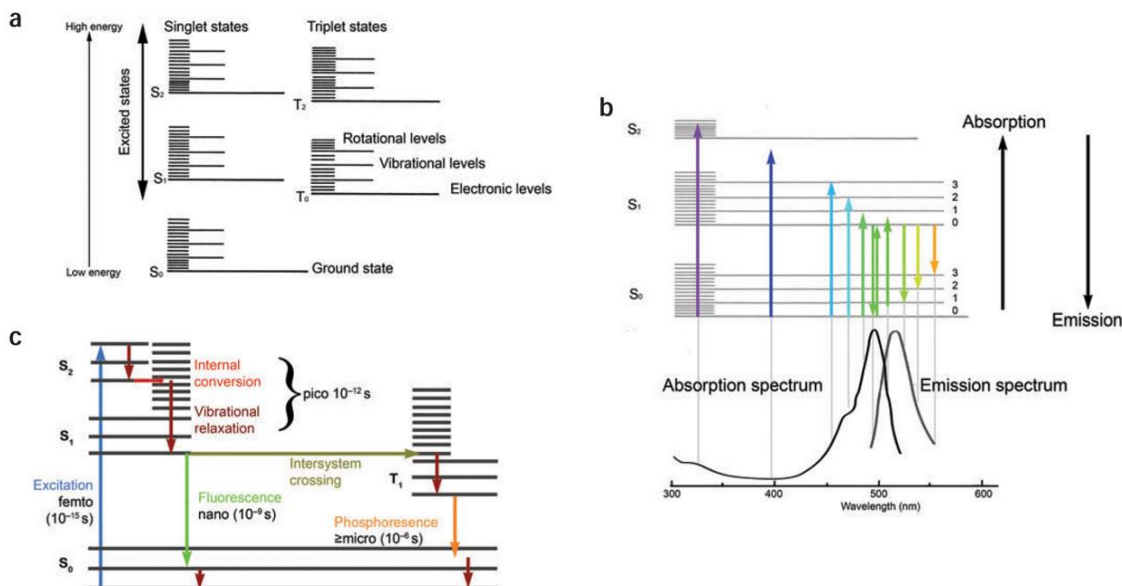
**Figure 1.2 Perrin-Jablonski schemes. (a)** *Jablonski scheme displaying the various electronic energy states (S – singlet; T- triplet) and the associated vibrational levels.* **(b)** *Absorption and emission characteristics of a fluorophore depend on the distribution of the energy levels and the energy steps necessary to bring the molecule to the various energy levels. The absorption and emission spectra of a common probe FITC and the associated Franck-Condon vertical transitions for the absorption (arrows pointing up) or emitted (arrows pointing down) photons are shown below the Jablonski scheme. The arrows are colored to represent the wavelength of the absorbed or emitted photons. For example, the purple arrow to the left signifies a probable transition upon ultraviolet photon absorption from the ground state to the second singlet excited state. The orange arrow on the right represents the transition from the lowest vibrational energy state of $S_1$ to a high vibrational state of $S_0$. In the region of overlap of the absorption and emission spectra, absorption of photon is not restricted to the lowest vibrational level. The symmetry of the absorption and emission curves arise from the similarity of transitions between $S_0$ and $S_1$ vibrational levels. **(c)** Characteristic times associated with various photophysical events. ([Lichtman & Conchello, 2005](#))*

## 1.4 DASPMI as a Unique Probe for Mitochondrial Membrane Potential

Mitochondria are an important organelle of eukaryotic cells, wherein it performs various important physiological functions, such as, oxidative phosphorylation, ionic homeostasis and thermoregulation. The morphology of mitochondria in situ varies from punctate to elongated form and big mitochondrial networks. This dynamic organelle undergoes fission-fusion events which are important to maintain mitochondrial homeostasis. Structurally, a mitochondrion consists of an outer membrane, an inner membrane, the intermembrane space and the matrix. The vital role of mitochondria is to provide the ATP and ATP equivalents as a universal source of metabolic energy. Electron transport chain consists of four respiratory enzyme complexes at the mitochondria inner membrane which undergo biochemical reactions to produce the proton gradient or the mitochondrial membrane potential. The membrane potential drives the synthesis of ATP by $F_oF_1ATPase$, which functions as a proton turbine.

The intracellular distribution of mitochondria and its dynamic membrane potential can be visualized by staining with numerous fluorescent probes including rhodamine 123 or dimethylaminostyryl pyridinium methiodide. The membrane-potential-dependent Nernst partitioning of charged lipophilic cations allows the selective mitochondrial staining by fluorochromes. Mitochondria selective staining was first reported for rhodamine applied to plant cells (Johannes, 1941), and was attributed to a specific rhodamine isoform, rhodamine 123 (Rh123), by Lan Bo Chen's group in 1978 (Johnson et al., 1980). In 1976, DASPMI was described to selectively accumulate in the mitochondria (Bereiter-Hahn, 1976) of a variety of cells (Figure 1.3; Eng et al., 1989; Fuchs et al., 1987; Irion et al., 1993; Leip et al., 1994; McCormick, 1990).

DASPMI is a low toxicity ($< 5 \times 10^{-7}$ M) specific vital stain of mitochondria and its emission intensity in mitochondria is influenced by uncouplers and inhibitors of oxidative phosphorylation. The very fast response of DASPMI to transmembrane potential changes, high sensitivity and well definable potentiometric response makes it a unique valuable probe for precise monitoring of the dynamic changes in membrane
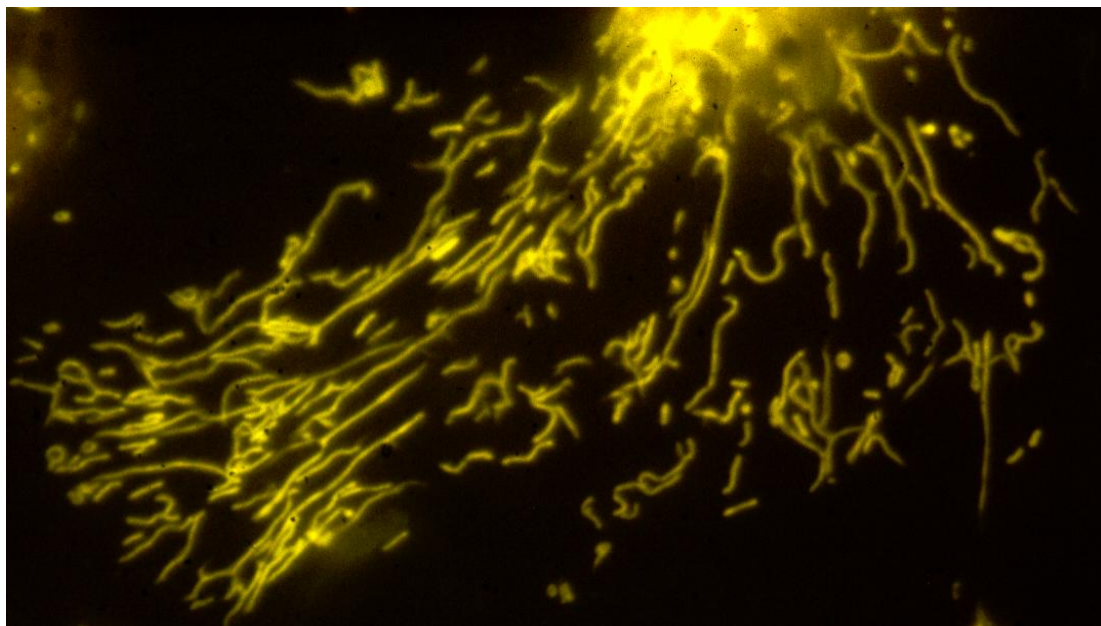
**Figure 1.3** *Mitochondria in living XTH2 cells stained with DASPMI. (Courtesy: Prof. Dr. Jürgen Bereiter-Hahn)*

potential across different mitochondria in a single living cell and within intramitochondrial zones. For instance, high membrane potential regions within in a cell required for ATP production during cell growth, cell differentiation and cell motility (James & Bohman, 1981; Darzynkiewicz et al., 1982; Collins & Foster, 1983; Johnson et al., 1981; Diaz et al., 1999) may well be precisely visualized with such optical probes.
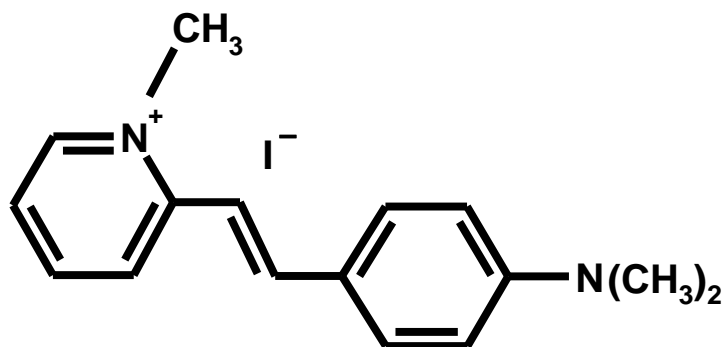


**Figure 1.4** *Structure of 2-(4-(dimethylamino)styryl)-1-methylpyridinium iodide.*

DASPMI is a lipophilic compound with a delocalized $\pi$ – electron system ([Figure 1.4](#)) and its spectra in mitochondria corresponds to those in a phospholipid environment (excitation wavelength maximum around 470 nm, emission 560 – 570 nm). The fluorescence characteristics of DASPMI are influenced by both polarity and viscosity of the environment which, in general, are not discernible. The polarity based influences manifest themselves as a red shift in the emission spectra, blue shift in the absorption spectrum and a decrease in quantum efficiency and lifetime in the case of increasing polarity of the environment. The increase in viscosity results in enhancement of fluorescence. Although DASPMI has many such interesting molecular properties, its potential as a fluorescent probe for mitochondria have not been fully exert to benefit. This requires comprehension of the mechanism of voltage-sensitive molecular fluorescence, localisation in mitochondria and its behaviour under the conditions influencing mitochondria energy status in living cells.

## Objectives of this Dissertation

The aspiration of this doctoral work was to establish novel time- and space-correlated single photon counting system; capable of obtaining spectrally and spatially resolved fluorescence decays with picosecond time resolution in living cells. The necessity of such an advanced system in my scientific endeavour was to understand the complex behaviour of a mitochondria selective potentiometric styryl probe 2-(4-(dimethylamino)styryl)-1-methylpyridinium iodide (DASPMI) in living cells. Fluorescence intensity of DASPMI is a dynamic measure of energization of mitochondria and thus is influenced by inhibitors and uncouplers of oxidative phosphorylation. The presumed localisation of DASPMI at the mitochondrial inner membrane suggested the possible interactions with respiratory chain complexes, flavins and cytochromes.

In this endeavour, a systematic approach of first revealing DASPMI photophysics in various solvents and use these inferences to determine the localisation and possible interactions inside the mitochondria. Both steady-state and time-resolved fluorescence approaches will be used as an investigative tool.

## Time- and Space-Correlated Single Photon Counting

The success of fluorescence microscopy as an investigative tool for envisaging the structure and dynamics of living systems arises from its ability to provide spatial and temporal information with high degree of sensitivity. The temporal information is important in comprehending the photophysical, photochemical, and photobiological processes. The emergence of ultrafast lasers with higher repletion rate and the use of micro-channel plate photomultipliers for photodetection have increased the time-resolution up to a few picoseconds.

At present almost all time-domain measurements are performed using time-correlated single-photon counting (TCSPC). It is a technique to record low-level light signals with picosecond time resolution and single photon sensitivity. The current state-of-the-art of

this technique uses high-repetition-rate picosecond or femtosecond light sources and high-speed microchannel plate photomultipliers. Typical applications apart from fluorescence lifetime measurements include - detection and identification of single molecules, fluorescence correlation spectroscopy (FCS), fluorescence resonance energy transfer (FRET) and fluorescence anisotropy.

In the field of FLIM in living cells, the most universal method is time- and space-correlated single photon counting (TSCSPC) in the picosecond range. The core of a time and space correlated single photon counting spectroscope is a fast detector (time resolution 25 − 80 ps ) which resolves space either along a line of measurement (DL-detector) or over a two dimensional light sensitive area (QA-detector). The image of a fluorescence microscope is projected on the photocathode of such a detector. The photocathode reacts by a burst of electrons when hit by a photon; the resulting current is amplified via two micro channel plates (MCP) and finally reaches a delay-line or a quadrant anode. This provides an electric signal which is time correlated to the fluorescence excitation pulse and space correlated to the position the photon impinged onto the photocathode. Thus for each point of measurement a fluorescence decay curve can be generated. Introducing a spectrograph before the DL-detector allows determining spectrally resolved fluorescence decays.

**Photophysical Properties of DASPMI in Solvents**

The photophysics and photochemistry of stilbazolium and related (aminophenyl)pyridinium dyes, have been a subject of extensive investigation, owing to its many interesting applications, such as, to detect membrane potential in biological materials and several other applications in polymer science and analytical chemistry due to its strong viscosity dependence. The simultaneous dependence of photophysics on solvent viscosity and polarity was explained as due to the internal charge transfer processes between the electron donor and acceptor substituent groups by single-bond twisting in the excited state toward a "twisted intramolecular charge transfer" (TICT)
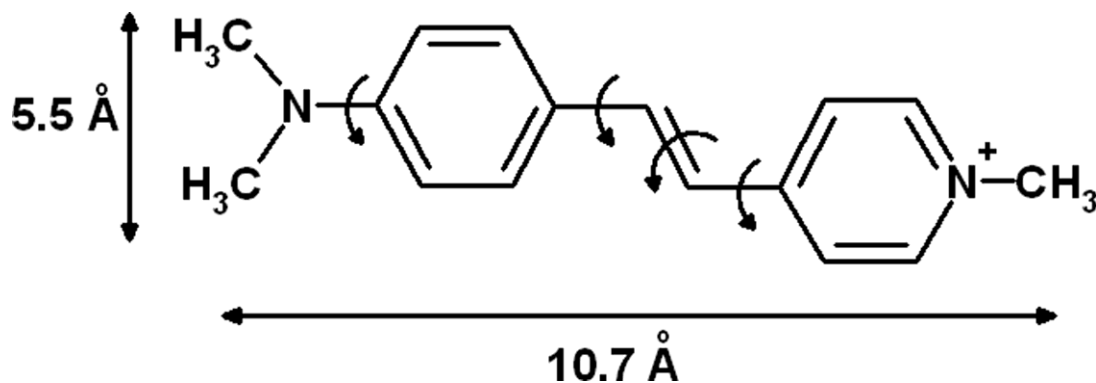
**Figure 1.5** *Molecular structure of trans-4-[4-(dimethylamino)-styryl]-1-methylpyridinium iodide (DASPI) and the possible twisted conformations predicted based on previous experimental and theoretical approaches*. *Twisting around the dimethylamino group was found to be unfavorable due to the possession of higher TICT state energy than the planar conformation. The trans-cis isomerization was as well found to be improbable in the excited state because of very low isomerization yield (<1 %). Twisting of the single bonds neighboring the olefinic double bond can result in de-activation of excited-state by fluorescence. (Adopted from Kim & Lee, 1999; and the references therein)*

state (Figure 1.5). The TICT-model was endorsed by synthesis of a model compound wherein the flexible single bond between the pyridinium and anilino group was bridged to obtain a rigid molecule (2-methyl- 7-(dimethylamino)-2-azafluorenium), possessing higher quantum yield of about 50 % (Fromherz & Heilemann, 1992). The quantum efficiency of the twistable compound ((aminophenyl)pyridinium) was 0.05 % in solvents of high polarity and fluidity.

In this work, the complex photophysical properties of DASPMI were investigated by obtaining spectrally resolved fluorescence decays in solvents of various polarity and viscosity. The picosecond lifetime dynamics in solvents required the optimisation of the lifetime setup for obtaining a good instrument response function with a time resolution of only few picoseconds. The formation of new excited-state species from the initially excited state was approached by constructing decay associated spectra (DAS). The strong viscosity dependence was examined in varying ratios of ethanol/glycerol mixtures. The time dependence of fluorescence emission characteristics was studied by constructing

time-resolved emission spectra from the obtained spectrally resolved fluorescence decays. Finally, a comprehensive photophysical model of DASPMI excited-stated kinetics was to be obtained.

**Behaviour of DASPMI in Living Cells**

Fluorescence microscopy including time- and space-resolved single photon counting was embarked to investigate the interactions, localization and the mechanism of voltage sensitive fluorescence of DASPMI in mitochondria of living cells. The amphibian endothelial cell line XTH2 (cells from Xenopus laevis tadpole hearts) will be used for this study. Fluorescence microscopy will be applied to obtain quantitative information on the membrane-potential-dependent uptake kinetics and the intracellular distribution of emission intensity. The uptake kinetic differences of DASPMI in a single cell revealed the presence of more than one population in mitochondria. Previously, such populations have been distinguished as differing by matrix density, RNA content or as in XTH2 cells due to differing mtDNA synthesis. Emission fingerprints of DASPMI from various regions of interest in living XTH2 cells will be examined to obtain the contribution of various excited-state species.

Spatially resolved fluorescence decays obtained from various mitochondrial regions of interest would reveal the changes in excited-sate kinetics of DASPMI, under conditions manipulating mitochondrial membrane potential. Mitochondrial energy status shall be manipulated as are for instance cyanide (KCN) to inhibit respiration by blocking complex IV function, nigericin which is known to increase inner mitochondrial membrane potential by electroneutral $K^+/H^+$ exchange, and CCCP a powerful uncoupler of respiratory chain activity from oxidative phosphorylation due to its protonophore character. The external control of mitochondrial energy status was undertaken by permeabilizing the cells with saponin and assessing the influence of ATP and substrate (glutamate and malate) on DASPMI decay kinetics. The fluorescence decays extracted from various ROI including nucleus, nucleoli and cytoplasm shall be used to explain its

phtophysical properties in living cells. The excited state lifetime changes in relation to morphology and other influences such as photodamage shall as well be investigated.

Anisotropy is a dimensionless quantity and has information on the rotational mobility of a molecule in relation to its excited state lifetime. The flexibility of DASPMI under varying mitochondrial energy status will be monitored by simultaneously acquiring the polarization resolved fluorescence images and hence determining its emission anisotropy in living cells. Determination of emission wavelength dependent anisotropy and lifetime distribution of DASPMI under various conditions manipulating mitochondrial membrane potential would enable to draw inferences on its localization and ground state charge distribution. Because of the severe loss of mitochondrial DASPMI fluorescence under the influence of inhibitors and uncouplers, ageing model of avian cells will be used to demonstrate the differences of DASPMI anisotropy due to changing mitochondrial membrane potential.

## 2. MATERIALS AND METHODS

### 2.1 Time- and Space-Resolved Fluorescence Decay Microscopy

A Millennia Xs (Nd:YVO$_4$ gain medium; Spectra-Physics, Darmstadt, Germany) pumped, mode-locked Ti:sapphire laser (Titanium-doped sapphire; Tsunami, Spectra-Physics, Darmstadt, Germany) with a repetition rate of 82 MHz and about 50 femtosecond pulse width was tuned to 880 nm. For the stable operation at the wavelength tuned, it had to be purged in nitrogen. The Ti: saphire laser was coupled to a pulse stretcher, pulse selector and frequency doubler (Model 3980; Spectra-Physics, Darmstadt, Germany) to obtain excitation wavelength of 440 nm at 4 MHz repetition rate and less than two picosecond pulse width. The frequency doubled laser pulses were expanded, spatially filtered and optically aligned to the condenser of an inverted fluorescence microscope (epi-illumination, Olympus IX70, Hamburg, Germany) to obtain uniform illumination over the sample area. An adapter (Double lamp housing; U-DULHA, Olympus) containing a switchable mirror was used to change the illumination between laser pulses and mercury lamp (U-ULS100G; Olympus, Hamburg, Germany). A part of the infrared laser beam (one percent) from Ti: Saphire laser was used to monitor its pulse width and wavelength characteristics using an autocorrelator (APE, Berlin, Germany) and spectrometer (APE, Berlin, APE, Berlin, Germany), respectively.

The core of the fluorescence decay microscope are delay-line (Kemnitz et al., 1995) and quadrant anode (Kemnitz et al., 1996) single-photon counting detectors, which resolve space along a line of measurement (DL-detector; Euro-photon GmbH, Berlin, Germany) and over a two-dimensional area (QA-detector; Euro Photon GmbH, Berlin, Germany). These detectors react by a burst of electrons when hit by a photon; the resulting current is amplified via two multichannel plates (MCP) and finally reaches a delay-line or a quadrant anode. The position of impinge of the centroid of the charge cloud on the anodes provides an electric signal which is time correlated to the fluorescence excitation pulse and space correlated to the position the photon impinged onto the photocathode.
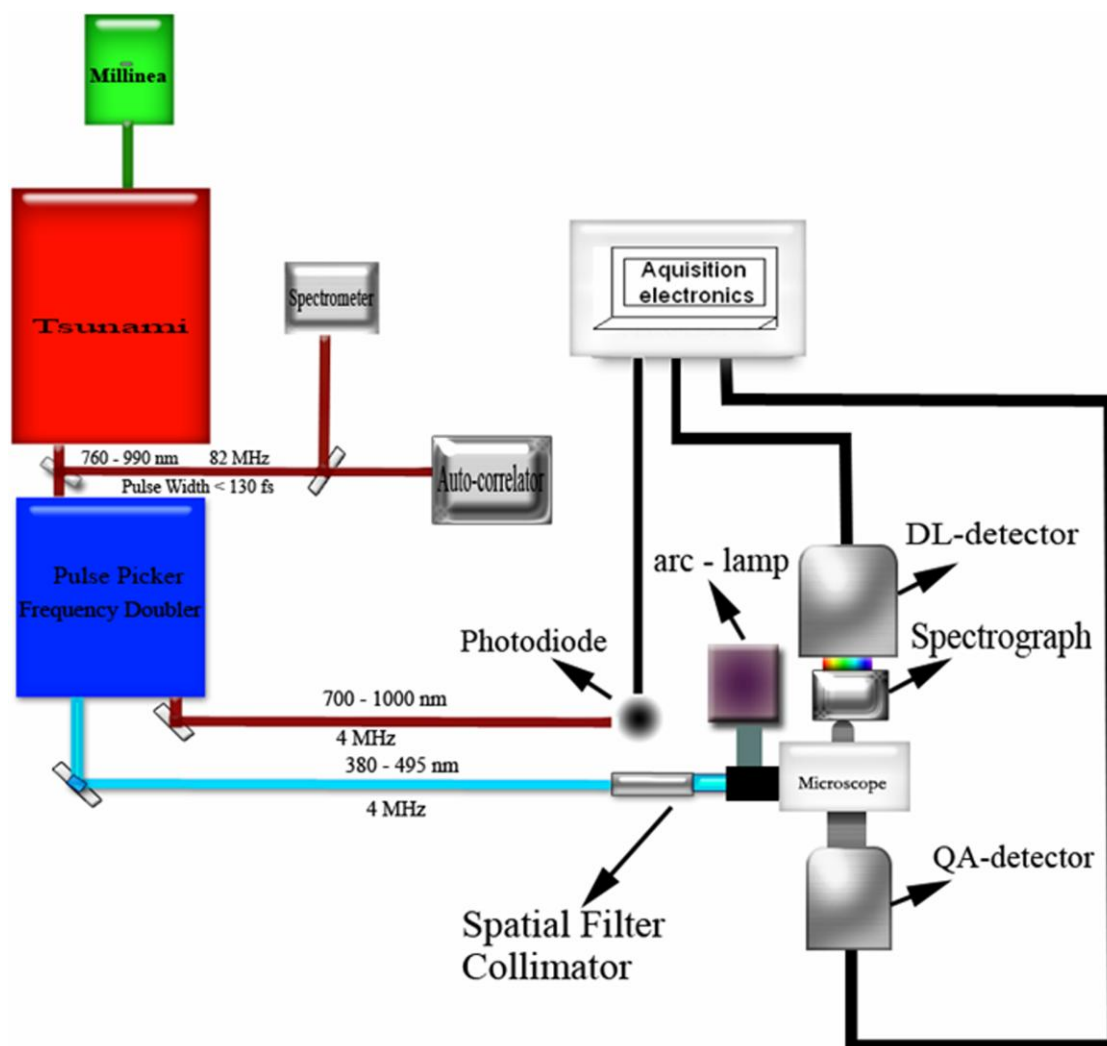
**Figure 2.1** *Scheme of Picosecond Fluorescence Decay Microscope. Picosecond laser excitation pulses obtained after pulse stretching, pulse picking and frequency doubling are spatially filtered and collimated into the microscope. A photodiode signal is used by the acquisition electronics as a reference to measure the time difference between the laser pulse and the spatially resolved single photon emission counted by the detector. Time-correlated single photon counting detectors DL and QA, resolve space either along a line of measurement or over a two-dimensional light sensitive area, respectively. Introducing a spectrograph in front of the DL-detector allows determining spectrally resolved fluorescence decays (Figure 3.2 b and d).*

Thus, for each point of measurement a fluorescence decay curve can be generated. The time information correlated with laser excitation pulses is achieved by acquisition of signals from the second MCP and an amplified (Fast Preamp; VT120; EG & G Ortec, Tennessee, USA) photo-diode signal (S5972, Hamamatsu, Photonics Deutschland Gmbh, Herrsching, Germany) generated by the infra-red laser pulses surpassing the frequency doubling crystal (BBO). The scheme of picosecond fluorescence decay microscope is shown in Figure 2.1. Further details concerning the optical layout, electronic schemes and the various problems encountered during the establishment of the setup, including remedies have been described in Appendix.

### 2.1.1 DL-Detector (Spectrally Resolved Fluorescence Decays)

Spectrally resolved fluorescence decays were obtained by introducing a 120 mm Czerny-Turner spectrograph (77400-M; LOT, Oriel instruments; Darmstadt, Germany) between the microscope and the DL-detector. Light from the sample was collected through one of the detection ports of the microscope and focused on the entrance of a Czerny-Turner spectrograph, using a plano-convex lens. The spectrograph has an F/number of 3.7, a focal length of 120 mm and is equipped with a ruled grating (600 lines/mm) with blaze wavelength at 400 nm. The DL-detector was placed in the focus of the spectrum projected by the spectrograph.

The amplified signals (Fast Preamp; VT120; EG & G Ortec) of the DL-detector were connected to constant fraction discriminators (CFD; Ortec Electronics, Tennessee, USA). The logical pulses produced by CFD's were used to start and stop the time-to-amplitude converters (TAC; Ortec Electronics Tennessee, USA) which output an analog voltage pulse proportional to the start and stop signals. The position of the centroid of the charge clouds that exit MCP are calculated by the difference of arrival time at the two ends of the delay. Since the delay line anode is symmetric (Figure 2.2), an additional delay to one of the signals from the ends of the delay line was given after the CFD to make sure that the start pulse always arrives before the stop pulse. The spatial resolution of the position determination is dependent on the accuracy of temporal measurement. Hence a careful
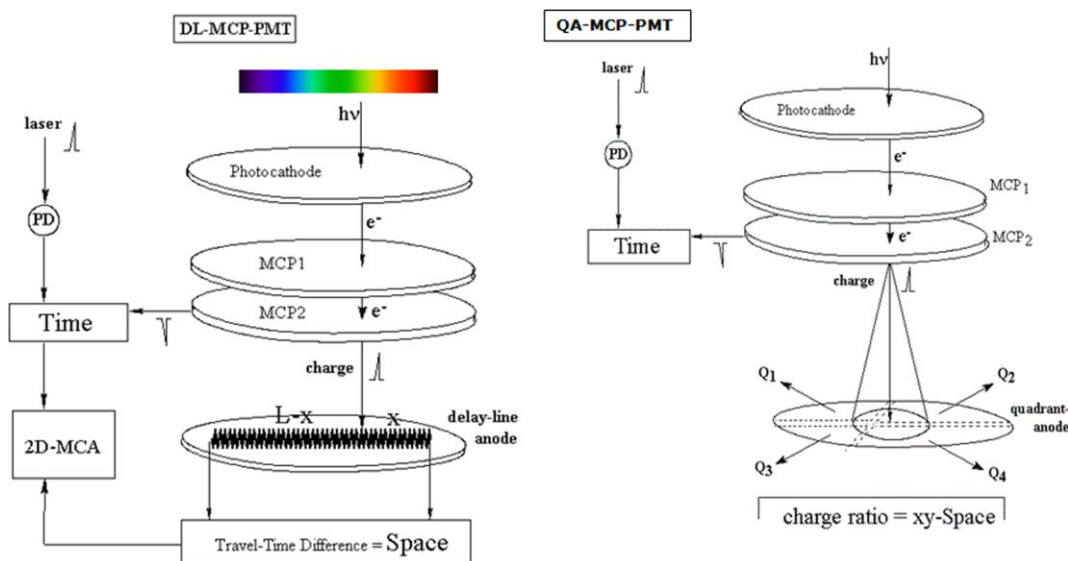
**Figure 2.2** *Scheme of delay-line and quadrant anode detector.*

optimization of the readout electronics (CFD, TAC & analogue digital converters) is required, in particular of the optimum fraction and delay for CFD's.

The time information from the TAC's are sent to a 2D multi-channel analyser (ADWin, Lorsch, Germany), which generates a two-dimensional histogram of 256 channels for wavelength and 1024 channels for time. With the histogram from the transputer, the aqusition program (SPCView, Europhoton, Berlin) displays spectrally resolved fluorescence decays. Calibration of the wavelength channel was carefully done using the light guided through a fiber from the monochromator (Photon Technology International, New Jersey, USA). The time channels were calibrated by giving a fixed time delay to the photodiode signal. The spectral resolution was changed by adjusting the entrance slit width of the spectrograph.

### 2.1.2 QA-Detector (Spatially Resolved Fluorescence Decays)

Spatially resolved fluorescence decays from the projection of the magnified two-dimensional area of the sample in focus, was obtained using QA-detector. The positions of impinging of the photons are determined by the relative charge distributions

throughout the four quadrants and a fifth correction component ([Figure 2.2](#)). The fifth correction component is determined from the charges collected in the detector area encircling the four quadrants. Simultaneously, for time correlation, a time-to-amplitude converter is used between signal coming from the second microchannel plate and signal from a fast photodiode triggered by the pulsed excitation source. The online acquisition program records a three dimensional matrix with temporal and spatial resolution in each pixel of the two-dimensional sample image ($256 \times 256$ pixels). Hence every pixel has the information regarding the relative time of arrival of each photon, number of photons in each pixel and the correlated time information between the excitation pulses and fluorescence emission. This allows construction of fluorescence decays (in up to 4096 channels) from different regions of sample, at different acquisition times. The detector was water cooled to 4°C before the start of experiments to reduce the thermal noise. The full width half maxima of the instrument response function were less than 150 ps. The spatial resolution was determined by placing a micrometer scale in the sample area of the microscope.

## 2.2 TRPV4-Microfilament Interactions

### 2.2.1 Cell Culture

HaCaT keratinocyte cells (passage 47 – 52) were cultivated in keratinocyte SFM medium (Invitrogen, Karlsruhe, Germany), containing 10 % fetal calf serum (FCS), 10 mM Hepes (Invitrogen) at 37°C in 5 % CO2 atmosphere. CHO-K1 cells (passage 28 – 50) were cultivated in F-12 HAMs cell medium (Invitrogen), containing 10% FCS and 10 mM Hepes (Invitrogen) buffer at 37°C in 5 % $CO_2$ atmosphere.

HaCaT and CHO cells were either transfected with Effectene transfection reagent (Quiagen, Hildern, Germany) according to manufacturer's instructions or by electroporation (BTX electro cell manipulator 600, Holliston, USA). The transfected cells were seeded onto coverslips after 24 h.

For F-actin staining, cells (72 h post transfection) were washed twice with PBS and fixed with 10 % formaldehyde in PBS for 20 min at room temperature. Fixed cells were washed thrice and stained for 20 min with 2 μg/ml TRITC-Phalloidin (Sigma-Aldrich, Munich, Germany) in PBS at RT. Cells were washed 3 times and embedded in Mowiol.

### 2.2.2 Constructs

For construction of TRPV4-CFP, TRPV4-GFP (Becker et al., 2005) was digested with BamH1 and Not1 and the GFP tag was exchanged for the CFP tag of plasmid CFP-C1 (Clontech, California, USA). For construction of actin-YFP, actin-GFP (Clontech) was digested using BamH1 and BglII and cloned into the EcoR1 and BglII sites of the vector YFP-C1 (Clontech, California, USA).

### 2.2.3 Steady-State Fluorescence Images

Co-localization studies were performed using a Leica TCS 4D confocal laser scanning microscope fitted with the appropriate filters and PL Fluotar objective (100x, 1.3 NA) that was controlled by the SCAN Ware 5.10 software (Leica, Bensheim, Germany). Images were processed using Imaris v. 4.1.3 and auto deblur, edition gold v. 9.3.

Steady state fluorescence imaging was done using an IX70 (Olympus, Hamburg, Germany) inverted fluorescence microscope. Mercury arc lamp (50 W) was used for excitation, in combination with filters: 450 – 490 nm band pass filter, 480/30 nm (Omega opticals, Vermont, USA) filter and BP530 – 550 nm (Omega opticals, Vermont, USA) emission filters. Imaging was done using a 100x oil objective and 12 bit sensi-cam (Imago).

### 2.2.4 Spectrally Resolved Fluorescence Decays

The full-width half maximum of the instrument response function in the case of DL-detector was about 75 ps for the temporal resolution and 30 ($\Delta\lambda/\lambda$) for spectral resolution.

All the measurements were performed at 27°C, using a 60x oil objective (1.25NA, Olympus), 450DCLP (Omega filters, Vermont, USA) and LP460 nm (Omega filters, Vermont, USA).

### 2.2.5 Spatially Resolved Fluorescence Decays

All measurements were done at 27°C, using a 100x oil objective (Olympus, Hamburg, Germany) with 1.3 NA to obtain a uniform illumination area of 80 μm diameter. 450DCLP and one of these filters: D480/30, BP530 − 550 nm (Omega filters, Vermont, USA) was used for imaging.

### 2.2.6 Data Analysis

Fluorescence lifetimes were obtained by analysing the fluorescence decays by iterative re-convolution with instrument response function (IRF) in MATLAB (The MathWorks, Natick, MA). The convolution integral was defined as

$$F(t) = \int_{-\infty}^{t} dt' \left\{ B + D(t - t') \right\} I(t')$$

where F is the convoluted decay curve, B is the constant background, D is the decay curve assumed in the analysis and I is the instrument response function. The Marquardt nonlinear least-square algorithm used to reduced goodness-of-fit $\chi^2$ parameter was defined by

$$\chi^2 = \left[ \sum_{k=1}^{n} [I(t_k) - I_c(t_k)]^2 \Big/ I(t_k) \right] \Big/ (N - p)$$

where $I(t_k)$ is the data and $I_c(t_k)$ the fit value at the $k^{th}$ time point, $t_k$. N is the number of time points and p the number of variable fit parameters. In analysis of the decay curves, an exponential decay model was assumed for all the fluorescent proteins used.

Global analysis ([Knutson et al., 1983](#)) of the spectrally resolved fluorescence decays by linking the lifetimes indicated bi-exponential decay kinetics for CFP. For the calculation of FRET efficiency using spectrally resolved fluorescence data, the lifetime of the donor alone and in the presence of acceptor was obtained from the region 460 – 490 nm.

The decay associated spectra (DAS) i.e relative contribution of different species (characterized by their decay) to emission spectra was calculated using the relationship

$$DAS(\lambda, \tau_i) = \frac{\alpha_i(\lambda)\tau_i}{\sum\limits_{j=1}^{n}\alpha_i(\lambda)\tau_i} ISS(\lambda)$$

where $\alpha_i(\lambda)$ is the relative contribution of the fluorescent species at wavelength $\lambda$, $\tau_i(\lambda)$ is the corresponding fluorescence lifetime and $ISS(\lambda)$ is the steady state intensity at wavelength $\lambda$.

Independent pixel lifetime analysis of the QA images was done and the average lifetime obtained from the analysis was used to construct the pixelated average lifetime image. This reduction of bi-exponential decay to average lifetime corresponds to the situation for intensity measurements. Bi-exponential decay kinetics was necessary to describe the CFP fluorescence kinetics. Mono-exponential decay modelling was sufficient to describe the kinetics of YFP.

The FRET efficiency (E) was calculated according to the relationship:

$$E = 1 - \frac{\langle\tau_{DA}\rangle}{\langle\tau_D\rangle}$$

where $\langle\tau_{DA}\rangle$ and $\langle\tau_D\rangle$ are the mean donor lifetimes in the presence and absence of acceptor.

## 2.3 Photophysical Properties of DASPMI

### 2.3.1 Materials

DASPMI was a chromatographically pure preparation generously provided by the Bayer research laboratory (Leverkusen). All solvents (Glycerol, Chloroform, Methanol, Ethanol and DMSO) used for measurements were purchased from Aldrich. Double distilled millipore water was used for fluorescence measurements. Freshly prepared solutions of DASPMI with a final concentration of 10 μM were used for all delay-line measurements.

### 2.3.2 Steady-State Spectra

Absorption and emission spectra were obtained using Milton Roy (Spectronic 3000 array, Fischer, Germany) spectrophotometer and Carry Eclipse fluorescence spectrophotometer (Varian), respectively. The corrected emission spectra were obtained at the 5 – 10 μM DASPMI concentration at 298 K. Temperature dependent emission spectra were obtained by using a temperature controlled ancillary water bath.

Emission wavelength dependent anisotropy spectrum was measured using an L-format Jobin Yvon SPEX fluorimeter (FLUOLOG 3; France). Anisotropy was calculated using the formula

$$\langle r \rangle = \frac{I_{VV} - G * I_{VH}}{I_{VV} + 2G * I_{VH}}$$

where G is the grating factor that has been included to correct for the wavelength response to polarization of the emission optics and detector. $I_{VV}$ and $I_{VH}$ are the emission intensities measured parallel and perpendicular to the vertically polarized excitation, respectively.

**2.3.3 Spectrally Resolved Fluorescence Decays**

The full-width half maximum of the instrument response function in the case of DL-detector was about 35 ps for the temporal resolution and 30 ($\Delta\lambda/\lambda$) for spectral resolution. All the measurements were performed with a 20x or 60x oil objective (1.25 NA, Olympus), 450DCLP (Omega filters, Vermont, USA) and LP460 nm (Omega filters, Vermont, USA). Samples were placed on a coverslide with a microwell and measured at room temperature. Ethanol and ethanol/glycerol mixtures were filled in an air tight micro-capillary for the lifetime measurements.

**2.3.4 Data Analysis**

Fluorescence lifetimes were obtained by analysing the fluorescence decays by iterative re-convolution with instrument response function (IRF) in MATLAB (The MathWorks, Natick, MA). The convolution integral was defined as

$$F(t) = \int\limits_{-\infty}^{t} dt' \left\{ B + D(t - t') \right\} I(t')$$

where F is convoluted decay curve, B is the constant background, D is the decay curve assumed in the analysis and I the instrument response function. The reduced goodness-of-fit, $\chi^2$, parameter was defined as

$$\chi^2 = \left[ \sum_{k=1}^{n} [I(t_k) - I_c(t_k)]^2 \Big/ I(t_k) \right] \Big/ (N - p)$$

where $I(t_k)$ is the data and $I_c(t_k)$ the fit value at the $k^{th}$ time point, $t_k$. N is the number of time points and p the number of variable fit parameters. In analysis of the decay curves, an exponential decay model was assumed for all the solvents used.

The decay associated spectra (DAS) i.e. relative contribution of different species to emission spectra was calculated using the relationship

$$DAS(\lambda, \tau_i) = \frac{\alpha_i(\lambda)\tau_i}{\sum\limits_{j=1}^{n} \alpha_i(\lambda)\tau_i} ISS(\lambda)$$

where $\alpha_i(\lambda)$ is the relative contribution of the fluorescent species at wavelength $\lambda$, $\tau_i(\lambda)$ is the corresponding fluorescence lifetime and $ISS(\lambda)$ is the steady state intensity at wavelength $\lambda$.

Time-resolved emission spectra were fitted to log-normal function as described by Maroncelli and Fleming (1987). Briefly, the emission intensity at a time t and given wavelength $\lambda$ was reconstructed from the fitted decay parameters using the equation:

$$I(\lambda;t) = \frac{I^{ss}(\lambda)}{\tau_{avg}(\lambda)} \sum\limits_{i=1}^{n} \alpha_i(\lambda)\exp(-t/\tau_i)$$

where $I^{ss}$ is the intensity of steady state spectrum, $\tau_{avg}$ is the average lifetime, $\tau_i$ is the wavelength independent lifetime and $\alpha_i$ represents the wavelength-dependent contributions of the lifetime. The time-resolved emission spectra were fitted to log-normal function (Siano et al., 1969) of the form

$$\varepsilon(v) = \frac{\varepsilon_0 b}{v_{max} - a} \exp(-c^2)\exp\left\{\frac{-1}{2c^2}\left[\ln\left(\frac{v-a}{b}\right)\right]^2\right\}$$

$v > a$ and $\varepsilon(v) = 0$ for $v \leq a$

where $v$ is wavenumber in cm$^{-1}$, $\varepsilon_0$ is the amplitude and $v_{max}$ is the peak frequency. The parameters a, b and c can be evaluated from asymmetry parameter $\rho$, full-width at half maxima H and the wavenumber of the maximum $v_{max}$ by the following relations:

$$a = v_{max} - H\left[\frac{\rho}{\rho^2 - 1}\right]; \quad b = H\left[\frac{\rho}{\rho^2 - 1}\right]\exp(c^2); \quad c = \frac{\ln \rho}{(2\ln 2)^{1/2}}$$

## 2.4 Fluorescence Dynamics of DASPMI in Living Cell

### 2.4.1 Chemicals

DASPMI was a chromatographically pure preparation generously provided by the Bayer research laboratory (Leverkusen). Nigericin, oligomycin, carbonyl cyanide m-chlorophenylhydrazone (CCCP) and valinomycin were purchased from Sigma-Aldrich Chemie Gmbh, Steinheim, Germany. Potassium cyanide (KCN) was purchased from Merck, Darmstadt, Germany. ATP was purchased from Serva Electrophoresis GmbH, Heidelberg, Germany. Saponin, glutamate and malate were purchased from Sigma-Aldrich chemie Gmbh, Steinheim, Germany.

### 2.4.2 Cell Culture and DASPMI Staining

XTH-2 cells , an endothelial cell line derived from Xenopus laevis tadpole hearts (Schlage et al., 1981) were grown in Dulbecco's modified minimal essential medium (Gibco, Cergy-Pontoise, France), supplemented with 5 % fetal calf serum. Cells seeded on 24 mm diameter cover glasses at preconfluent density were used for experiments after 48 hours of trypsinisation. These cells were then incubated with 3 µM DASPMI (diluted from aqueous stock solution) for 40 minutes at 28 $^{\circ}$C. For observations under microscope, the coverslips were mounted onto a custom made chamber and rinsed with HBSS (Hank's balanced salt solution with 20 % water in excess to adjust tonicity to values adequate for amphibian tissues), to remove the extra cellular DASPMI. For lifetime experiments, cells were kept under HBSS to avoid background fluorescence. XTH2 cells kept at room temperature (approx. 25°C) during the experimentation time remained very flat and allowed the observation of single mitochondria.

For permeabilization, cells were incubated for 15 minutes with 0.01 % saponin and 0.5 mM ATP in culture medium (Jacob et al., 1991; Saks et al., 1998). Cells rinsed with culture medium were then incubated with DASPMI alone or containing substrates (malate and glutamate).

For uptake measurements, cells under the microscope were given 3 µmol/L DASPMI and imaged every 30 seconds.

### 2.4.3 Steady-State Imaging

Steady-state fluorescence images were obtained using an IX70 (Olympus, Hamburg, Germany) inverted fluorescence microscope. Mercury arc lamp (50 W) was used for excitation, in combination with FT510 dichroic mirror, 450 – 490  nm band pass excitation filter and 570DF20  filter, 560DF40, BP515-565 nm, BA590 and BP530 – 550 nm emission filters (Omega opticals, VT, USA). Imaging was done using a 100x oil objective and 12 bit Sensi-Cam (Imago, Till Photonics, Herrsching, Germany). Neutral density filters were used to image at low light level, for avoiding photobleaching effects.

Emission fingerprinting was done using laser scanning microscopy (Zesis LSM 510 Meta). DASPMI-stained XTH2 cells kept in diluted HBSS solution were excited at 450 nm and the emission was measured in the range of 500 – 670 nm.

Anisotropy measurements were done using a dual-View Micro-Imager™ with a polarization/anisotropy filter cube (MSMI-DV-FC, Optical Insights, USA) mounted in front of the 12 bit Sensi-Cam. Polarisation of the excitation light from the mercury arc lamp was controlled by introducing appropriate polarization filters (AHF Analysentechnik AG, Tübingen, Germany). The resulting dual-view images on Sensi-Cam are two spatially identical images of the sample in focus that differ only in their polarization content. The resulting spatially identical vertically and horizontally polarized images were modified using image processing functions in MATLAB (The MathWorks,

Natick, MA) environment to achieve precisely aligned images. Anisotropy was then calculated using the formula

$$\langle r \rangle = \frac{I_{VV} - G * I_{VH}}{I_{VV} + 2G * I_{VH}}$$

where G is the grating factor that has been included to correct for the wavelength response to polarization of the emission optics and detector. $I_{VV}$ and $I_{VH}$ are the emission intensities measured parallel and perpendicular to the vertically polarized excitation, respectively.

### 2.4.4 Spatially Resolved Fluorescence Decays

All measurements were performed at room temperature (approx. 25 $^{o}$C), using an apochromate 100x oil objective (Olympus, Hamburg, Germany), 1.3 NA to obtain a uniform illumination area of 80 μm diameter. FT510 dichroic and one of these emission filters: 570DF20, BP530 – 550 nm and BA590 (Omega filters, VT, USA) were used for imaging.

Fluorescence lifetimes were obtained by analyzing the fluorescence decays by iterative re-convolution with the instrument response function (IRF) in MATLAB (The MathWorks, Natick, MA). The $\chi^2$ goodness-of-fit parameter was reduced by using Marquardt nonlinear least-square algorithm. The fluorescence decays obtained from different regions of DASPMI stained XTH2 cells were best fitted for a three-exponential fit ([Figure 2.3](#)). The regions of interest in some examples were as small as a single mitochondrium. For calculations, a minimum number of 10000 photon counts were required to achieve a reliable fit of $\chi^2$ in the range of 0.9 – 1.1. The $\chi_R^2$ surfaces were examined to determine the range of parameters consistent with the fluorescence decay. Confidence intervals obtained from the surface support analysis were in the range 10 – 150 ps for all the data analyzed ([Figure 2.4](#)). Mean lifetime proportional to steady-state intensity was calculated as $\langle \tau \rangle = \sum a_i \tau_i$, where $a_i$ is the normalized relative contribution

($\sum a_i = 1$) of the i fluorescent species characterized by its fluorescent lifetime $\tau_i$. The fractional contributions of each decay time to the steady-state intensity were calculated as $f_i = a_i \tau_i \Big/ \sum_j a_j \tau_j$ .
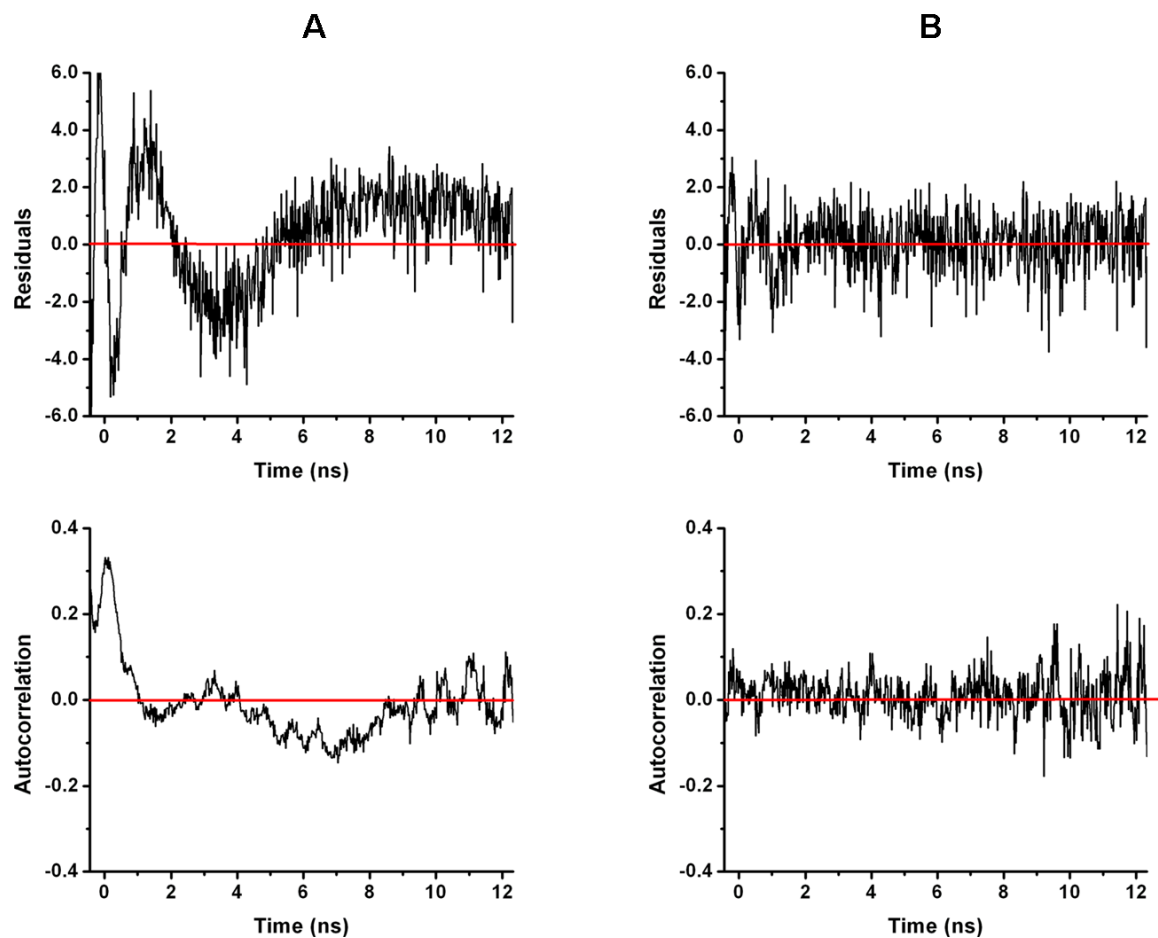


**Figure 2.3** *Residue and autocorrelation curves of (A) two- and (B) three-component fit of decay obtained from a mitochondrial region of interest.* **(A)** *Residuals (top) and autocorrelation (bottom) obtained by a bi-exponential fit showed large deviations from zero.* **(B)** *A four fold decrease in $\chi^2$ value for the three-decay-time model was adequate to reject the bi-exponential decay model. This significant improvement in the quality of fit when fitted with a three-exponential decay model is apparent from the random distribution of residues (top) and autocorrelation (bottom) around zero.*
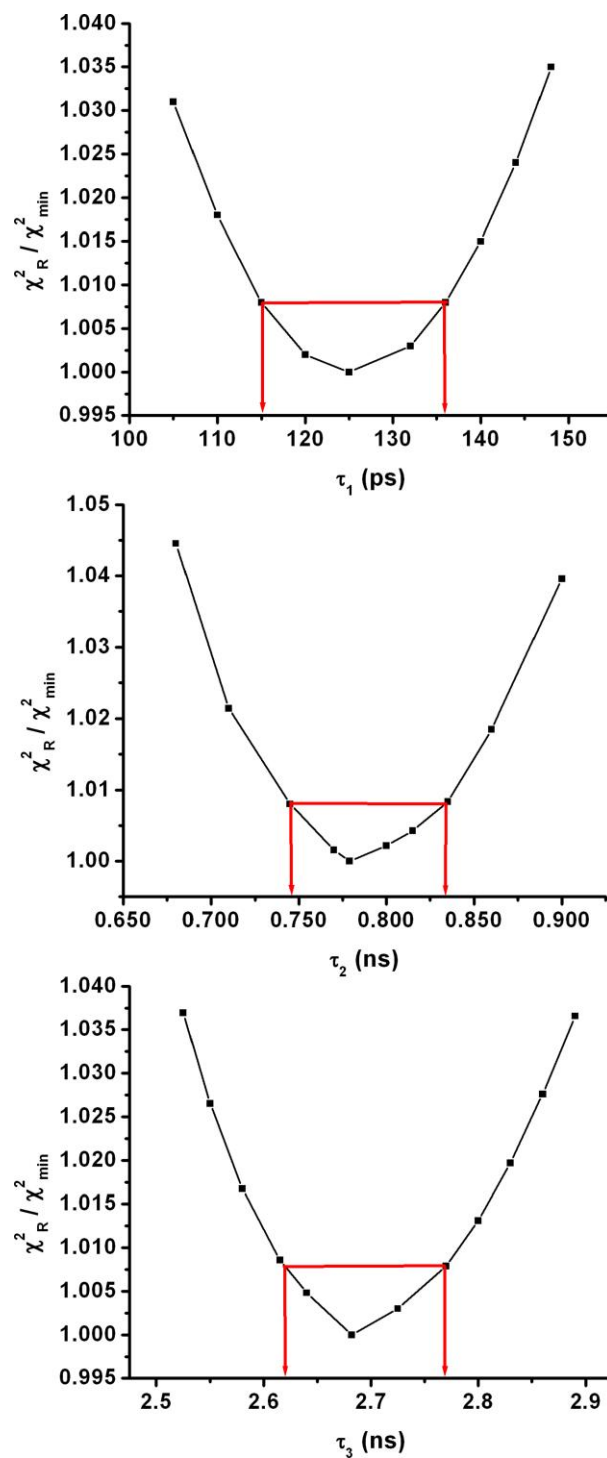
**Figure 2.4** *Representative lifetime* $\chi_R^2$ *surfaces for the various* $\tau_i$ *values obtained from the three-exponential fit of fluorescence from DASPMI stained mitochondria.* *The confidence intervals are shown by the intercepts of the red horizontal line on the* $\chi_R^2$ *surfaces.*

# 3. RESULTS AND DISCUSSIONS

## 3.1 TRPV4-Microfilament Interactions

### 3.1.1 Introduction

Investigation of protein-protein interactions in living cells is essential to understand the underlying signal cascade mechanisms in their natural environment. Many interactions in living cells are made probable by the creation of specific environment like complex organisation and compartmentalisation for the molecules to interact. Using fluorescence microscopy, the sub-cellular localisation and the distribution of proteins could be easily determined. To envisage and study the extent of interaction of proteins in a complex, dynamic and highly dense environment like in a living cell; a non-invasive approach with high spatial sensitivity in the range of few nanometers is necessary.

Förster resonance energy transfer (FRET) is a non-radiative phenomenon between two fluorochromes requiring the emission spectra of the donor molecule overlapping with the absorption spectrum of the acceptor molecule. This energy transfer due to long-range dipole-dipole interactions (Förster et al., 1948) occurs only when the interacting molecules are in the distance of 10 − 100 Angstroms. Hence FRET can be used as a spectroscopic ruler to study the interactions of proteins in living cells (Selvin et al., 2000). Proteins fused with green fluorescent protein and its variants make the study of protein-protein interactions in living cells possible (Elangovan et al., 2002; Wouters et al., 2001; Pepperkok et al., 1999; Stubbs et al., 2005).

However, resonance energy transfer measurements based on steady-state fluorescence signal change and acceptor photobleaching are not sufficient proof to confirm the interactions, especially, when the photophysics of the fluorochrome is not fully understood (Valentin et al., 2005). Fluorescence lifetime imaging based on time- and space-correlated single photon counting is a non-destructive, non-invasive and reliable method to investigate interactions of proteins in living cells (Tony et al., 1999; Tramier et

al., 2002). Fluorescence lifetime imaging microscopy (FLIM; Lakowicz & Berndt, 1991; Lakowicz, 1999; Gadella et al., 1993; Dowling et al., 1998) based experiments are independent of fluorochrome concentration and excitation intensity in contrast to intensity based FRET measurements. Single photon counting methods (O'Connor & Phillips, 1984) have the striking benefits of using low level excitation light and picosecond time resolution to directly investigate the photophysical process involved.

Resonance energy transfers are revealed by a wavelength related shift in the emission spectrum and fluorescence lifetime changes in the donor molecules. Spectrally resolved fluorescence decays offer an insight into the different ground state species of the donor and acceptor molecules and the nature of their interaction. Spatially resolved fluorescence decays over a two-dimensional image of a living cell can be used to elucidate the key mechanisms involved in the regulation of protein interactions in differing environments in the different regions of single living cells. Hence the method of choice is time- and space-correlated fluorescence lifetime imaging including spectral resolution to prove interactions on a molecular basis by Förster resonance energy transfer determinations.

In this study, I investigated the proximity of the membrane protein TRPV4 involved in volume regulation with the actin cytoskeleton, by applying spectrally and spatially resolved fluorescence decay measurements, for the detection of FRET. TRPV4 is a $Ca^{2+}$ permeable non-selective cation channel and is a member of the vanilloid subfamily of transient receptor potential (TRP) channels, which preferentially form homo- oligomeric complexes (Hellwig et al., 2004; Liedtke et al., 2000). TRPV4 has six predicted membrane-spanning subunits with a pore loop (Pedersen et al., 2005). The amino-terminal domains with three ankyrin repeats as well as the C-terminus are located on the cytoplasmic side (Liedtke et al., 2000). Its wide distribution in mammals including heart, brain, lung, kidney and liver indicates its prominent physiological function (O´Neil et al., 2005). The ability for cells to adapt to changed osmotic conditions is essential for cellular homeostasis and disequilibrium could lead to dramatic events like apoptosis and necrosis (Liedtke et al., 2003). Therefore, many cell types are able to counteract to anisotonic environment by processes called regulatory volume decrease (RVD) and regulatory

volume increase (RVI). Recently, a direct participation of TRPV4 in RVD at cellular level and osmosensing in whole organism has been shown (Arniges et al., 2004; Becker et al., 2005; Liedtke & Friedman, 2003; Shen et al., 2001).

The exposure of cells to a hypotonic medium results in activation of TRPV4, as indicated by $Ca^{2+}$ influx (Strotmann et al., 2000). During RVD many cell types show a transient intracellular $Ca^{2+}$ increase, which may be mediated through TRPV4 (Arniges et al., 2004; Becker et al., 2005; Boudreault & Grygorczyk, 2004; O´Connor & Kimelberg, 1993; Light et al., 2003; Okada et al., 2001; Nilius et al., 2004). An intact cytoskeleton, mainly microfilaments have been shown to be required for the mechanosensitive or swelling-induced $Ca^{2+}$-entry in several cell types, suggesting possible interaction of TRPV4 and F-actin (Suzuki et al., 2003).

The sub-cellular localisation of exogenously expressed green fluorescent protein (GFP) fused to TRPV4 and counterstained with TRITC-Phalloidin in different cell lines revealed co-localization of TRPV4 in the cell membrane with the underlying cortical actin cytoskeleton. Whether this co-localization represents molecular interactions in living cells can be assessed by FRET measurements. For this purpose, TRPV4-CFP and actin-YFP plasmids were transfected in vertebrate cells; to evaluate the possible interactions by FLIM. Both, spectrally and spatially resolved fluorescence decays indicated an interaction of these proteins. Apart from the fluorescence lifetime changes of the donor in the presence of acceptor, an additional emission peak appeared at 527 nm. This is a stringent indication of the energy transfer taking place. In addition, spatially resolved fluorescence decays were used to check for the spatial heterogeneity of environment and interaction.

### 3.1.2 TRPV4-Microfilament Spatial Proximity

TRPV4 is a calcium permeable non-selective cation channel and responds to various physical (heat, cell swelling; Vriens et al., 2004) and chemical stimuli (4a-phorbol-12, 13-didecanoate, endocannabinoid anandamide, arachidonic acid; (Vriens et al., 2004;

Watanabe et al., 2003). An intact actin cytoskeleton is necessary for the activation of TRPV4, as many cell types lack hypotonicity-induced intracellular $Ca^{2+}$ increase, after disruption of actin cytoskeleton (Ebner et al., 2005; Pritchard & Guilak, 2004). The mechanism of activation of TRPV4 after hypotonic shock is presumed to occur via mechanical stretching of the plasma membrane or the cortical network. $Ca^{2+}$ ion influx represents an obligatory factor for volume decrease upon hypotonic challenge as can be deduced from experiments in the absence of $Ca^{2+}$ or by inhibiting $Ca^{2+}$ - influx. Cessation of RVD in the presence of reagents interfering with the integrity of microfilaments suggested a possible interaction of TRPV4 with the actin cytoskeleton.

### 3.1.3 Distribution of TRPV4 and F-actin

Subcellular localization of TRPV4 and actin in different cell lines has been investigated using confocal laser scanning microscopy (Figure 3.1A and B). In transiently double transfected HaCaT cells, TRPV4-CFP (Figure 3.1A a), actin-YFP (Figure 3.1A b) and their merged image (Figure 3.1A c) showed a clear co-localization. The cross sections (bottom, right) show that TRPV4 fluorescence almost exclusively is found in the membrane. CHO cells were transiently transfected with TRPV4-GFP and counterstained with TRITC-Phalloidin for detection of F-actin (Figure 3.1B). The images show different xy-planes, at the basal membrane (Figure 3.1B a-c), slightly above the basal membrane (Figure 3.1B d-f) and the apical side of the cells (Figure 3.1B g-i). TRPV4-GFP is localized in the plasma membrane with an accumulation in microspikes (Figure 3.1B d, g) and lamellipodia edges (arrowhead). The latter localization could be related to the evidence that at the leading edge of epithelial cells (Mittal & Bereiter-Hahn, 1985) and of fibroblasts (Wang & Dembo, 2004) is sensitive to inhibition of stretch activated calcium channels while this does not apply to the trailing edge. In microspikes as well as in leading edges F-actin is a predominant compound as shown by TRITC-phalloidin staining (Figure 3.1B f, i). The merged images (Figure 3.1B c, f, i) show a strong co-localization of these proteins (indicated in yellow). In some cases, however, only TRPV4-GFP was observed in membrane structures. Since both proteins colocalize at very specific sites, also functional interaction is likely. To confirm this, fluorescence lifetime imaging studies were performed.
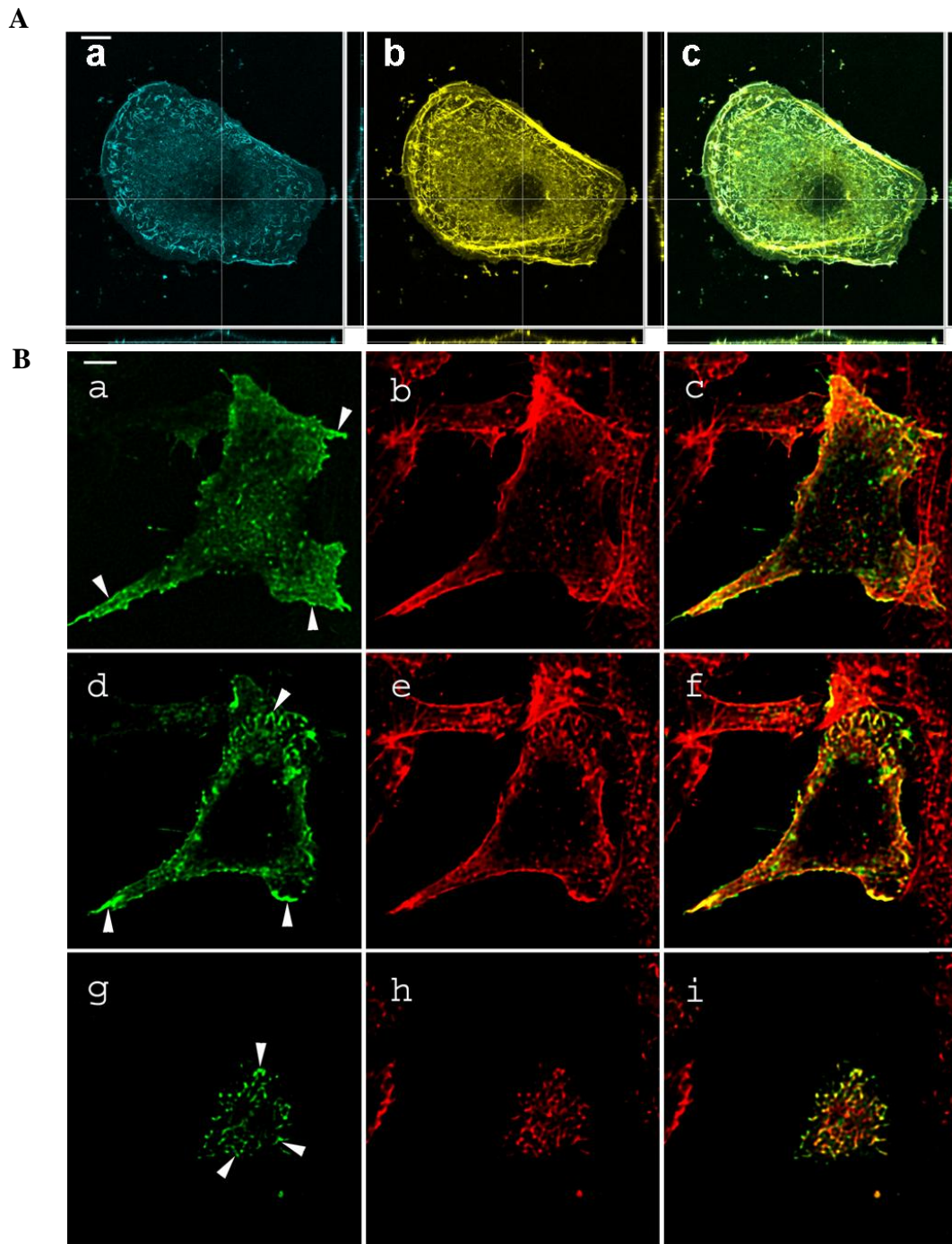
**Figure 3.1** *Co-localization of TRPV4 and F-actin in different cell lines.* **(A)** *HaCaT cells transiently double transfected with TRPV4-CFP (a) and actin-YFP (b) and the merged image (c) showing co-localization.* **(B)** *CHO cells were transiently transfected with TRPV4-GFP (green) and counterstained 72 h after transfection with TRITC-Phalloidin (red). Confocal laser scanning microscopy show xy-planes at different layers of the cell, from the very basal cell region (upper row) to the apical cell region (lower row). (Bar 5 μm)*

### 3.1.4 Investigation of TRPV4-actin Interactions Using FLIM

In HaCaT cells, TRPV4 is expressed constitutively whilst CHO cells are devoid of this channel. Therefore, CHO cells provide a good model cell type to investigate TRPV4 interaction with cellular constituents without interferring with the genuine protein.

CHO transfected cells were cultured on coverslips and 72 hours after transfection they were used for the FLIM studies. During the measurement, cells were kept in Hank´s balanced salt solution (HBSS) to avoid background fluorescence from the culture medium. In many cases, cells double transfected with TRPV4-CFP and actin-YFP displayed an altered morphology in comparison to single transfected cells. Only those cells which still seemed to be intact, i.e. exhibited normal well spread morphology have been used for the experiments.

### a. Proximity of TRPV4-actin Assessed by Spectrally Resolved FLIM

CFP-fluorescence of single transfected living CHO cells was obtained at 440 nm excitation wavelength and LP460 nm filter on the emission side (DL-detector). Emitted photons were counted in correlation to the time and space channels over a period of 10 min. The spectrally resolved fluorescence decays and the emission spectrum were extracted from the two-dimensional histogram (Figure 3.2 b & d). For recording instrument response function (IRF), the intensity of the exciting laser pulses was reduced using grey filters. In some cases, the excitation light was strong enough for considerable photons to accumulate at the channels corresponding to IRF despite the presence of the long pass filter. The slit of the spectrograph and acquisition electronics were adjusted to a wavelength resolution of 1.3 nm per channel. The count rates in all the measurements were up to 2500 photons per second.

Representative images of single transfected (TRPV4-CFP) and double transfected (TRPV4-CFP & actin-YFP) cells are shown in Figure 3.2a and Figure 3.2 c, respectively. The two-dimensional pseudo colour image (Figure 3.2 b) of TRPV4-CFP single
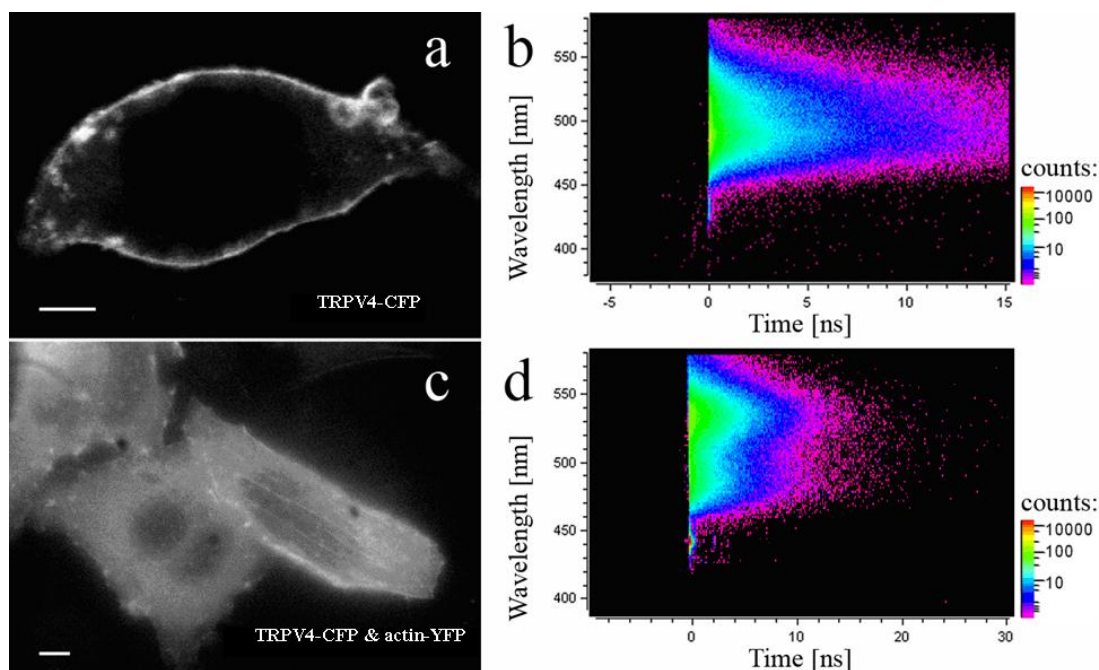
**Figure 3.2** *Spectrally resolved fluorescent decays (b, d) and their representative steady state images (a, c) of living CHO cells after 72 h of transfection. The cells were kept in HBSS solution during imaging.* **(a)** *and* **(c)** *Mercury arc lamp with 450 - 490 nm band pass filter was used for excitation, in combination with filters 480/30nm and BP530 - 550 nm for single (TRPV4-CFP; a) and double (TRPV4-CFP & actin-YFP; c) transfected cells, respectively.* **(b)** *Pseudo colour two–dimensional histogram of single (TRPV4-CFP) transfection.* **(d)** *Pseudo colour two–dimensional histogram of double (TRPV4-CFP& actin-YFP) transfection. Apart from decrease in donor lifetimes (Table 1), there was an increase in fluorescence at 530 nm region (d), indicating FRET and hence the interaction of TRPV4 and actin microfilaments.*

transfected cells encodes emission wavelengths (ordinate), number of counted photons (colour) and time of emission (abscissa) in correlation to the exciting laser pulses. In living cells, an emission peak is found at 476 nm and a bi-exponential fluorescence lifetime analysis (Figure 3.3) in the wavelength region $460 - 490$ nm yielded $\tau_1 = 1.04 \pm 0.29$ ns and $\tau_2 = 3.58 \pm 0.47$ ns. When the TRPV4-CFP and actin-YFP double transfected cells were imaged at 440 nm excitation, an additional peak appeared with a maximum at 527 nm corresponding to YFP fluorescence emission (Figure 3.2 d). The donor lifetimes obtained from the wavelength band $460 - 490$ nm were $\tau_1 = 0.54 \pm 0.06$ ns
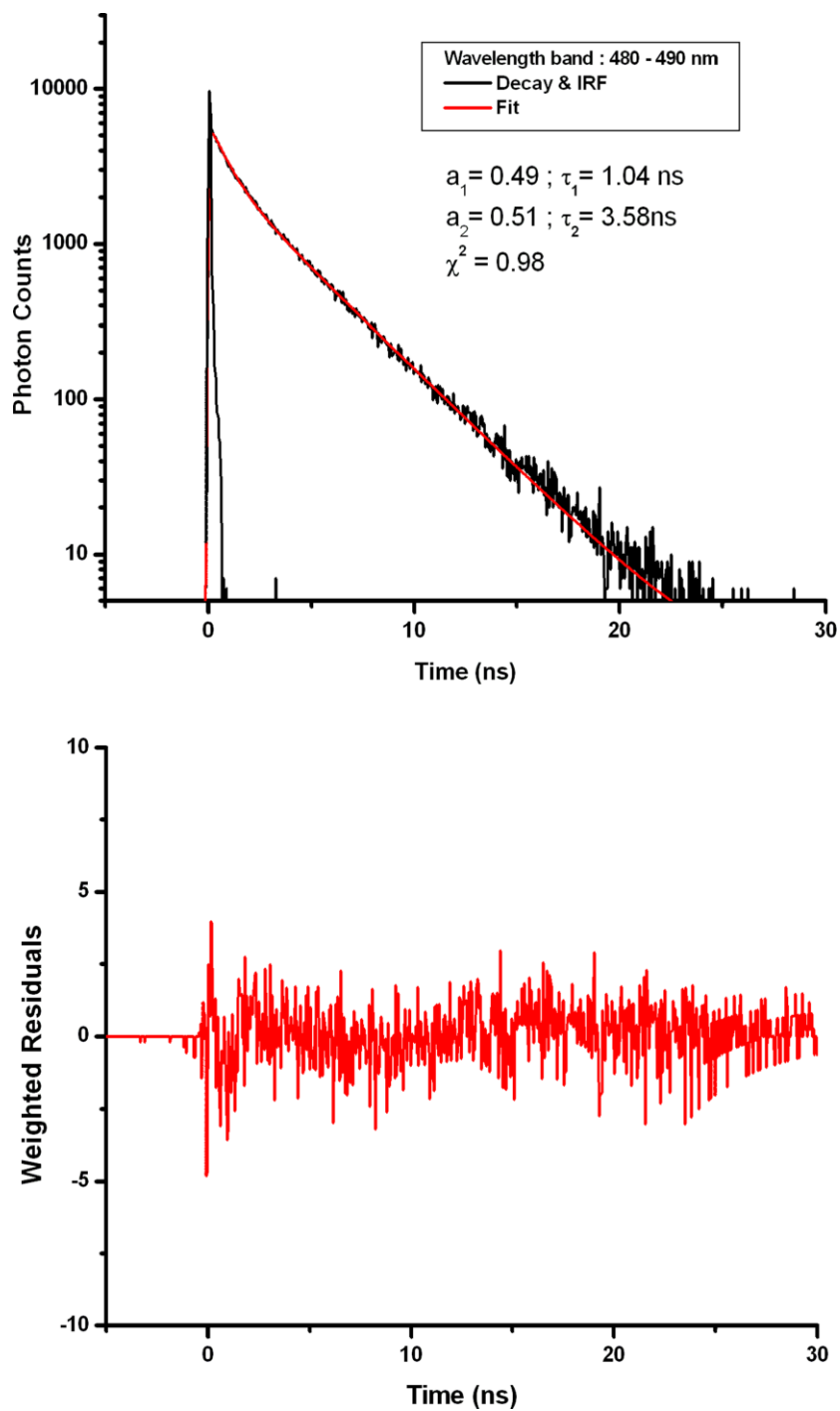
**Figure 3.3** *Bi-exponential fit of fluorescence decay from single transfected TRPV4-CFP (in the wavelength band 480 - 490 nm).*

**Table 3.1 Fluorescence lifetime (DL-detector) calculations performed for the spectral range 460 nm to 490 nm.**

| Proteins | $a_1$ | $\tau_1$ (ns) | $a_2$ | $\tau_2$ (ns) | $<\tau>$ | n |
|---|---|---|---|---|---|---|
| TRPV4-CFP | $0.54 \pm 0.06$ | $1.04 \pm 0.29$ | $0.46 \pm 0.06$ | $3.58 \pm 0.47$ | $2.21 \pm 0.25$ | 9 |
| TRPV4-CFP/actin-YFP | $0.52 \pm 0.03$ | $0.54 \pm 0.06$ | $0.48 \pm 0.03$ | $3.06 \pm 0.09$ | $1.75 \pm 0.11$ | 4 |
| actin-YFP | | | | | $3.02 \pm 0.06$ | 3 |

$a_i$ is the fractional contribution of the i fluorescent species characterized by its fluorescence lifetime $\tau_i$ and n is the number of experiments. The error corresponds to the standard deviation.

and $\tau_2 = 3.06 \pm 0.09$ ns, indicating quenching of the donor fluorescence by energy transfer to the acceptor. The lifetime data from spectrally resolved decays are summarized in Table 3.1. However, in a few cases, fluorescence emission of YFP (<10 % with respect to CFP peak) was found and the donor lifetime in the wavelength band 460 – 490 nm did not change, indicating direct excitation of YFP. The YFP quantum efficiency being 1.5 times higher than CFP quantum efficiency and strong expression levels of actin-YFP in comparison to TRPV4-CFP could explain this discrepancy. To confirm this, living CHO cells that were single transfected with actin-YFP where imaged at 440 nm excitation. They showed a very low count rate ($\leq$ 200 photons per second) and an emission peak appeared at 527 nm corresponding to YFP. There was no significant YFP-actin fluorescence detected in the wavelength region (460 – 490 nm) used for the FRET analysis. The spectra extracted from the spectrally resolved fluorescence decays are presented in Figure 3.4. An energy migration analysis would not provide precise data because of the existence of direct excitation of YFP (< 10 % with respect to CFP peak) and bi-exponential decay kinetics of TRPV4-CFP.

The spectral dependence of lifetime changes were examined by the construction of decay associated spectra (DAS). The DAS were evaluated from the emission spectra obtained from DL-measurements and the lifetimes obtained by the global analysis of fluorescence decays obtained by binning over 8 wavelength channels (corresponding to 10 nm). As the lifetime of YFP and the longer lifetime of CFP are very close, bi-exponential analysis was sufficient to describe the CFP and YFP fluorescence over the entire spectrum. In the
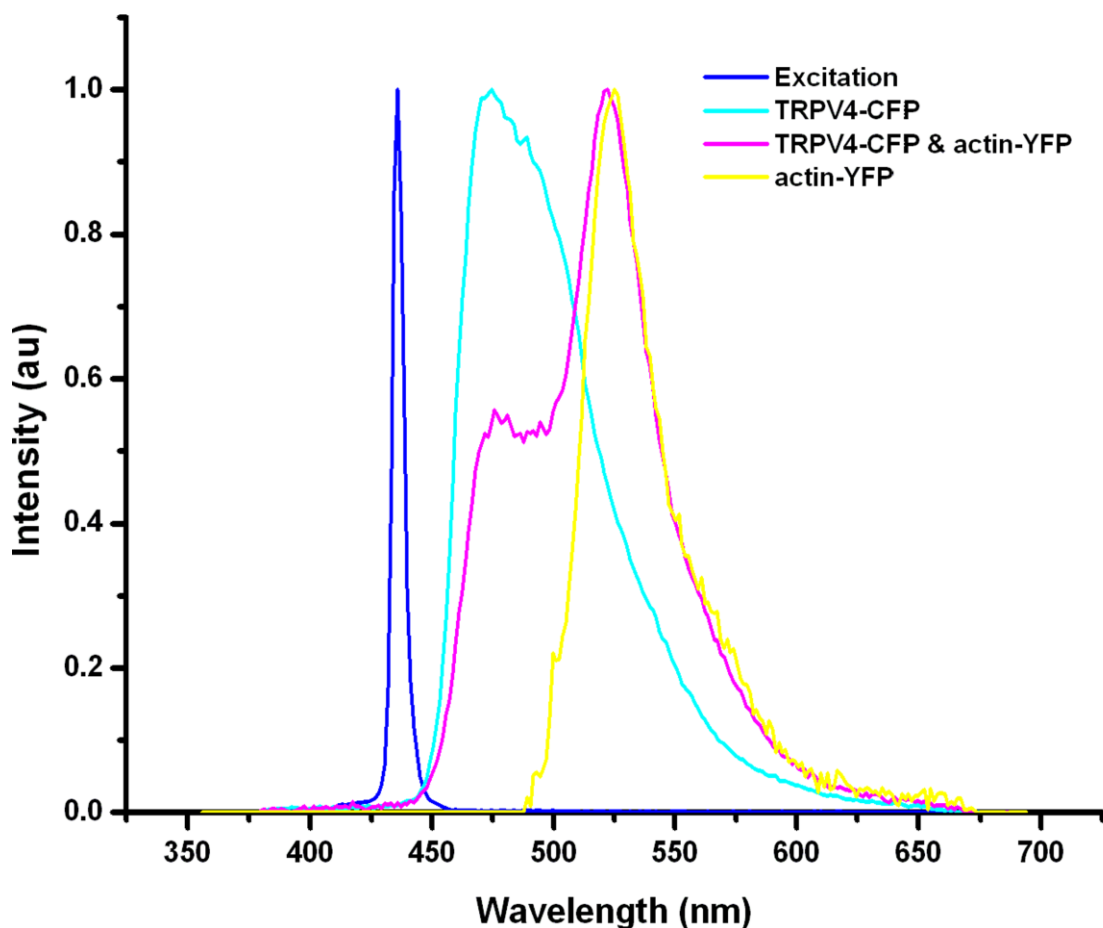
**Figure 3.4** *Normalized excitation and fluorescence emission spectra extracted from two-dimensional histograms (DL-detector) of single and double transfected cells.*

DAS spectra plotted (Figure 3.5), the contribution of the longer lifetime increases with increasing wavelength indicating the contribution of YFP fluorescence.

The mean lifetimes obtained in the region of 460 – 490 nm were used to calculate the apparent FRET efficiency. This procedure compares to intensity based FRET calculations. The apparent FRET efficiency calculated using the mean lifetimes of the donor in the presence ($<\tau> = 1.75$ ns) and in the absence ($<\tau> = 2.21$ ns) of acceptor was 20.8 %, indicating the nanometer scale proximity of TRPV4 and F-actin

.
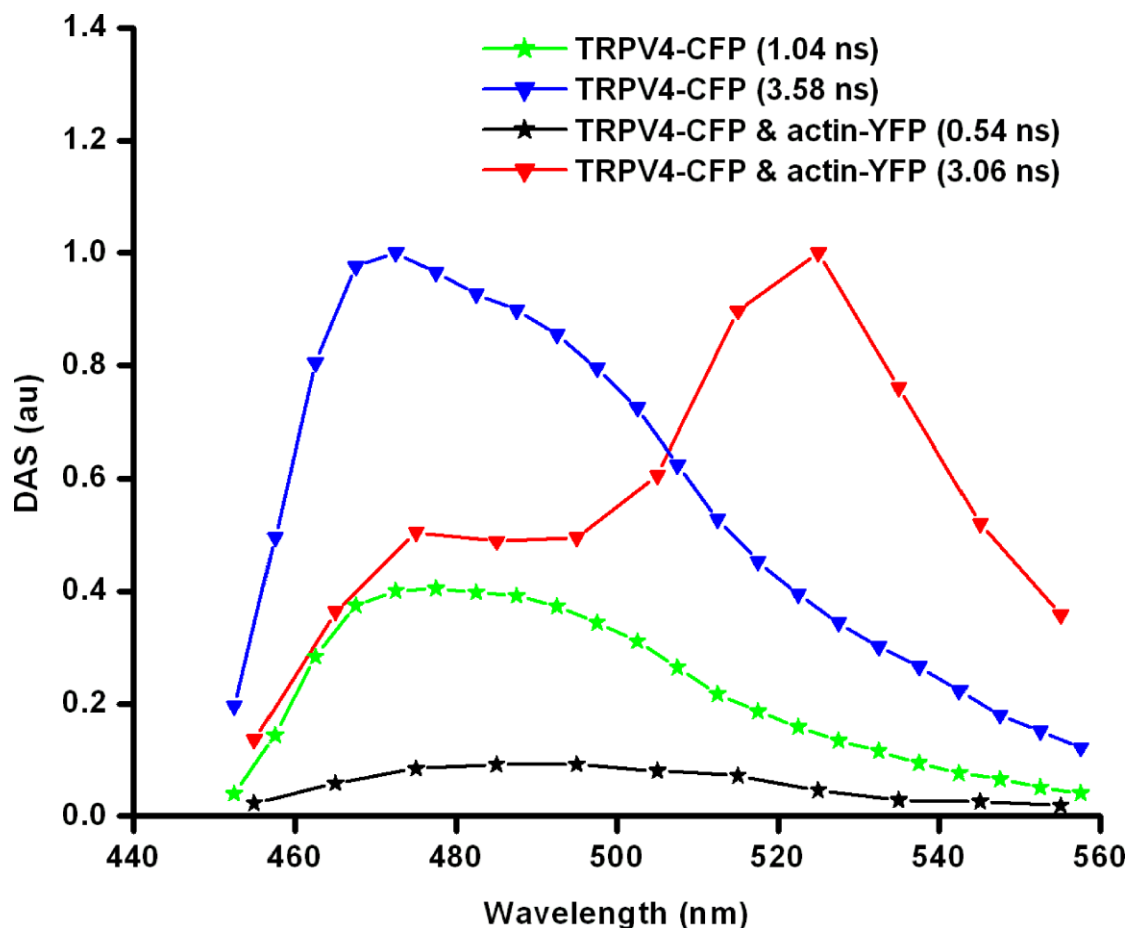
**Figure 3.5** *Decay associated spectra of single transfected (TRPV4-CFP) and double transfected (TRPV4-CFP and actin-YFP) in living CHO cells. There was no distinction made between the longer lifetime of TRPV4-CFP and actin-YFP lifetime. In the presence of YFP the contributions of both the CFP lifetimes decrease, as is a typical indicator for donor behaviour if FRET takes place.*

Spectrally resolved FLIM has the advantage of obtaining the donor and acceptor fluorescence simultaneously and allowing for spectrally resolved energy transfer determination. Decrease in donor lifetime and corresponding increase in acceptor fluorescence are the most reliable indications of FRET. Such an analysis excludes the possibilities of decrease in donor lifetime due to photoconversion (Valentin et al., 2005) or other undesired quenching processes (Grailhe et al., 2006). Although this is the most reliable approach for the study of fluorochrome interactions, spatially resolved FLIM gives a better insight into the subcellular locations favouring these close associations.

### b. Proximity of TRPV4-actin Assessed by Spatially Resolved FLIM

The close spatial arrangement between TRPV4 and F-actin may well depend on their locations within the cell. Therefore fluorescence decay at 440 nm excitation was determined using QA-detector with good spatial resolution (Figure 3.6). The spatially resolved fluorescence decays of the CHO cells were obtained using a band pass filter 480/30 in front of the detector. Photon acquisition occurred over several minutes and the fluorescence decays were obtained by binning the space and time channels to get a $100 \times 100$ pixel three-dimensional matrix. Fluorescence decay was calculated for each pixel containing up to 20,000 photons by fitting linked lifetimes and using the algorithm described above. In some cases, specific regions of interest (ROI) were analysed.

The steady state image, time–integrated image and fluorescence lifetime image of single transfected TRPV4-CFP cells are shown in Figure 3.6. Bi-exponential decay model was necessary for the best-fit of the CFP fluorescence decays with lifetimes 0.98 ns and 3.6 ns ($<\tau> = 2.26 \pm 0.13$ ns; Figure 3.6, Table 3.2). The mean lifetimes of CFP, both in the absence and in the presence of the acceptor YFP were calculated for several ROIs of different cells. Mono-exponential decay analysis with a lifetime of $3.05 \pm 0.05$ ns was sufficient to describe the fluorescence kinetics of actin-YFP single transfected cells

**Table 3.2 Fluorescence lifetimes (QA-detector).**

| Proteins | $a_1$ | $\tau_1$ (ns) | $a_2$ | $\tau_2$ (ns) | $<\tau>$ |
|---|---|---|---|---|---|
| TRPV4-CFP | $0.54 \pm 0.04$ | $0.98 \pm 0.17$ | $0.46 \pm 0.04$ | $3.6 \pm 0.13$ | $2.26 \pm 0.13$ |
| TRPV4-CFP/actin-YFP | $0.56 \pm 0.08$ | $0.77 \pm 0.36$ | $0.44 \pm 0.06$ | $3.29 \pm 0.18$ | $1.85 \pm 0.16$ |
| actin-YFP | | | | | $3.05 \pm 0.05$ |
| TRPV4-CFP& cytosol YFP | $0.56 \pm 0.14$ | $0.85 \pm 0.05$ | $0.44 \pm 0.05$ | $3.74 \pm 0.15$ | $2.12 \pm 0.15$ |

$a_i$ is the fractional contribution of the i fluorescent species characterized by its fluorescence lifetime $\tau_i$. The error corresponds to the standard deviation.
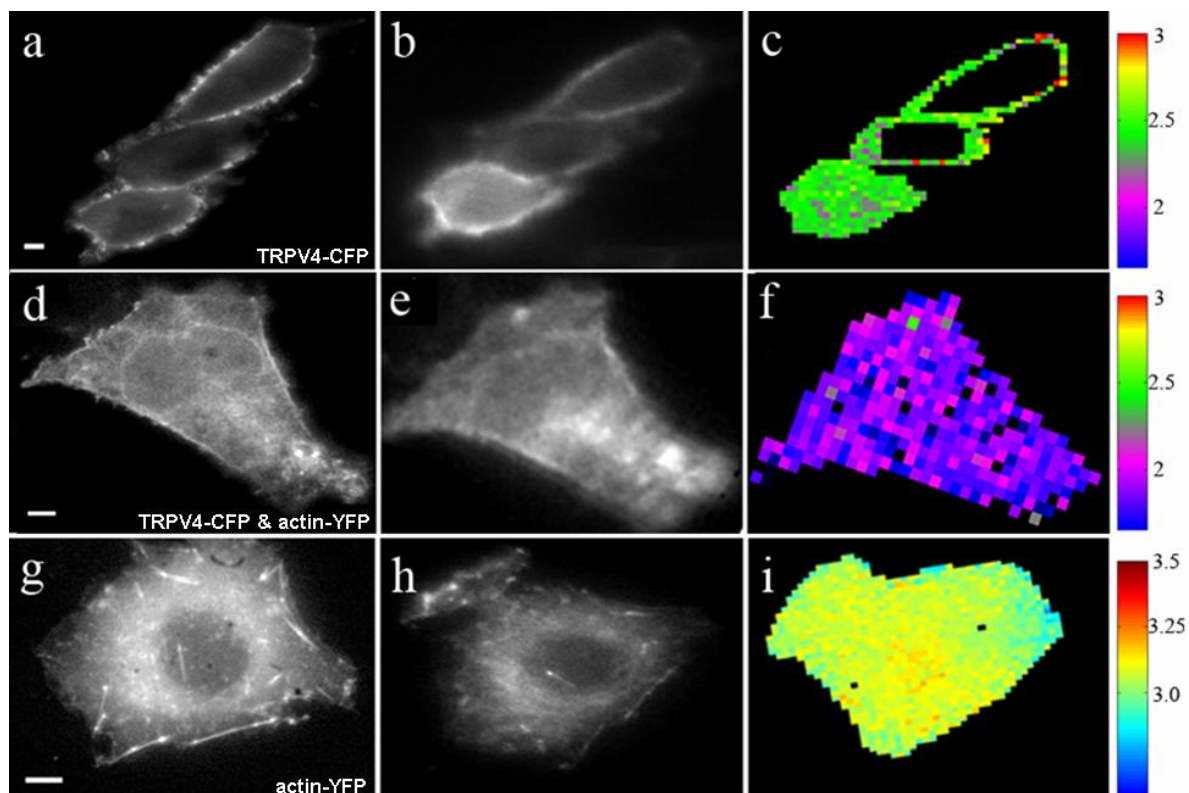
**Figure 3.6** *Fluorescence lifetime analyses of single and double transfected cells. Fluorescence lifetime imaging of living CHO cells (QA-detector) and their pixelated average lifetime distribution (c, f, i). All the steady state images (a, d and g) were acquired using a 50 W mercury arc lamp immediately before being imaged using QA-detector. Images b, e and h (400 × 400 pixel) are time integrated images obtained from QA-detector by exciting at 440 nm using the laser system described above. The slight tilt in the steady state image and QA-image could be observed due to the difference in positioning of CCD camera. Single (a & g) and double transfected (d) cells were kept in HBSS and imaged after 72 h of transfection, using 480/30 nm filter. YFP-actin monotransfected cells (g and h) were acquired using BP530–550 nm filter. The spatial channels of QA-images correlated with time in each pixel were binned to 100 × 100 pixel and fitted using the program described in data analysis section (c, f, i). (Bar 5 μm)*

([Figure 3.6 i]) in different regions of cells. There was no YFP fluorescence detected in YFP actin transfected cells alone, using the CFP fluorescence filter set (480/30 nm) and excitation at 440 nm. In the presence of an interacting partner (actin-YFP), the mean lifetime of CFP was 1.85 ± 0.16 ns. Control experiments performed with TRPV4-CFP and plenty of unbound YFP in the cytoplasm revealed a donor lifetime of 0.85 ± 0.05 ns

and 3.74 ± 0.15 ns ($<\tau>$ = 2.12 ± 0.15 ns). In comparison to FRET measurements, control measurements had more than twice the number of photons in YFP channel for similar counts in CFP channel. This indicates the abundance of YFP-cytosol and likelihood of FRET by chance due to distance and orientation of the fluorophores as minimal. This is in accordance to previous experimental observations (Grailhe et al., 2006). Thus, energy transfer to YFP which is not bound to actin is very low and supports the interpretation that quenching of CFP fluorescence in the presence of actin-YFP was due to FRET by stabilised proximity between the labelled proteins. Considering the mean lifetimes, the energy transfer efficiency was 18.1 %. This is in good agreement with the transfer efficiency obtained from the DL-measurements (20.8 %). The small differences in fluorescence lifetimes and energy transfer efficiency obtained from spatially resolved fluorescence decays and spectrally resolved fluorescence decays can well result from local differences within the cells which are not differentiated by the DL-measurements or may be attributed to different temporal resolution of the acquisition electronics.

## 3.2 Photophysical Properties of DASPMI

### 3.2.1 Introduction

Photophysical properties of ionic styryl dyes are of considerable interest because they respond to changes in trans-membrane potential by a fast, electrochromic mechanism (Loew et al., 1978; Loew et al., 1979; Loew & Simpson, 1981). The chromophore's positive charge is concentrated in the pyridine ring in the ground state and shifts to the amino-naphthalene in the excited state (Loew et al., 1978; Loew et al., 1979). This charge-shift couples with an electric field within a cell membrane, resulting in electrochromism. For example, styryl dye 2-(4-(dimethylamino)styryl)-1-methylpyridinium iodide (DASPMI; Figure 3.7) selectively stains mitochondria in living cells. Fluorescence intensity of DASPMI is a dynamic measure for the membrane potential of mitochondria (Bereiter-Hahn, 1976; Bereiter-Hahn et al., 1983). In living cells, uptake of the dye is strongly influenced by inhibitors of oxidative phosphorylation such as CCCP (carbonylcyanide-m-chlorophenylhydrazone). Other styryl dyes, such as di-4-ANEPPS have been reported to indicate plasma membrane potential strongly (Loew, 1996). While the quantum yield of fluorescence is determined by the polarity of the environment, the dissipation by twisted intramolecular charge transfer (TICT) is determined by the microviscosity of the environment (Strehmel & Rettig, 1996). This simultaneous dependence of styryl dye photophysics on viscosity and polarity has offered several applications in polymer science and in cell biology (Loew et al., 1979; Spooner & Whitten, 1991; Ulmann, 1991; Ephardt & Fromherz, 1991).
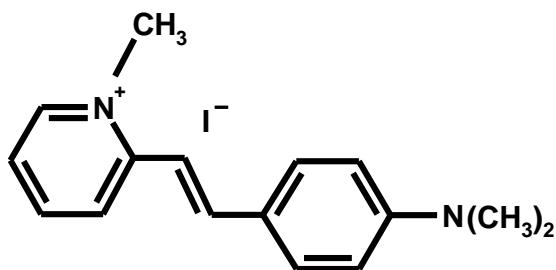


**Figure 3.7** *Structure of o-DASPMI.*

While the changes in intensity and shifts in emission spectrum of styryl dyes are evident from stationary fluorescence experiments, an ambiguity exists in the interpretation of these changes whether based on polarity or viscosity influences. This can be elucidated by taking into consideration the complex emission behaviour of these dyes. Previous experimental and theoretical approaches have independently used the model of TICT and solvent relaxation to explain the fluorescence dynamics of DASPMI. The twists of olefinic double bond and its neighbouring single bonds had been attributed to the multiple nature of DASPMI fluorescence (Strehmel et al., 1997). Solvation dynamic studies in polar solvents indicated a bimodal solvent response function with an ultrafast initial decay component attributed to inertial free streaming motions of the solvent molecules (Jonkman et al., 1996). Other photophysical mechanisms like trans-cis isomerization and excimer formation have been shown to be unlikely.

In this work, an advanced spectroscopic technique based on time- and space-correlated single photon counting (Kemnitz et al., 1995; Ramadass et al., 2007; O'Connor & Phillips, 1984) was used for simultaneous acquisition of wavelength dependent picosecond fluorescent decays at room temperature. Global analysis (Knutson et al., 1983) as a function of wavelength was performed to obtain the decay parameters. Decay associated spectra showed negative values in the red part of the emission spectrum signifying the generation of fluorescent species from the locally excited state. The examination of time-resolved fluorescence spectra was in favour of a three-state model of a generalised kinetic scheme explaining the excited state photophysics and dynamics of DASPMI.

### 3.2.2 Steady-State Spectra

Absorption and emission spectra of DASPMI were measured in various solutions (Figure 3.8). Excitation maxima of DASPMI varied from 487 nm (Chloroform; dielectric constant $\varepsilon = 4.8$) to 435 nm (water, $\varepsilon = 78.39$) in the visible region. This polarity dependent solvent-induced shift can be interpreted as the change in the relative contributions of resonance hybrids i.e. benzenoid and the quinoid forms (Tsukada et al.,

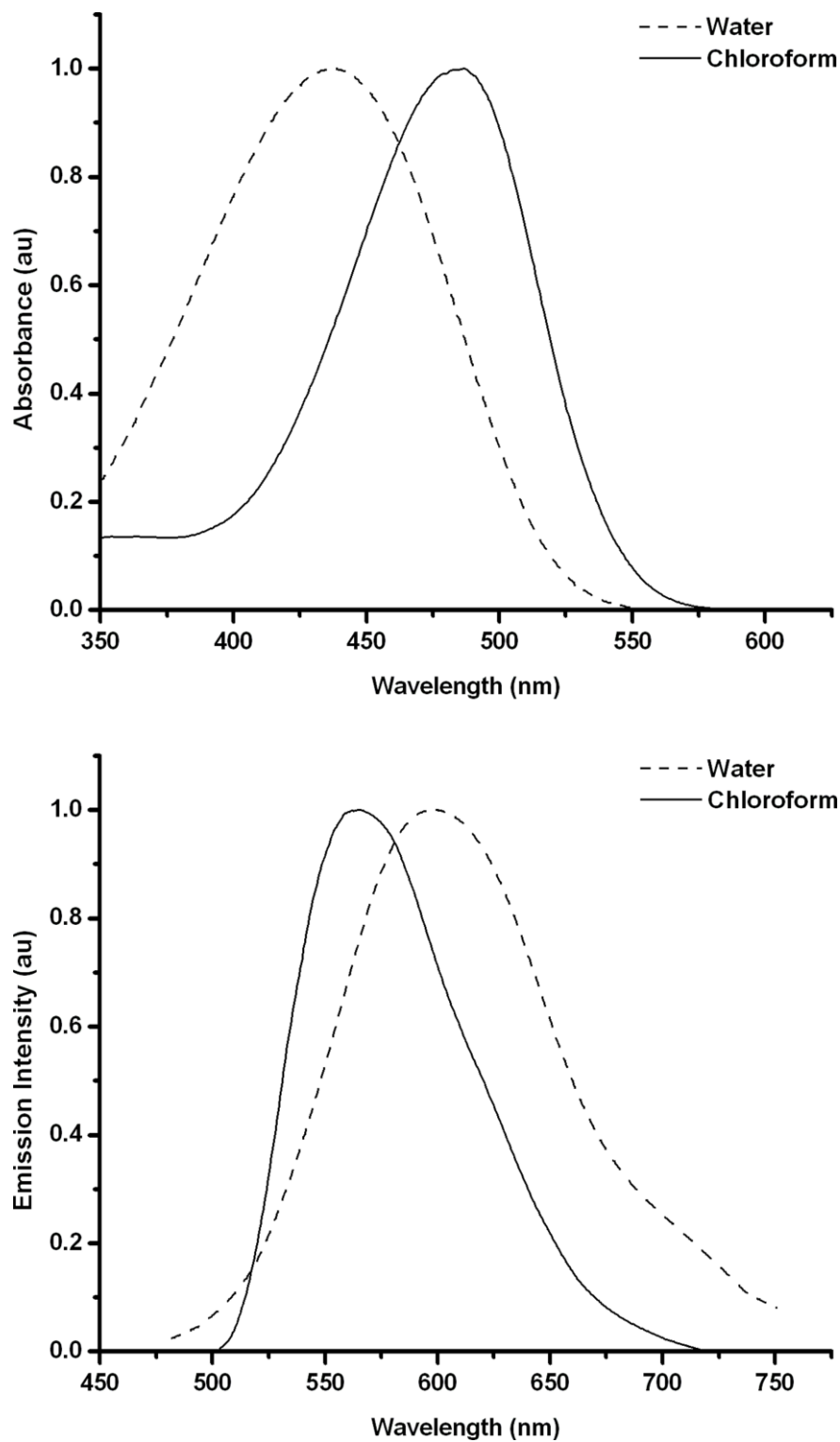**Figure 3.8** *Absorption and emission Spectra of DASPMI (10 μmol/L) in water and chloroform.*

1989). The polar nature of benzenoid form due to more localised $\pi$ - electrons make it more favourable in polar solvents and a consequent blue shift in the absorption spectrum. Apart from absorption in the visible spectrum, the protonated form of DASPMI absorbs in the near ultraviolet region as well (Bereiter-Hahn et al., 1983; Shibasaki & Itoh, 1991).

DASPMI shows appreciable Stokes shift as illustrated in the absorption and emission maxima in water to be 435 nm and 600 nm, respectively. After photoabsorption, rotational and translational motion of the solvent molecules leads to the dynamic relaxation and consequently red shift in the emission spectrum (Jonkman et al., 1996). This shift can be further enhanced by the solvent relaxation resulting in the formation of an excited state due to intramolecular twist. Additionally, the blue shift in absorption maxima and decrease in quantum yield in polar solvents like water implies the dissipation of energy by the formation of charge transfer state. Dual fluorescence, as has been observed for other TICT systems, was not observed for DASPMI, indicating effective non-radiative de-excitation for this state.

### 3.2.3 Emission Anisotropy

Emission anisotropy as a function of wavelength was measured in various solvents (Figure 3.9), to determine the torsional motions about the flexible bonds. A very high anisotropy in the initial part of the emission spectrum was found in all the solvents measured. This indicates that the molecule does not change its transition dipole moment and hence molecular configuration during the emission from initially excited state. In chloroform and the viscous solvent glycerol there was a very slight decrease of anisotropy with increasing wavelength; from an average value of 0.39 to 0.37. While in ethanol, a considerable decrease of anisotropy (from an average value of 0.34 to 0.2) with increasing emission wavelength could be observed. Addition of 40 % glycerol by volume to ethanol increased its anisotropy at the red edge to 0.29, with blue emission anisotropy (490 nm – 520 nm) remaining constant. The observed results indicate the gradual change in molecular configuration and hence transition dipole moment from the initially excited Franck-Condon level. This scenario could be imagined by the later formation of a charge transfer state, with the onset of torsional motions about the single bonds neighbouring the
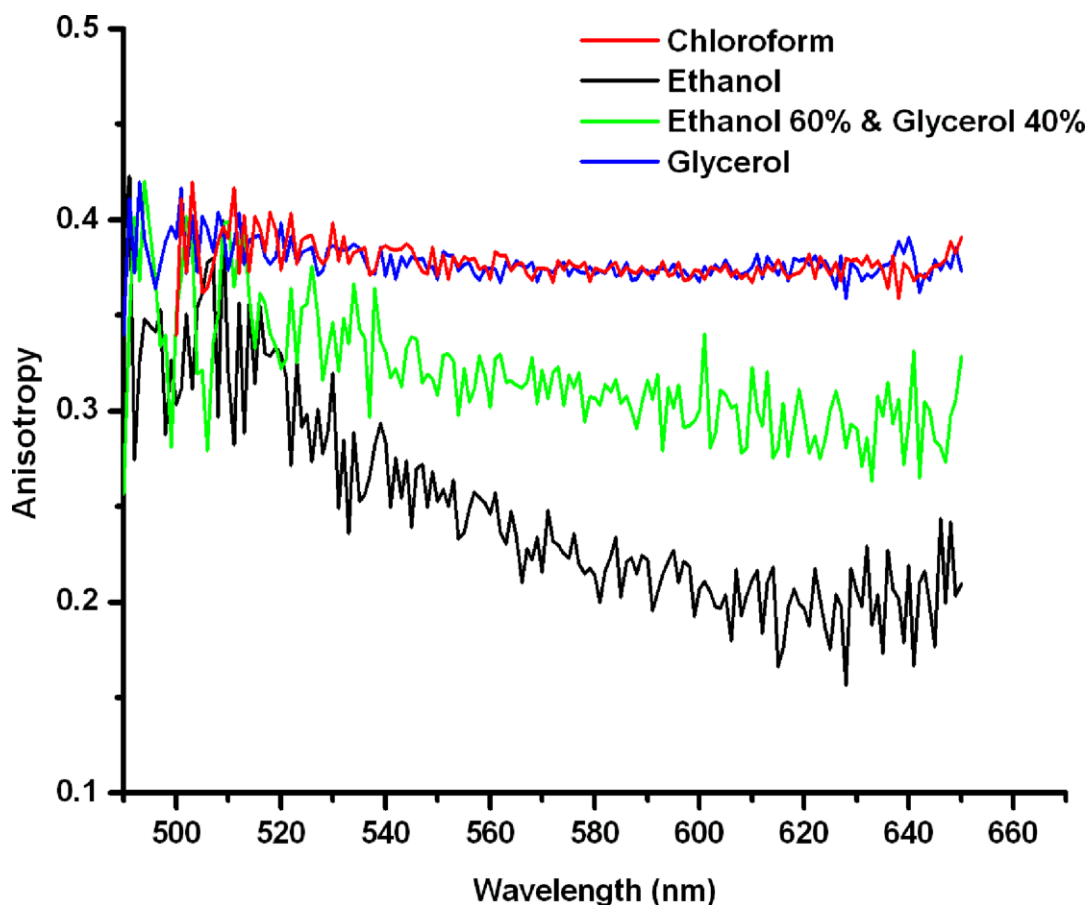
**Figure 3.9** *Steady-state emission anisotropy of DASPMI as a function of wavelength in various solvents.*

olefinic double bond. Similar anisotropy behaviour in chloroform and the highly viscous solvent glycerol could be explained by the restricted flexibility of single bonds either due to the presence of quinoid form or to the viscosity of the solvent, respectively.

### 3.2.4 Spectrally Resolved Fluorescence Lifetime Imaging

Spectrally resolved fluorescence decays of DASPMI were obtained in solvents of different polarity over a period of 5 minutes. The slit of the spectrograph was adjusted to yield a count rate of up to 2000 photons per second and a spectral resolution of ~ 2 nm per channel. The instrument response function (IRF) had a full width at half maxima (FWHM) of ~ 35 ps. Wavelength resolved fluorescence decays of DASPMI in ethanol
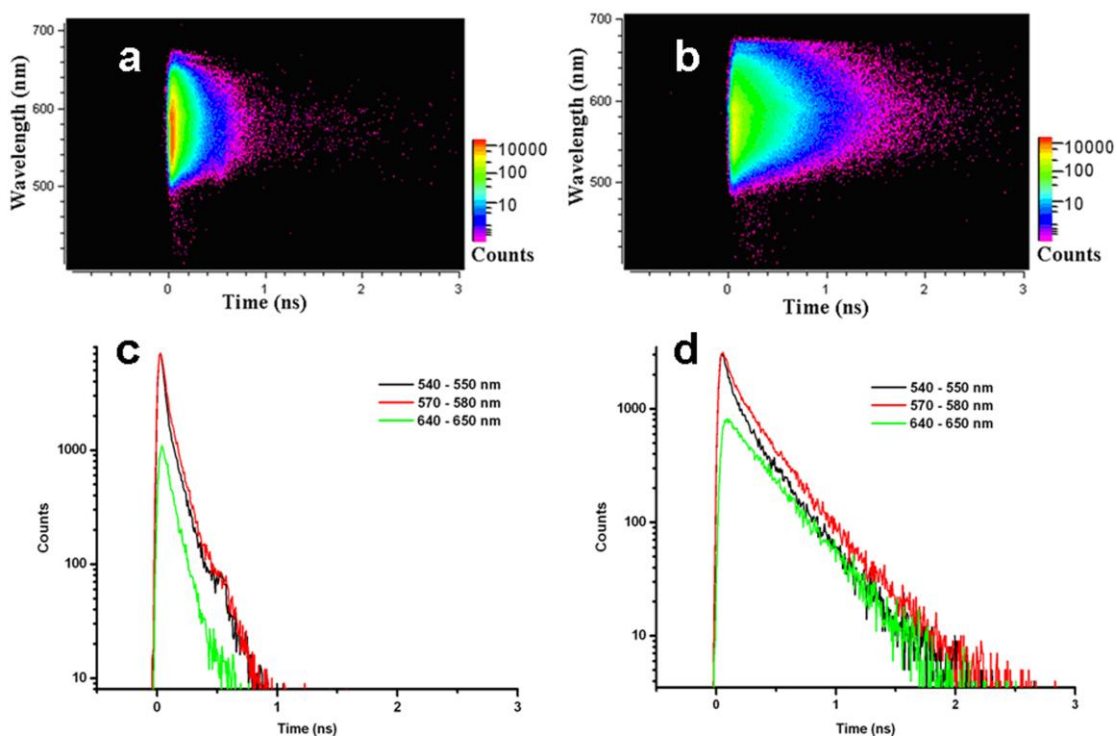
**Figure 3.10** *Spectrally resolved fluorescence decays of DASPMI in ethanol and glycerol (a & b, respectively) and their corresponding fluorescence decays at different emission wavelength bands (c & d, respectively).*

**Table 3.3 Results of the global analysis of Figure 3.10 c and d as a function of emission wavelength.** Best fit numerical values of the time constants and in parenthesis, their normalized relative contribution to decay.

| Solvent | $\lambda_{emission}$ (nm) | $\tau_1$ (ps) | $\tau_2$ (ps) | $\tau_3$ (ps) |
|---------|---------|---------|---------|---------|
| Ethanol | 540-550 | 4 (0.88) | 62 (0.12) | - |
|  | 570-580 | 4 (0.78) | 62 (0.22) | - |
|  | 640-650 | 4 (0.28) | 62 (0.72) | - |
|  |  |  |  |  |
| Glycerol | 540-550 | 23 (0.67) | 104 (0.22) | 309 (0.11) |
|  | 570-580 | 23 (0.53) | 104 (0.28) | 309 (0.19) |
|  | 640-650 | 23 (-0.32) | 104 (0.39) | 309 (0.61) |
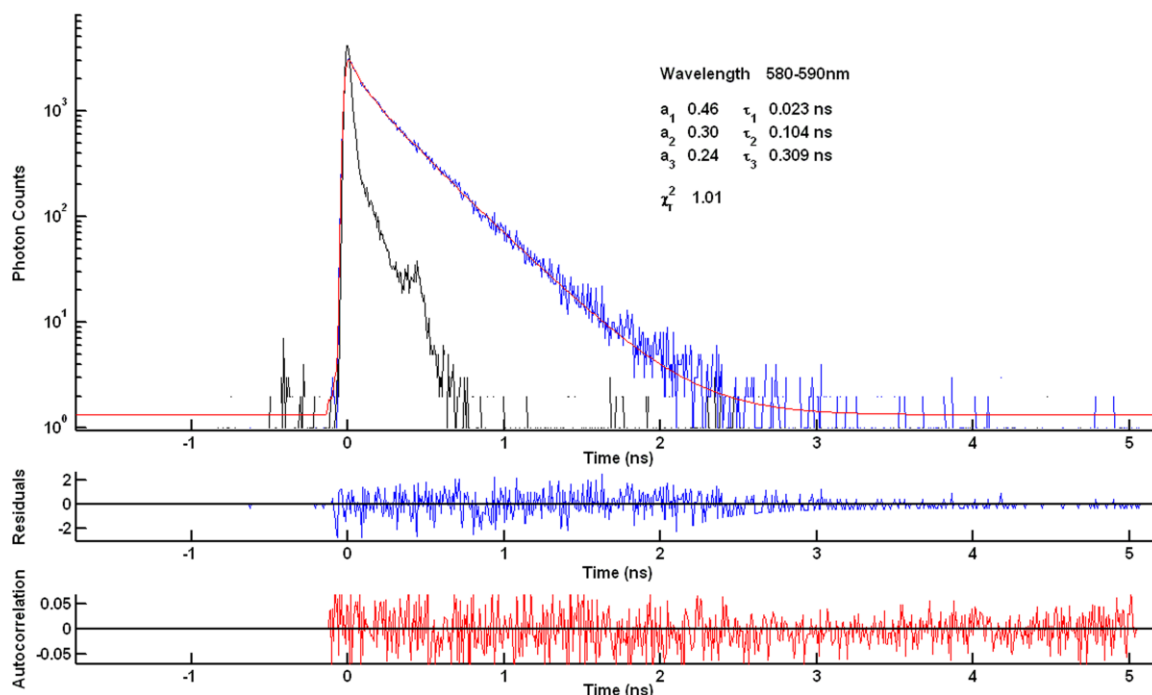
**Figure 3.11** *Three exponential fit of DASPMI in glycerol with corresponding residuals and autocorrelation curve.*

and glycerol at room temperature are shown in Figure 3.10. The two-dimensional pseudo-colour images (Figure 3.10 a, b) represent wavelength on y-axis and time on x-axis. Fluorescence decays extracted from different wavelength bands (~10 nm) clearly show the domination of longer lifetime components with red shift (Figure 3.10 c, d and Table 3.3). This signifies the multiple photophysical mechanisms of DASPMI. In the highly polar solvent water, mono-exponential fluorescence decay with lifetime in the low-picosecond region (6 ps) was found. Quenching due to high solvent polarity and effective non-radiative decay due to low solvent viscosity might be attributed to this extremely short lifetime. Bi-exponential decay kinetics was necessary to globally describe the fluorescence decays in all other medium polar solvents measured. Only in glycerol three-exponential decay kinetics was necessary (Figure 3.11). All the lifetimes are summarized in Table 3.4. Optimum description parameters have been deduced from $\chi^2$ values.

**Table 3.4 Decay kinetics of DASPMI in different solvents.**

| Solvent (Dielectric constant ε) | $\tau_1$ (ps) | $\tau_2$ (ps) | $\tau_3$ (ps) |
|---|---|---|---|
| Chloroform (4.8) | 34 | 79 | - |
| Ethanol (24.55) | 4 | 62 | - |
| Glycerol (42.5) | 23 | 104 | 309 |
| Water (78.39) | 6 | - | - |

Upon photo-excitation, the internal charge transfer from the electron donating aniline moiety to the electron accepting methylpyridinium moiety results in the excited ICT state. The new electronic charge distribution sets the relaxation of solvation energy by the reorganization of solvent molecules. This relaxation process is of the order of few tens of picoseconds (Lakowicz, 1983). Further, the molecules can rotate about the pyridyl and aniline ring leading to the near complete charge transfer and formation of TICT state.

The potential barrier for twist about the aniline ring is high and is possible only in solvents of higher polarity at room temperature. Fluorescence up-conversion studies of DASPMI had shown a bi-modal solvent response in various polar solvents (Jonkman et al., 1996). The ultrafast initial component was attributed to the inertial free streaming motion of solvent molecules and the slower component to rotational and translational motion of solvent molecules. It is of interest to note that the short lifetime component of ethanol reported here is in agreement with the values obtained by Jonkman et al. (1996).

The presence of a TICT state had been previously asserted by synthesizing a model compound in which the flexible single bond between the pyridinium and anilino group (Fromherz & Heilemann, 1992) was bridged to obtain a rigid molecule (2-methyl-7-(dimethylamino)-2-azafluorenium) The rigid dye had a higher quantum yield by 50 %. Viscosity dependent studies of glycerol/ethanol mixtures were performed by us to analyse the influence. The intensity of emission maxima was found to increase linearly with higher glycerol concentrations (Figure 3.12 A). Fluorescence decay kinetics of
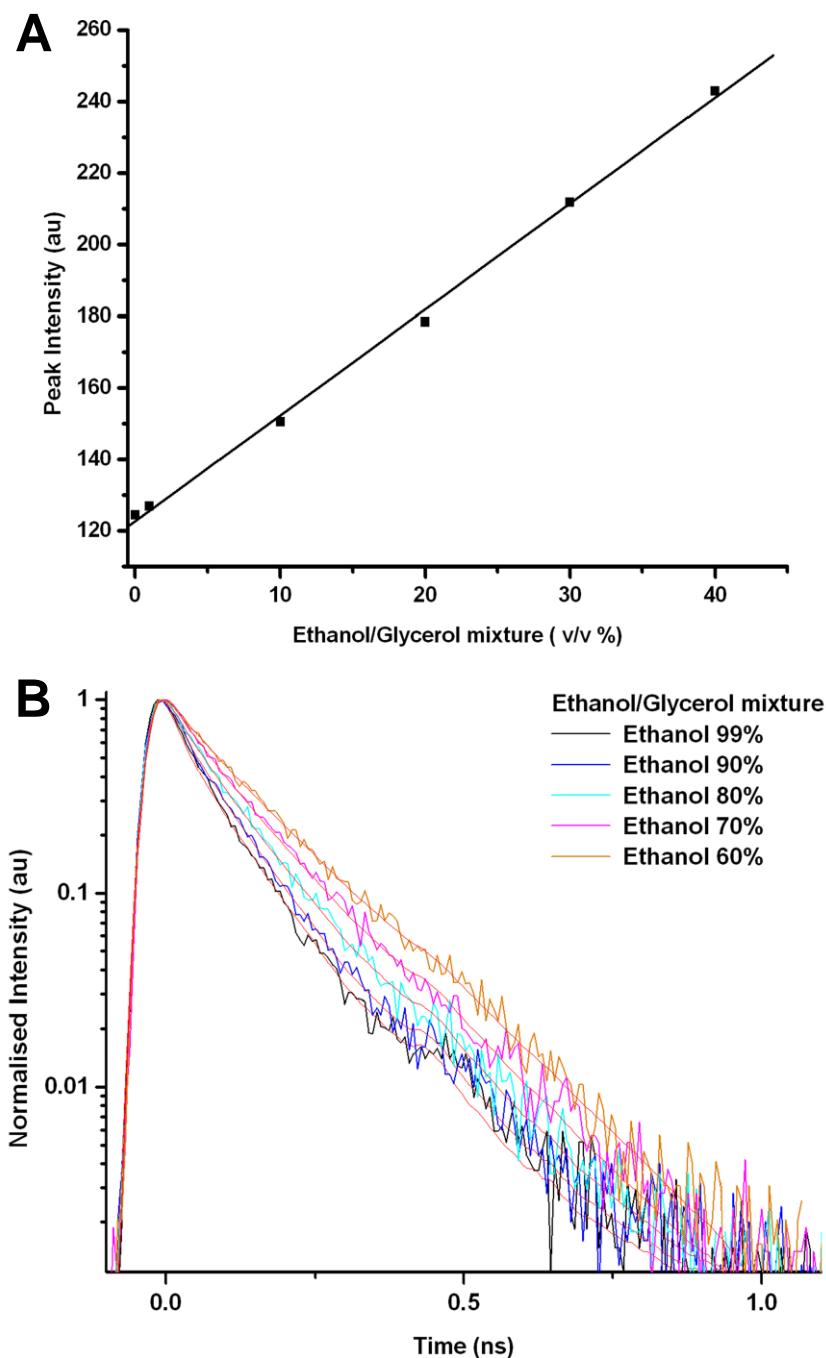
**Figure 3.12** (**A**) *Dependence of the emission maxima intensity of DASPMI in glycerol for various volume ratios of ethanol/glycerol (at constant temperature 298 K).* (**B**) *Normalised fluorescence decay of ethanol/glycerol mixtures.* All fluorescence decays have been fitted with a bi-exponential decay model (shown in red for all the decays). The measurements were done at 465 nm excitation.*

**Table 3.5 Decay kinetics of DASPMI (10 µmol/L) in ethanol/glycerol Mixtures.**

| Ethanol/Glycerol (V/V %) | $\tau_1$ (ps) | $\tau_2$ (ps) | $\tau_3$ (ps) | $<\tau>$ (ps)[a] |
|---|---|---|---|---|
| 0 (pure ethanol) | 4 | 62 | - | 19 |
| 1 | 6.6 | 64 | - | 25 |
| 10 | 8.6 | 71 | - | 32 |
| 20 | 12 | 84 | - | 43 |
| 30 | 14 | 99 | - | 51 |
| 40 | 15 | 114 | - | 62 |
| 100 (pure glycerol) | 23 | 104 | 309 | 144 |

[a] Mean lifetime for the 600 – 605 nm wavelength band was calculated as $<\tau> = \sum a_i \tau_i$, where $a_i$ is the normalized relative contribution ($\sum a_i = 1$) of the i fluorescent species characterized by its fluorescent lifetime $\tau_i$.

DASPMI in various glycerol/ethanol mixtures are summarized in Table 3.5. The longer lifetimes became increasingly prominent with the increasing addition of glycerol (Figure 3.12 B). This is consistent with the hypothesis that the torsional dynamics about the single bonded flexible groups exhibit increased inertia with increasing viscosity. The calculated mean lifetime (Table 3.5) can be fitted against the volume ratio for second order polynomial with negligible contribution of the coefficient of the quadratic term.

The parameters obtained by global analysis were used to construct decay associated spectra (DAS) in chloroform and glycerol (Figure 3.13). In contrast to glycerol, the contributions of DAS from shorter and longer lifetime components are almost equal in chloroform. The higher polarity of glycerol reduces the potential barrier for rotation and hence facilitates conversion from the Franck-Condon state to the TICT state. This is evident from the relative contribution of the shorter component with increasing solvent polarity in Figure 3.13. The negative DAS values ($\tau_1$) in chloroform and glycerol are indications of the formation of new fluorescence species from locally excited state. The DAS of longer lifetime components ($\tau_2$ & $\tau_3$) remained positive throughout the measured emission spectrum.
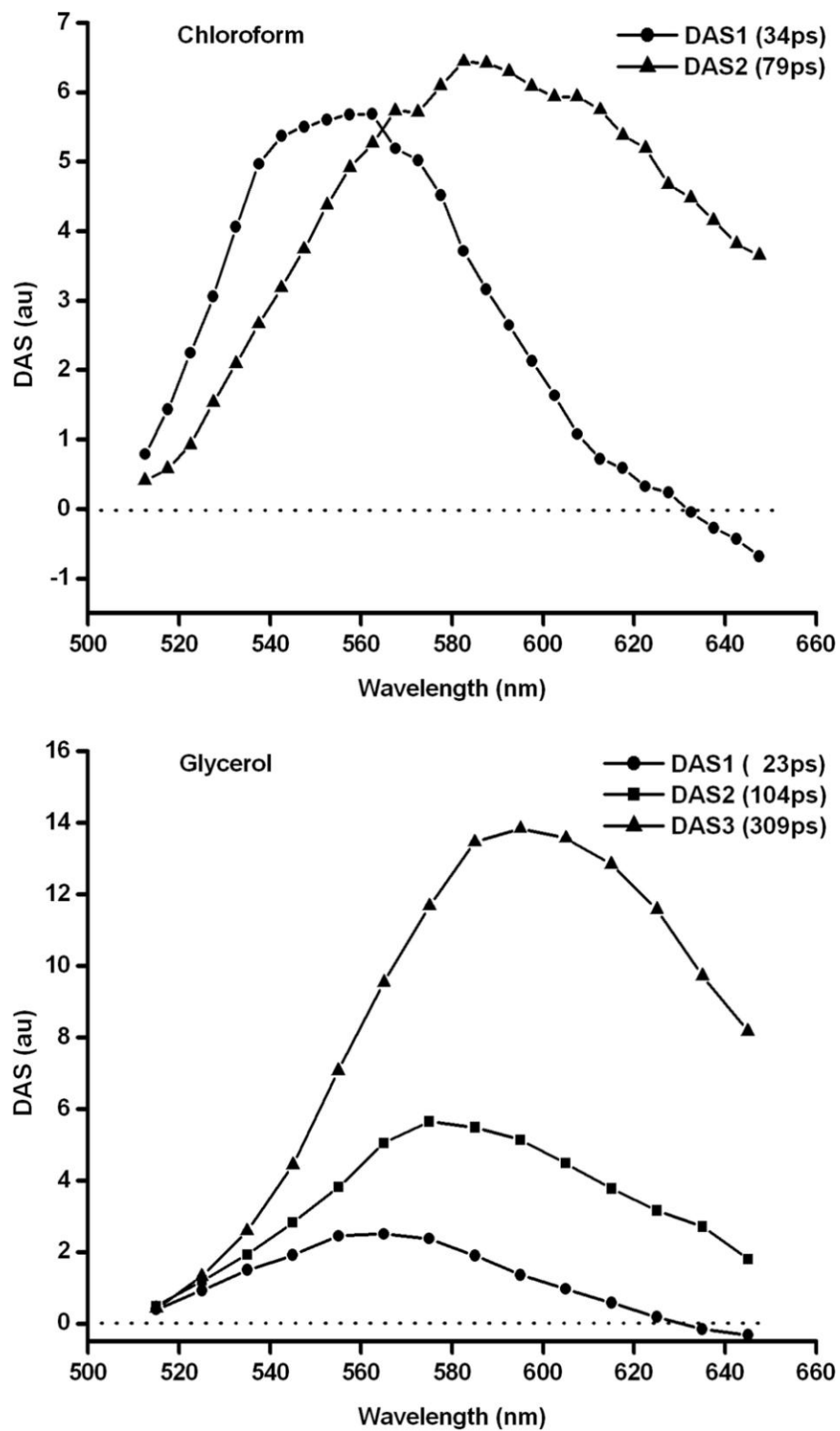
**Figure 3.13** *Decay associated spectra (DAS) of DASPMI in chloroform and glycerol.*

**3.2.5 Time-Resolved Emission Spectra**

Time-resolved emission spectra (TRES) of DASPMI were constructed and fitted to log-normal function as described by Maroncelli and Fleming (1987). Normalised fluorescence emission spectra in chloroform and glycerol after delay times 7, 54, 102 and 510 ps are shown in Figure 3.14. The spectra were fitted to log-normal function. The asymmetry parameter (c) varied from 0.21 to 0.27 in chloroform and 0.07 to 0.11 in glycerol. Apart from a red-shift in the spectra, an increasing fluorescence in the red flank could be observed. This red edge effect is more pronounced in the case of the non-polar solvent choloroform, in comparison to the polar solvent glycerol. Spectral-peak relaxation and changes in FWHM over time are shown in Figure 3.15. The spectral peak is shifted more to red in the case of glycerol. The spectral-peak relaxations in chloroform and glycerol were best fitted to bi-exponential decays. The time constants in chloroform are $44 \pm 2$ ps (amplitude -2113 cm$^{-1}$) and $65 \pm 3$ ps (2911 cm$^{-1}$). In the case of glycerol, two well separated time constants $38 \pm 3$ ps (62 %) and $134 \pm 17$ ps (38 %) gave the best fit. The changes in FWHM of TRES plotted in Figure 3.15 indicate the initial increase from a common value of spectral width $\sim$ 2450 cm$^{-1}$ in glycerol and chloroform. The spectral width reaches maximum at 3200 cm$^{-1}$ in the non-polar solvent chloroform and at 2750 cm$^{-1}$ in the polar solvent glycerol. The bi-exponential relaxation of emission maxima indicates a continuous solvent relaxation mechanism. However, initial fast increases of spectral width and nearly constant behaviour at later times are evident from Figure 3.15B.

An initial fast decrease of the peak amplitude with minor red-shift was observed for time delays less than 40 ps (Figure 3.14, Figure 3.16 and Figure 3.17) in chloroform. This is revealed as negative amplitude for the fast component of spectral peak relaxation. This behaviour can be interpreted as due to the presence of two different excited states, a locally excited (LE) nonpolar state and the subsequent formation of internal charge-transfer (ICT) state which undergoes solvation. An indication of fluorescence from LE state is apparent from the shoulder visible at the initial delay times, in the short-

wavelength side ([Figure 3.16](#)). In more polar solvents, the charge-transfer state becomes the low-energy state and emission occurs at longer wavelengths.
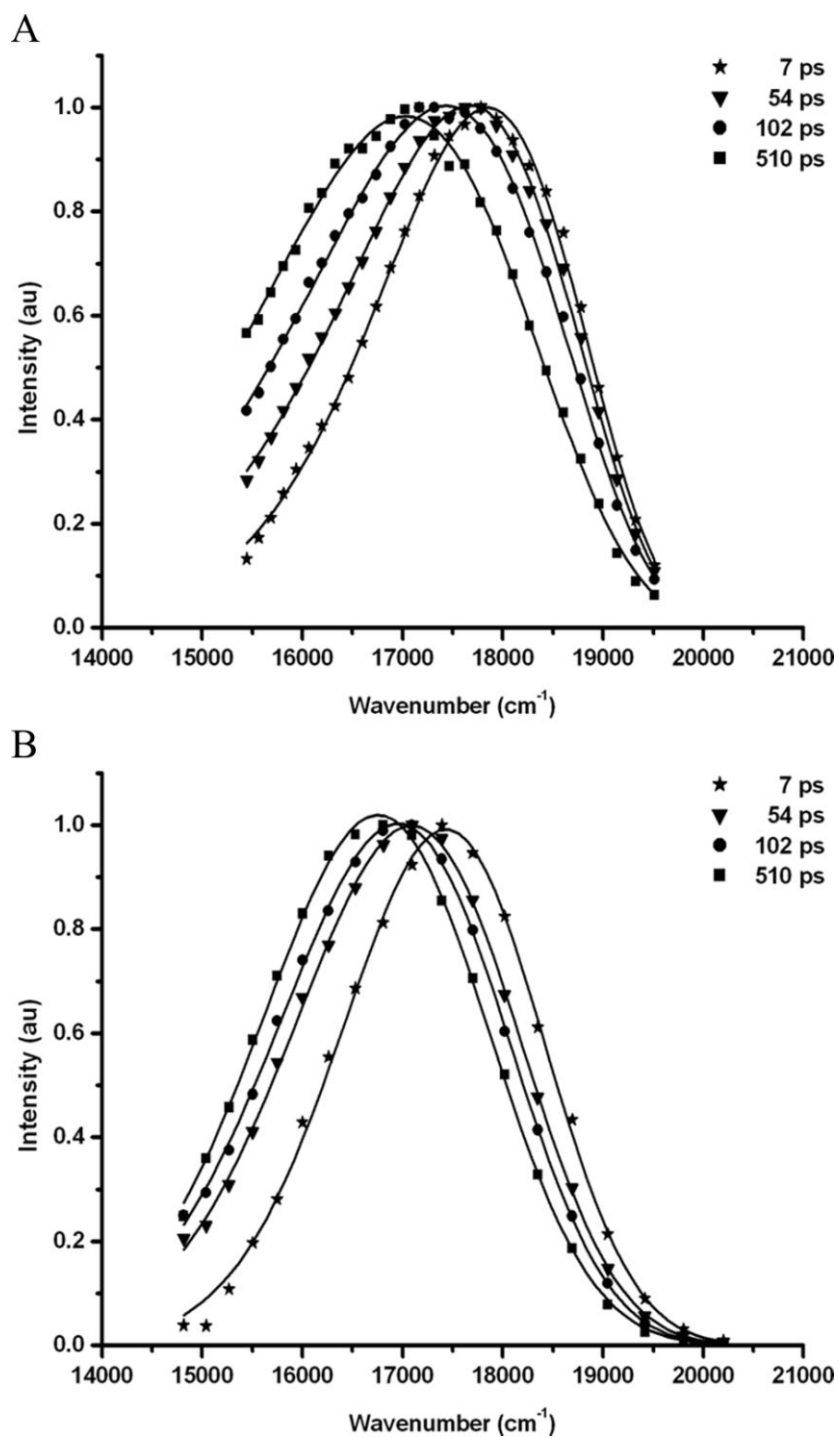


**Figure 3.14** *Time-resolved emission spectra of DASPMI in chloroform (A) and glycerol (B).*
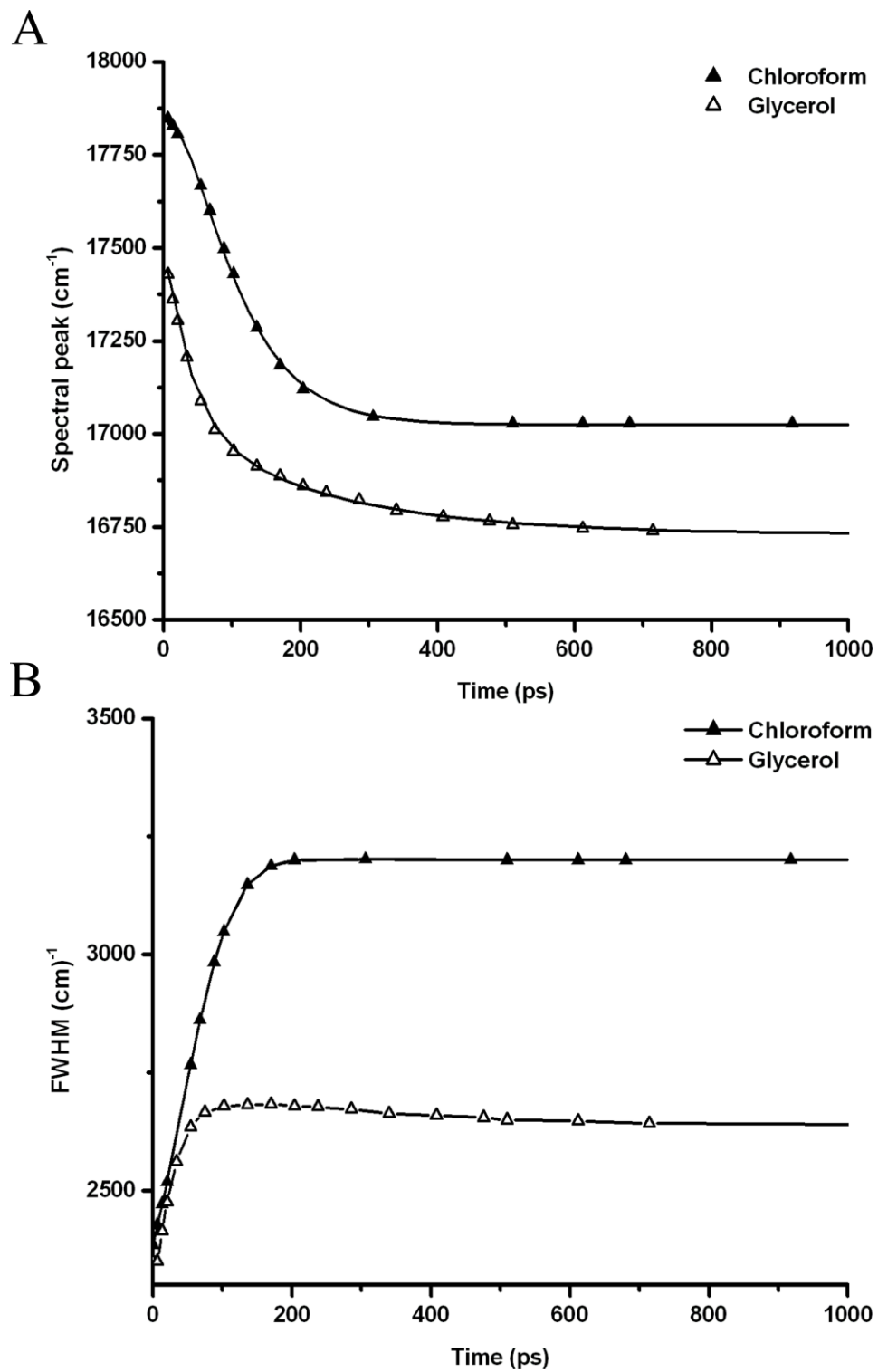
**Figure 3.15** *Dependence of spectral-peak relaxation (A) and spectral bandwidths (B) of DASPMI in chloroform and glycerol.*
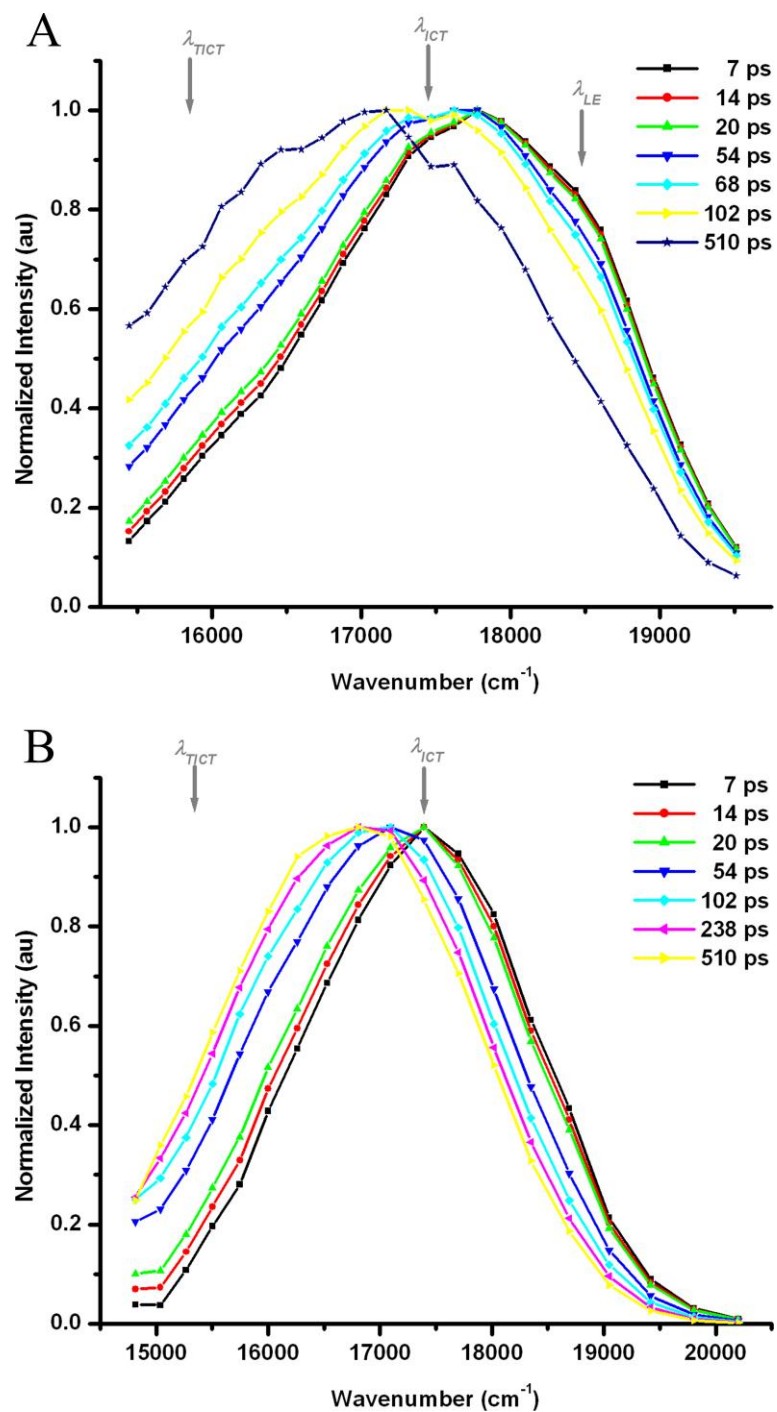
**Figure 3.16** *Time-resolved emission spectra of DASPMI in (A) chloroform and (B) glycerol at 298 K, reconstructed from spectrally-resolved fluorescence decays. A steady increase of fluorescence at the red edge of the spectra was observed in both the solvents. In comparison to glycerol, shift in emission maxima of chloroform is less pronounced at the initial time delays after excitation.*

A



B
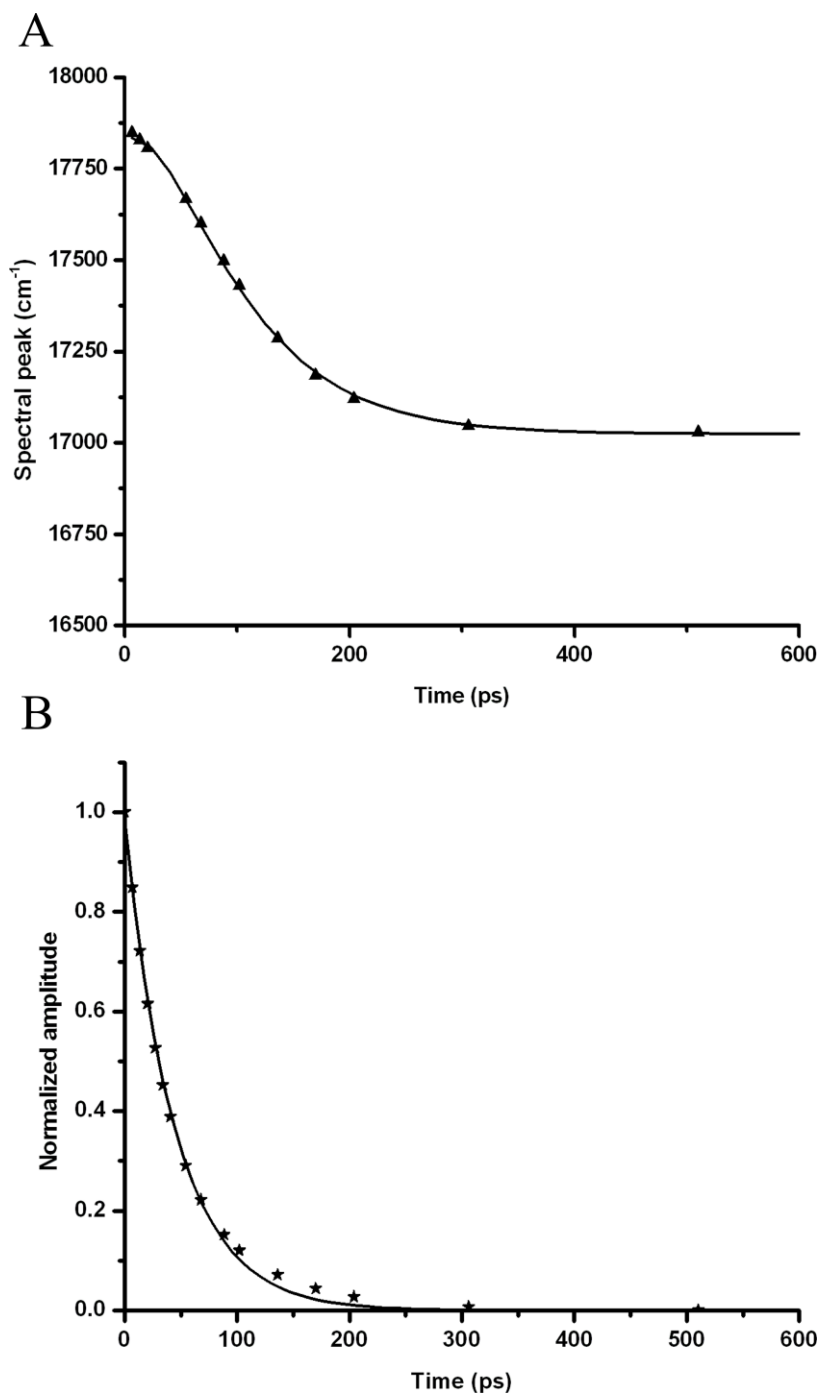


**Figure 3.17** *Time-resolved emission spectra of DASPMI in chloroform were fitted to a log-normal line shape function to extract amplitude and peak-shift.* (**A**) *Spectral peak relaxation* (**B**) *Decay of normalized spectral amplitudes. The time constants for spectral relaxation in are 44 ± 2 ps (amplitude -2113 cm$^{-1}$) and 65 ± 3 ps (2911 cm$^{-1}$). The decay of normalized spectral amplitudes was best fitted by a mono-exponential decay with time constant 45 ± 1 ps.*
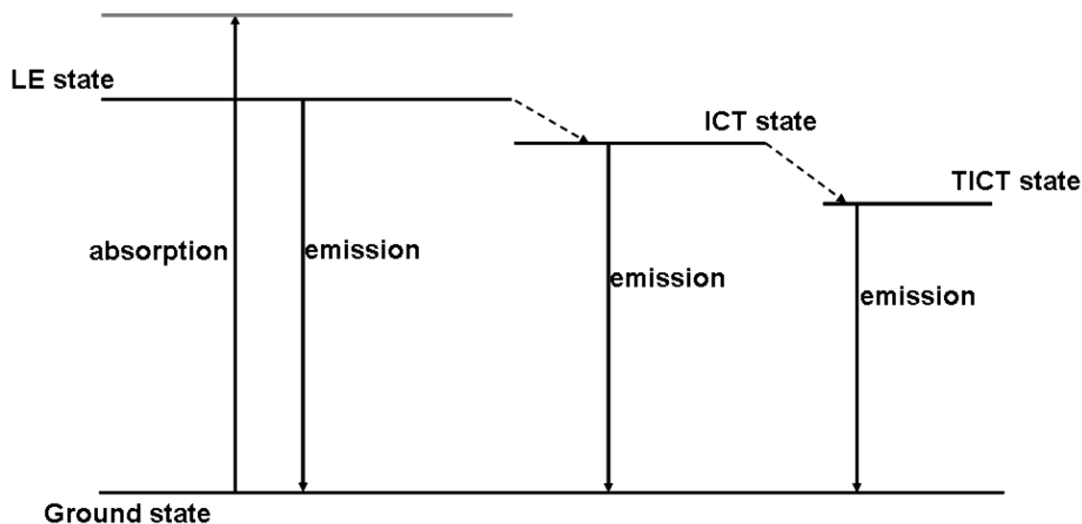
**Figure 3.18** *Generalized excited-state kinetics scheme. All the excited-states are associated with non-radiative deactivation as well and are predominantly rapid from TICT state in polar low-viscous solvents.*

### 3.2.6 Two-State Spectral Relaxation

The observed excited-state kinetics of DASPMI can be understood as the commencement of solvent relaxation from the charge transfer state. The dynamic relaxation of the solvation energy by reorientation of solvent dipoles lowers the energy of the excited state, leading to the red-shift. In addition to spectral shift, broadening of emission spectra has been observed in our TRES data. This trend of broadening is accompanied by the enhancement of fluorescence intensity at the red flank ([Figure 3.16](#)). One of the possible mechanisms accounting for this increase is by the formation of twisted-states about the single bonds neighbouring the olefinic double bond. These rotameric states are formed from the non-relaxed solvation shell. The two distinct structures (initially-excited Franck-Condon structure and the geometry attained by enhanced twist) undergoing solvent relaxation can be described as a two-state spectral relaxation process. This model is consistent with the gradual decrease of steady-state anisotropy with increasing emission wavelength and the presence of negative decay amplitudes for the short lifetime component in solvents of different polarity. Hence a three-state model of a generalised kinetic scheme is adequate to describe the excited-state kinetics of DASPMI

quantitatively (Figure 3.18). In apolar solvents or solvents impairing twist movements of the di-methyl pyridine and the aniline moiety the primary fluorescence gives rise to secondary fluorescence which contributes to the high quantum yield under these conditions whilst in low viscosity, polar solvents radiationless energy dissipation occurs.

The negative DAS values in chloroform and glycerol at the longer wavelengths explain the heterogeneity of fluorescence by the formation of new species from the initially excited state. This is in accordance to the low temperature studies by Strehmel et al. (1997), where the domination of a consecutive reaction mechanism was found. Several experimental and theoretical studies have revealed the twists around the single bonds, neighbouring the olefinic double bond, as the main mechanism of relaxation. Solvation relaxation of DASPMI in the lower picosecond regime has been reported by Jonkman et al. (1996) and Bringemann et al. (1995) as well. Hence a two-state spectral progression based on solvent relaxation and twist about the single bonds neighbouring the olefinic double bond will be sufficient to describe the fluorescence because relaxation by twist of the dimethyl amino group and the olefinic double bond is less probable as shown previously.

Upon photoabsorption, a substantial change in the electronic distribution of DASPMI results in an ICT state with the same geometry as in the ground state. Now enhanced twists about the aniline moiety and methylpyridinium ring support the formation of rotameric states. The rotameric states are assumed to form from the non-relaxed solvation shell of the ICT state. This scenario is similar to the model proposed by Röcker et al. (1996) for hemicyanine dyes without CC double bond and with one CC single bond. The solvations of both the geometries are assumed to move with a constant spectral width and asymmetry to the red edge of the emission spectrum. Based on these assumptions, bi-lognormal decomposition of TRES of DASPMI in chloroform and glycerol were performed (Figure 3.19 & 3.20). In chloroform and glycerol, the asymmetry parameter was taken as 0.23 and 0.11 respectively. For both solvents, spectral width of primary fluorescence (LE and ICT state) was assumed as 2450 $cm^{-1}$ and for secondary fluorescence (TICT state) 4680 $cm^{-1}$.
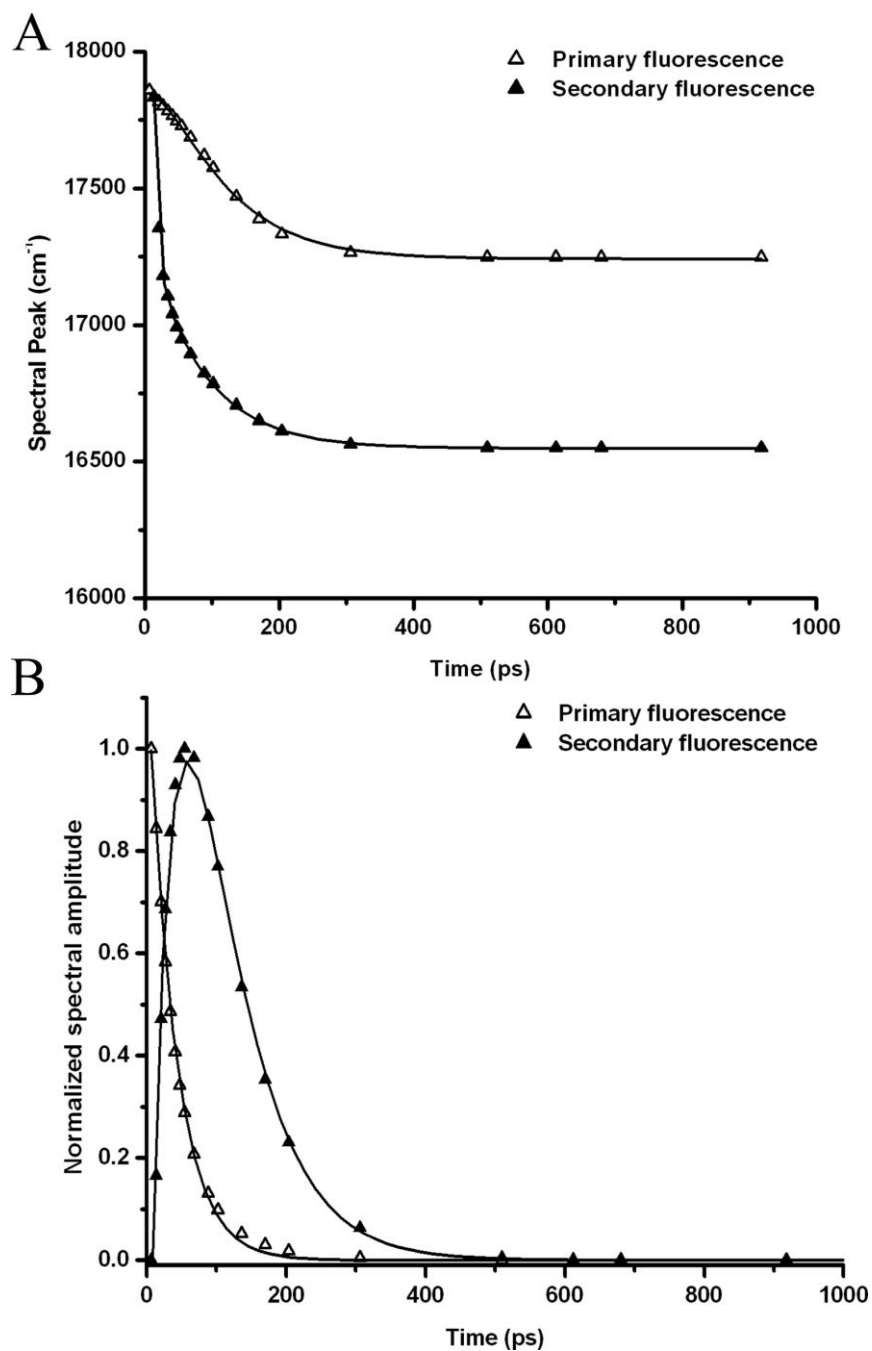
**Figure 3.19** *Bi-lognormal fit of TRES of DASPMI in chloroform into primary (open symbols) and secondary fluorescence (closed symbols).* **(A)** *Spectral peak relaxation.* **(B)** *Decay of normalized spectral amplitudes. The amplitude values of the secondary fluorescence have been increased 15.3 times relative to those of the primary fluorescence.*
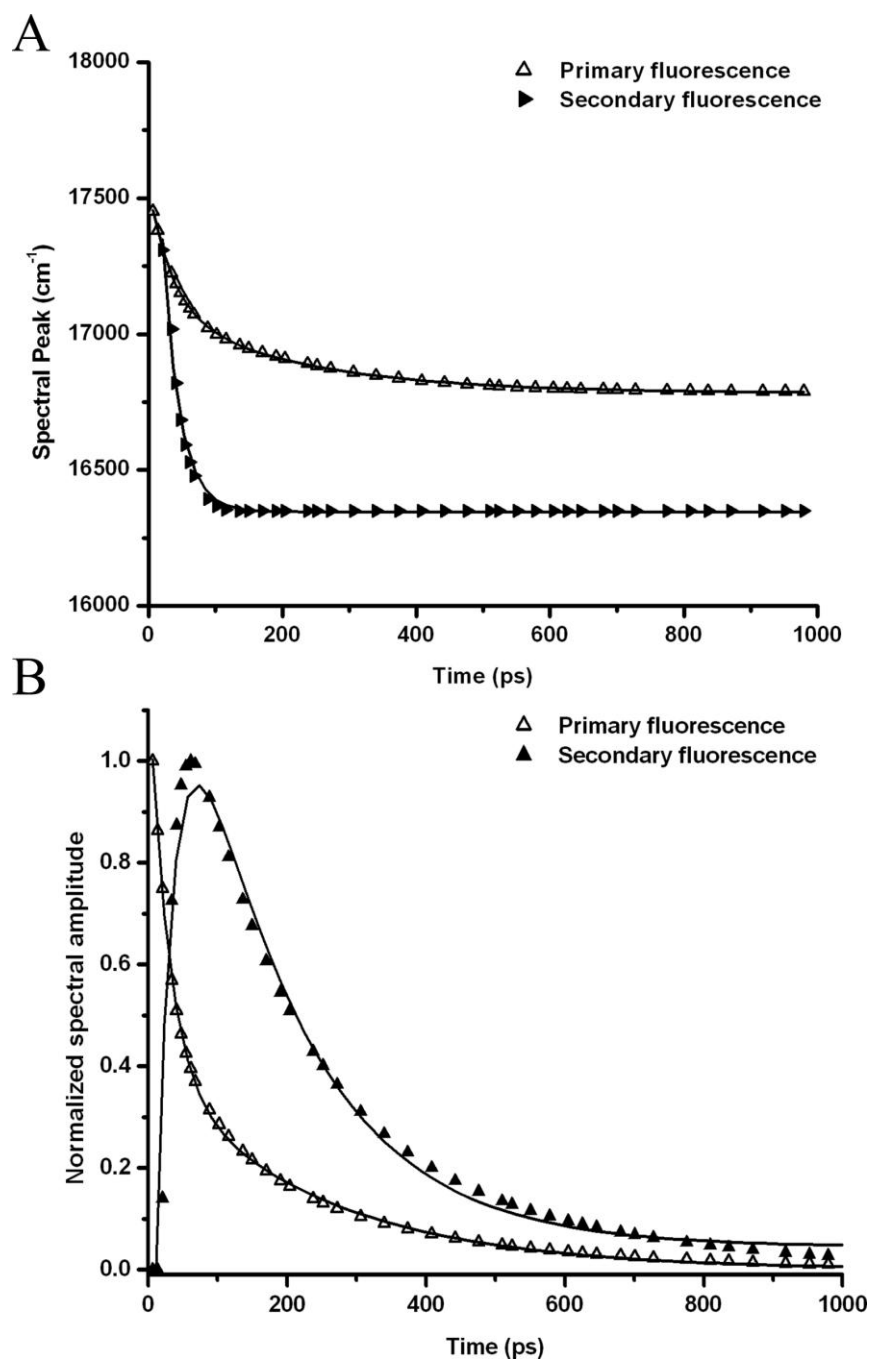
**Figure 3.20** *Bi-lognormal fit of TRES of DASPMI in glycerol into primary (open symbols) and secondary fluorescence (closed symbols).* **(A)** *Spectral peak relaxation.* **(B)** *Decay of normalized spectral amplitudes. The amplitude values of the secondary fluorescence have been increased 19.7 times relative to those of the primary fluorescence.*

Spectral peak relaxation and changes in spectral amplitudes over time for primary and secondary fluorescence in the non-polar solvent chloroform are shown in [Figure 3.19](). The primary fluorescence relaxes to 17250 cm$^{-1}$ and secondary fluorescence is red shifted with a final emission at 16550 cm$^{-1}$. The decay of primary fluorescence was mono-exponential with 38 ps time constant. The secondary fluorescence rising during the decay of primary fluorescence attains maxima within 60 ps and thereafter decays. The secondary fluorescence was fitted with bi-exponential decay model with time constants 38 ps (amplitude -5) and 68 ps (amplitude +5). These results signify the decay of primary fluorescence and concomitant formation secondary fluorescent state. The greater spectral width of secondary fluorescence advocates the enhanced polarity due to the formation of twisted state.

The decomposition of TRES in glycerol ([Figure 3.20]()) exemplifies the relaxation of primary and secondary fluorescence to 16800 cm$^{-1}$ and 16350 cm$^{-1}$. The biphasic decay of primary fluorescence was fitted by a bi-exponential course with time constants of 28 ps (67%) and 240 ps (33%). The secondary fluorescence increases with the decay of primary fluorescence and reaches its maximum within 75 ps. The biphasic secondary fluorescence was fitted by bi-exponential decay with the time constants 28 ps (amplitude -2) and 161 ps (amplitude +2). In comparison to chloroform, stronger solvation in glycerol is due to the higher polarity of glycerol and enhanced intramolecular charge transfer. The high viscosity of glycerol determines the slow dynamics of the twisted states. It is of interest to note that the primary and secondary fluorescence in chloroform and glycerol decay with identical time constants for the fast phase only. This emphasises the consecutive reaction mechanism in the excited state with no back reaction. The early phases of spectral relaxation in chloroform were primarily dominated by the increase in fluorescence at the red edge ([Figure 3.15]()) and a less apparent shift in emission maxima. While in glycerol, spectral shifts are dominating with a simultaneous gradual increase at the red edge. This can be attributed to the more polar nature of glycerol leading to a stronger solvation of the initially excited benzenoid form. This is reflected in the monophasic and biphasic nature of amplitude decay of primary fluorescence in

chloroform and glycerol, respectively. The fast decay component in glycerol (28 ps) is supposed to be due to local reorganization of solvent molecules and the slow component (240 ps) to solvent relaxation of the charge transfer state.

Influence of polarity and viscosity of the solvent are reflected by decays of normalized spectral amplitudes in various proportions of glycerol/ethanol mixtures and glycerol. Viscosity and polarity changes result in delays in the onset of secondary fluorescence and different rise times (Figure 3.21). These observations validate the assumption of twist about the flexible single bonds in the styryl group.
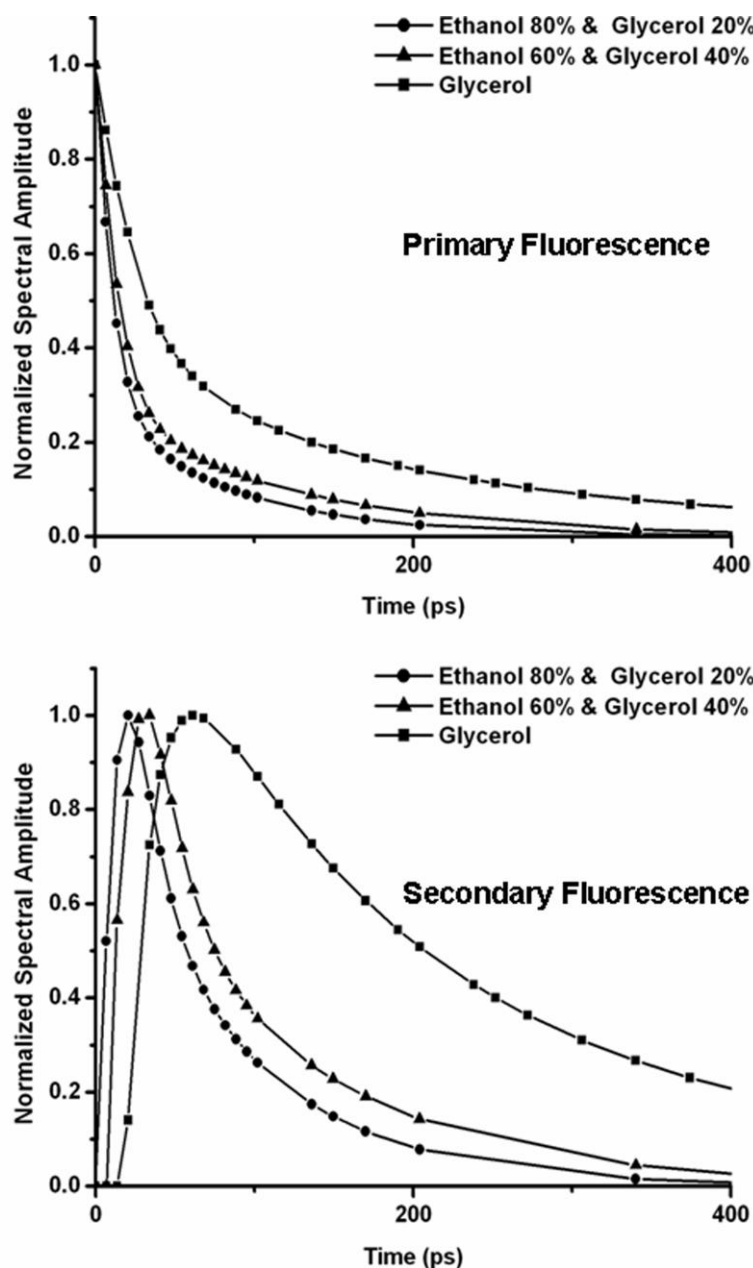
**Figure 3.21** *Decay of normalized spectral amplitudes in various proportions of glycerol/ethanol mixtures and glycerol. The delay times in the onset of secondary fluorescence and rise times of secondary fluorescence differ for various polarity and viscosity conditions. This validates the assumption of twist about the flexible single bonds in styryl group as the crucial factor in determining relaxation of the primary excited state.*

## 3.3 Fluorescence Dynamics of DASPMI in Living Cells

### 3.3.1 Introduction

Cellular energy metabolism is best represented by mitochondrial membrane potential in the range of 150 – 180 mV resulting from the proton gradient across the inner membrane (Chen, 1988; Bereiter-Hahn, 1990). Stress conditions as are for instance exposure to reactive oxygen species, uncoupling agents or ageing (Balaban et al., 2005; Lambert & Brand, 2007; Orrenius, 2007) strongly influence this potential. Thus visualzation of mitochondrial energy status is of significant physiological interest. Potentiometric probes such as cationic and zwitterionic styryl dyes, anionic and cationic cyanines, cationic rhodamines, and anionic and hybrid oxonols (Haughland, 2002) are potential tools for determining the membrane potential of mitochondria in living cells.

The styryl dye 2-[4-(dimethylamino)styryl]-1-methylpyridinium iodide (DASPMI) is a low toxicity ($< 5 \times 10^{-7}$ M) specific vital stain of mitochondria in living cells (Bereiter-Hahn, 1976; Bereiter-Hahn et al., 1983; Mewes & Rafael, 1981). Fluorescence intensity of DASPMI is a dynamic measure for the membrane potential of mitochondria and is presumed to be located in the inner mitochondrial membrane. Spectra of DASPMI stained mitochondria in living cells, correspond to those in a phospholipid environment (excitation wavelength maximum around 470 nm, emission 560 – 570 nm). The very fast response of DASPMI to transmembrane potential, high sensitivity and well definable potentiometric response make it a valuable probe for precise monitoring of the dynamic changes in membrane potential across different mitochondria in a single living cell and within intramitochondrial zones (Bereiter-Hahn, 1976; Loew et al., 1979; Mewes & Rafael, 1981; Bereiter-Hahn et al., 1983; Loew & Simpson, 1981). For example, higher membrane potential required for ATP production during cell growth, cell differentiation and cell motility (James & Bohman, 1981; Darzynkiewicz et al., 1982; Collins & Foster, 1983; Johnson et al., 1981; Diaz et al., 1999) may well be precisely visualized with such optical probes. The presence of sub-mitochondrial zones with higher membrane potential

has been reported previously using DASPMI and JC1 dyes (Bereiter-Hahn & Vöth, 1998). The uptake of DASPMI in mitochondria follows Nernst relations (Mewes & Rafael, 1981) and allows for straightforward determination of mitochondrial energization state (Bereiter-Hahn, 1976; Mewes & Rafael, 1981). The mechanism of voltage-sensitive molecular fluorescence and its behaviour under the conditions influencing mitochondria energy state in living cells, however, have not been comprehended yet. Interpretation of intensity measurements on single or submitochondrial level is difficult because of thickness variations, a problem overcome by intensity independent methods.

A three state model of fluorescence was sufficient to describe the solvent fluorescence of DASPMI, wherein an initially excited molecule undergoes twist and further solvation (Ramadass & Bereiter-Hahn, 2007). The fluorescence characteristics of DASPMI are influenced by both polarity and viscosity of the environment and are in general not discernible. The polarity based influences manifest themselves as red shift in the emission spectra, blue shift in absorption spectrum and decrease in quantum efficiency and lifetime. The increase in viscosity results in increase in lifetime and enhancement of fluorescence at the red-edge of the emission spectrum. While such differences exist, it is difficult to discern the individual influences of polarity and viscosity due to dependence of torsional dynamics of the dye on the intramolecular charge transfer state.

Here, we embark on a systematic approach of understanding the behaviour of DASPMI in living cells. The variation of fluorescence intensity of DASPMI in mitochondria of single cell was investigated by monitoring its uptake kinetics. Differences in its uptake kinetics and amount of accumulation determined by its final fluorescence intensity were found to vary for peri-nuclear and peripheri mitochondria in XTH cell line. From fluorescence decay determinations down to the level of single mitochondria, quantum efficiency and different speeds of mass accumulation of DASPMI have been identified as determinant factors in its behaviour revealing mitochondrial membrane potential. Extraction of emission finger prints among different mitochondria within a single cell exhibited variations in contribution of different excited states.

Fluorescence anisotropy is a dimensionless quantity independent of absolute intensity and environmental influences such as static quenching. Anisotropy is a measure of the mobility of the dye molecules in relation to the excited state lifetime. Emission anisotropy of DASPMI in mitochondria under high membrane potential conditions was high, suggesting restricted torsional flexibility under high membrane potential conditions. Similar high values were found as well, in sub-mitochondrial zones of higher membrane potential. Such behaviour of DASPMI in living cells is interpreted as an indication of a probably linear electrochromism and consequently restriction of its torsional dynamics. This has further been asserted by obtaining spatially-resolved fluorescence decays under various conditions altering the mitochondrial membrane potential. A three exponential decay model (Ramadass & Bereiter-Hahn, 2007) of successive formation of locally excited (LE) state, intramolecular charge transfer (ICT) state and twisted intramolecular charge transfer (TICT) state was applied to comprehend DASPMI fluorescence properties under differing conditions and at different regions inside a single living XTH2 cell. Under conditions of high membrane potential, there was a considerable decay time decrease of the shortest lifetime component with a concurrent increase in its contribution. This may well be related to its behaviour in highly polar solvents like water, wherein mono-exponential picosecond lifetime was found (Ramadass & Bereiter-Hahn, 2007). The other two lifetimes pertaining to ICT and TICT state increased with decreasing contribution to the decay. Such dramatic influences on locally excited state and disparate changes on other excited state lifetime indicate the partial insertion of DASPMI into the membrane wherein it undergoes electrochromism.

In regions of high membrane potential, de-localisation of $\pi$-electron system results in increase in stiffness of the single bonds neighbouring the olefinic double bond. Upon photo-excitation, the extent of electronic redistribution between the electron acceptor and donor moieties of DASPMI, depend on the potential across the mitochondrial inner membrane. Low anisotropy at lower mitochondrial membrane potential regions results from unhindered enhanced twists for an efficient charge transfer and relaxation of the excited probe DASPMI. Such fluorescence intensity independent emission anisotropy

could be used as a means to measure mitochondrial membrane potential in living cells and is devoid of discrepancies arising due to variances in dye uptake and the uneven staining in single cell studies using a fluorescence microscope.
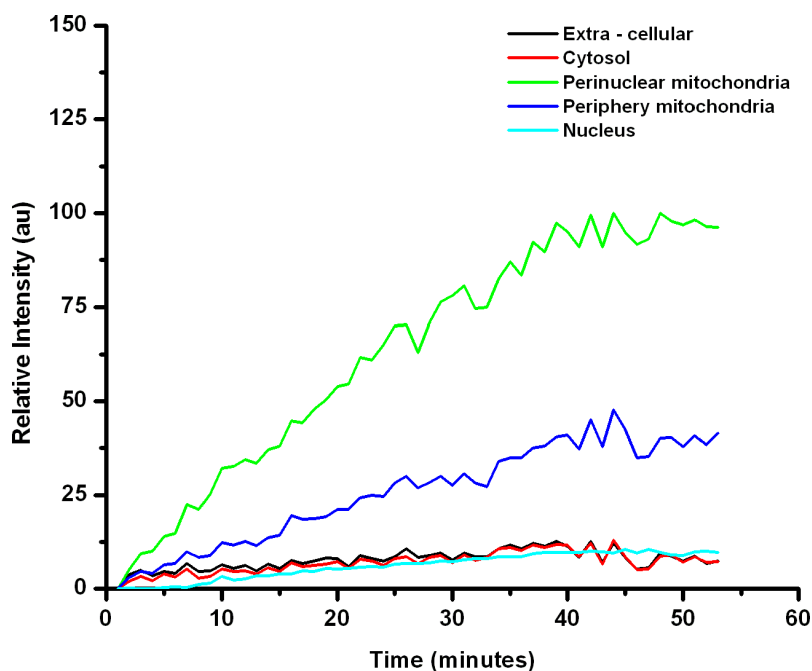


**Figure 3.22** *Uptake kinetics of DASPMI in a single XTH2 cell. Cells incubated in a medium containing 5 µM DASPMI were imaged successively for every minute and the measured integrated intensity density versus time were plotted for specific regions of interest. The uptake kinetics varied considerably for different cells.*

### 3.3.2 Kinetics of DASPMI Uptake

The lipophilic cationic dye DASPMI (2 µM) was dissolved in normal culture medium and the fluorescence intensity was measured by integrating brightness of CCD images showing several cells at successive time points at the desired regions of interest. At this high concentration DASPMI becomes accumulated in mitochondria and in the nucleus, the nucleoli in particular. Uptake rates of the dye varied in different regions of the cells. Time course of fluorescence changes upon uptake of DASPMI in a representative XTH2 cell is shown in Figure 3.22. In the peri-nuclear mitochondria (mean time to half maximal intensity − 18 ± 1 minutes) the uptake of the dye was faster in comparison to the

**70**

peripheral mitochondria (mean time to half maximal intensity − 22 ± 2 minutes). This difference is due to the higher membrane potential of mitochondria near the nucleus and charged molecules in the nucleoli. Apart from the uptake kinetics, the difference in fluorescence intensity in differing regions of a cell was apparent as well. Similar uptake kinetic behavior has been previously reported for XTH2 cells without any differentiation of various mitochondrial populations (Bereiter-Hahn et al., 1983). There exists a 3.5 fold emission intensity difference of total mitochondrial fluorescence in the perinuclear and in peripheral regions for this particular experiment (Figure 3.22). In a few cases, mitochondria having identical low intensity fluorescence inside a given single cell were found.

The differences in DASPMI accumulation between the peri-nuclear region and cell periphery, staining of mitochondria was investigated in saponin permeabilized XTH2. In contrast to the findings described above, a longer period (> 40 minutes) was required until fluorescence intensity reached stable values. This emphasizes the role of plasma membrane potential in channeling the DASPMI towards mitochondria. Representative images and average grey value distribution in permeabilized cells in the presence of ATP and substrate (ATP, glutamate and malate) are shown in Figure 3.23. Higher mitochondrial membrane potential apparent from higher fluorescence intensity and consequently, grey values in cells treated with ATP or substrate in comparison to the non-permeabilized cell is evident. Also the difference in intensity distribution of peripheral and peri-nuclear mitochondria decreases under these induced membrane potential conditions. Such changes are better distinguished from the average grey value distribution over 20 cells depicted in Figure 3.23. The grey values (abscissa) and their frequency (ordinate) of occurrence in perinuclear and peripheral mitochondria under control conditions and after ATP or substrate (glutamate & malate) treatment are plotted. Upon treatment with ATP and/or substrate, shifts to higher grey values with increased contribution are apparent for both mitochondrial populations. Also in comparison to control conditions, increased overlap of perinuclear and periphery grey value distribution is evident.
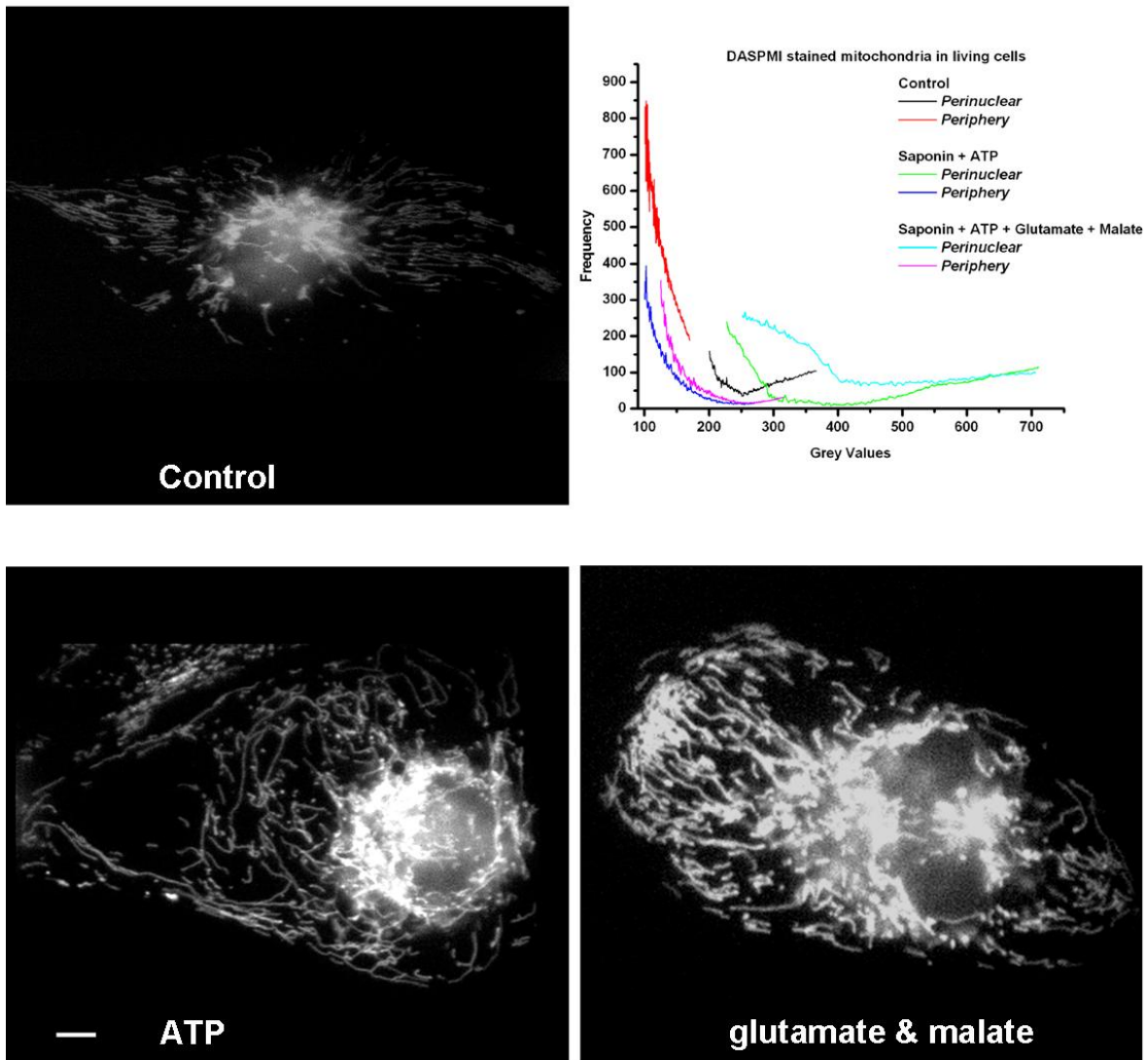
**Figure 3.23** *Representative images of DASPMI stained XTH2 cells after saponin permeabilisation under control conditions and after ATP or substrate (glutamate & malate) treatment. Average grey value distribution obtained from peri-nuclear and periphery mitochondrial regions of 20 cells in each case have been plotted against the frequency of their occurrence. Steady-state images were obtained under identical-optical conditions, electronic amplification and offset. In the presence of ATP or substrate, apart from shift to higher grey values, indicating increased fluorescence amplitude, decrease in the amplitude difference between perinuclear and peripheral mitochondria are evident. (Bar 5 µm)*

### 3.3.3 Emission Fingerprinting

Quantum efficiency and emission spectra of DASPMI considerably depend on solvent polarity and viscosity. Hence, the spectral fingerprint of DASPMI stained living XTH2 cells was performed at 458 nm excitation. The extracted emission spectra from mitochondria and nucleoli (at organelle conc. $\gg$ 2 $\mu$M) (Figure 3.24 A) exhibited emission maxima at 565 nm and 575 nm, respectively. Mitochondria emission spectrum has additional shoulders at about 535 nm and 590 nm. In DASPMI stained nucleoli, a single additional shoulder at about 610 nm can be observed. The emission spectra from the nucleus region, exhibits all the three peaks (535 nm, 565 nm and 590 nm). Based on the photophysical studies in solvents (Ramadass & Bereiter-Hahn, 2007), these shoulders in living cells can be attributed to the domination of locally excited state (~ 535 nm), the intramolecular charge transfer state (~ 565 nm) and the twisted intramolecular charge transfer state (> 590 nm). In the case of nucleoli, the decrease of fluorescence from LE state and the increased contribution of TICT state are evident.

The emission maximum of DASPMI in lipid environment was found to be at 545 nm and an excitation maximum of 430 nm. Accordingly the spectra in mitochondria indicate that DASPMI diffuses to the inner membrane of mitochondria (due to shoulder at ~ 535 nm) and aligns itself to the local electric field across the membrane. The polarity dependent red-shift of excitation maxima in mitochondria (470 nm) and the changes in fluorescence intensity of DASPMI at 565 nm could then be related to the membrane potential of mitochondria. Such membrane potential dependent changes in absorption and emission characteristics have been previously shown for p-DASPMI (Kim & Lee, 1999). The emission intensity due to torsional dynamics (TICT state) at longer emission wavelengths would then be dependent upon the compactness of the inner membrane and the local electric field.

Heterogeneous fluorescence of DASPMI along a single mitochondrion is depicted in Figure 3.24 B. Apart from changes in emission intensity; variations in spectral

characteristics due to different contributions of locally excited, ICT and TICT state are evident. Such changes may well be due to the influence of local electric field on its ground state electron distribution, the resistance of local electric field to align the transition dipole moment and on the local viscosity.
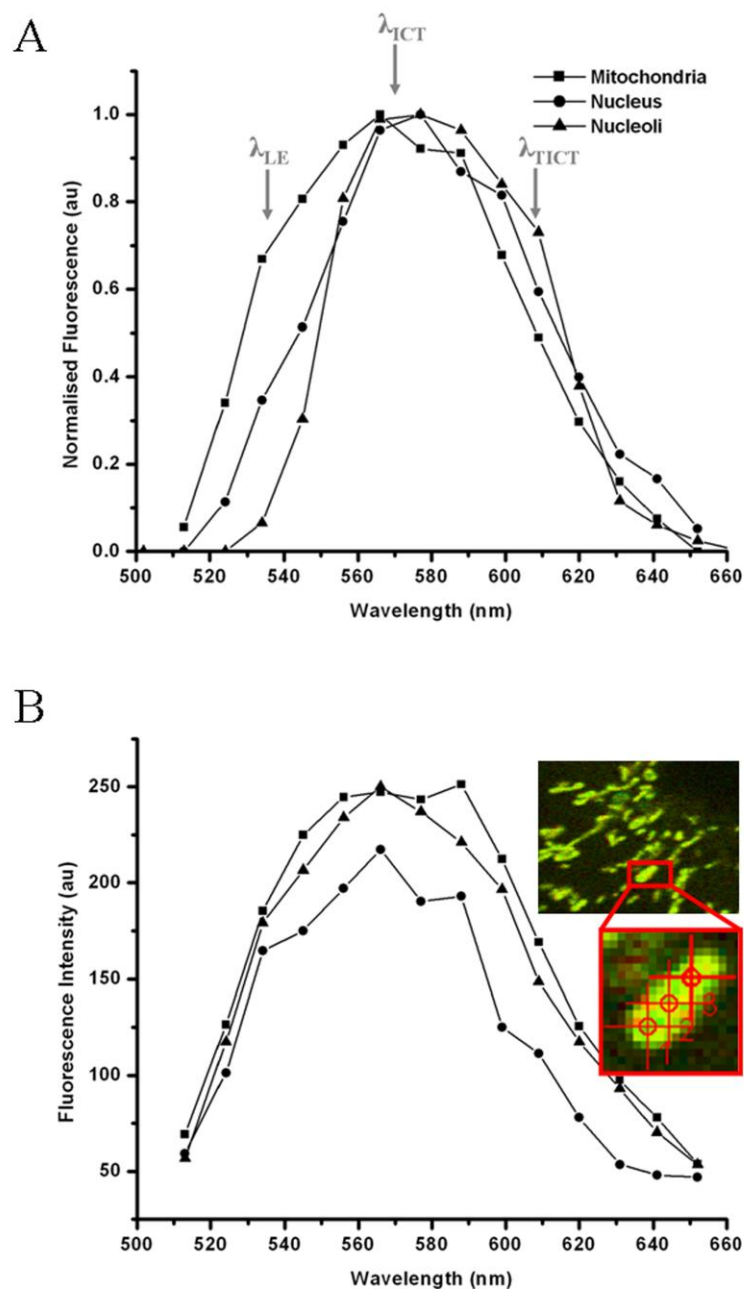


**Figure 3.24** *Emission fingerprints of DASPMI stained XTH2 cells.* **(A)** *average over a few mitochondria, nucleus and nucleoli regions* **(B)** *three different regions of interest along single mitochondria.*

### 3.3.4 Spatially Resolved Fluorescence Lifetime Imaging

### 3.3.4.1 Untreated Cells in Culture

Spatially resolved fluorescence lifetime imaging is the method of choice to relate the complex photophysics of DASPMI to its interaction with mitochondria at different physiological states, i.e. to elucidate how DASPMI fluorescence monitors mitochondrial membrane potential. Using a QA-detector, fluorescence decay values can be derived even for single mitochondria within living cells (Figures 3.25 – 3.26 & Tables 3.6 – 3.7). In Figures 3.25 and 3.26 fluorescence intensities have been color coded and fluorescence decay has been calculated for ROIs containing one mitochondrion or only very few organelles. Fluorescence intensity is highest in mitochondria in the perinuclear regions and decreases towards the cell periphery, a behavior often observed in larger cells. A whole cell is shown in Figure 3.25; the ROIs with the higher numbers lie in the cell periphery. In the very periphery single mitochondria no longer can be identified because this picture has been taken while the cells were alive and mitochondria were moving within the cytoplasm during the photon collection time. Figure 3.26 shows the peripheral part of an XTH-2 cell, ROI no. 1 is proximal towards the nuclear area and ROI no. 4 is the most peripheral. The higher membrane potential of mitochondria in Figure 3.25 is evident from its higher fluorescence intensity in comparison to mitochondria in Figure 3.26 taken at the same instrumental settings. The insert in Figure 3.26 shows that mitochondria in this cell exhibit clear morphological signs of photo-induced impairment (Bereiter-Hahn & Vöth, 1998).

Depending on intracellular location and physiological state notable variations of all the three lifetime components and relatively small changes in their contributions are evident. $\tau_1$ considerably increases with decreasing fluorescence intensity (Table 3.6, Figure 3.25), also its contribution to overall fluorescence increases. $\tau_2$ also increases, however with decreasing fraction. The longest lifetime, $\tau_3$, changes considerably and its contribution lies between 3 – 6 %. Average lifetime (proportional to area under the decay curve)

decreases at higher fluorescence intensities in the cell shown in Figure 3.25. The fractional contribution ($f_1$) of short decay time ($\tau_1$) to the steady-state intensity is weaker for regions of higher intensity; it is about half the fractional intensity of intramolecular charge transfer state ($f_2$) for regions of higher membrane potential. In Figure 3.26, the situation in photodynamically impaired mitochondria is shown by a consistent increase of lifetimes and their corresponding contributions, with increasing steady-state intensity (Table 3.7). Such decay kinetic behaviour is typical of viscosity influences as found in ethanol/glycerol mixtures. The longest lifetime $\tau_3$ is considerably longer (~ 1 ns) than that found in Figure 3.25 ROI's. The fractional intensity of the locally excited state ($f_1$) almost equals the fractional intensity of intramolecular charge transfer state ($f_2$) for ROI of higher mean lifetime.

At 3 µmol/L, DASPMI staining no longer is restricted to mitochondria rather this weak cation can also be accumulated in the nucleus, very prominently in the nucleolus and to a minor extent it may remain in the cytoplasm (cytosol; Table 3.8). In cytoplasm, nucleus and nucleolus, the long living component $\tau_3$ is longer lasting than in mitochondria and $f_3$ contributes more to the overall fluorescence. Also the other two decays have longer duration in the hydrophilic but highly charged environment of the nucleolus, and to a minor extent also in the nucleus and in cytosol.

**Figure 3.25** *Time-integrated QA image.*

**Table 3.6 Fluorescence lifetime analysis of various ROI in Figure 3.25.**

| ROI | $a_1$ | $\tau_1$ (ns) | $a_2$ | $\tau_2$ (ns) | $a_3$ | $\tau_3$ (ns) | $<\tau>$ (ns) | $f_1$ (%) | $f_2$ (%) | $f_3$ (%) |
|---|---|---|---|---|---|---|---|---|---|---|
| 1 | 0.65 | 0.091 | 0.31 | 0.544 | 0.04 | 2.343 | 0.322 | 19 | 52 | 29 |
| 2 | 0.74 | 0.085 | 0.23 | 0.528 | 0.03 | 2.162 | 0.249 | 25 | 49 | 26 |
| 3 | 0.70 | 0.118 | 0.24 | 0.739 | 0.06 | 2.711 | 0.423 | 20 | 42 | 38 |
| 4 | 0.71 | 0.101 | 0.26 | 0.591 | 0.03 | 2.286 | 0.294 | 25 | 52 | 23 |
| 5 | 0.74 | 0.221 | 0.22 | 0.747 | 0.04 | 2.357 | 0.422 | 39 | 39 | 22 |
| 6 | 0.75 | 0.216 | 0.22 | 0.780 | 0.03 | 2.503 | 0.409 | 40 | 42 | 18 |

**Figure 3.25** *Pseudo color time-integrated QA image and corresponding decay kinetics (Table 3.6) at various ROI of DASPMI stained XTH2 cell. The variable mitochondrial membrane potential can be inferred from its intensity distribution. Fluorescence lifetime analysis was performed over various regions of interest including single mitochondria or several organelles. Fluorescence from ROI 3 is primarily from nucleus, with a minor contribution from mitochondria only.*



**Figure 3.26** *Time-integrated QA image.*

**Table 3.7 Fluorescence lifetime analysis of various ROI in Figure 3.26.**

| ROI | $a_1$ | $\tau_1$ (ns) | $a_2$ | $\tau_2$ (ns) | $a_3$ | $\tau_3$ (ns) | $<\tau>$ (ns) | $f_1$ (%) | $f_2$ (%) | $f_3$ (%) |
|---|---|---|---|---|---|---|---|---|---|---|
| 1 | 0.75 | 0.271 | 0.21 | 1.006 | 0.04 | 3.445 | 0.561 | 37 | 38 | 25 |
| 2 | 0.73 | 0.233 | 0.23 | 0.910 | 0.04 | 3.430 | 0.513 | 33 | 41 | 26 |
| 3 | 0.71 | 0.197 | 0.25 | 0.779 | 0.04 | 3.174 | 0.453 | 30 | 42 | 28 |
| 4 | 0.69 | 0.122 | 0.28 | 0.618 | 0.03 | 2.888 | 0.352 | 25 | 50 | 25 |
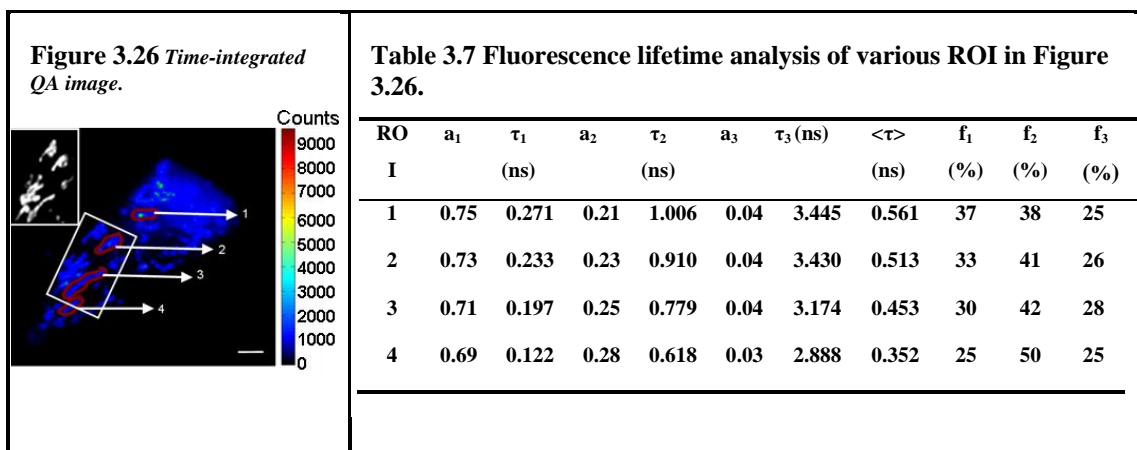
**Figure 3.26** *Pseudo color time-integrated QA image of DASPMI stained XTH2 cell having low mitochondrial membrane potential (in comparison to Figure 3.25) and the corresponding decay kinetics (Table 3.7) at various ROI. The inset figure shows several photo-damaged mitochondria. Electron micrographs of photo-damaged mitochondria have been shown previously to correspond to electron-translucent zones devoid of cristae.*

**Table 3.8 Fluorescence lifetime analysis of DASPMI stained living XTH2 cells.** The high standard deviations (shown below the decay parameters in parenthesis) result from biological variations occurring if measured on single cell or single mitochondrion level and not from instrumental inaccuracy (compare values in Table 3.6 and 3.7).

| Condition | $a_1$ | $\tau_1$ (ns) | $a_2$ | $\tau_2$ (ns) | $a_3$ | $\tau_3$ (ns) | $<\tau>$ (ns) | $f_1$ (%) | $f_2$ (%) | $f_3$ (%) |
|---|---|---|---|---|---|---|---|---|---|---|
| Punctated | 0.82 | 0.065 | 0.16 | 0.626 | 0.02 | 2.802 | 0.216 | 24 | 44 | 32 |
| | (0.09) | (0.023) | (0.08) | (0.082) | (0.01) | (0.410) | (0.065) | (3) | (5) | (4) |
| Elongated | 0.72 | 0.183 | 0.24 | 0.739 | 0.03 | 2.610 | 0.396 | 34 | 45 | 21 |
| | (0.04) | (0.041) | (0.03) | (0.114) | (0.01) | (0.241) | (0.068) | (5) | (3) | (4) |
| Nucleus | 0.67 | 0.190 | 0.25 | 0.963 | 0.08 | 3.020 | 0.603 | 21 | 39 | 40 |
| | (0.06) | (0.071) | (0.03) | (0.282) | (0.03) | (0.500) | (0.170) | (3) | (5) | (8) |
| Nucleoli | 0.64 | 0.225 | 0.26 | 1.257 | 0.10 | 3.576 | 0.816 | 18 | 39 | 43 |
| | (0.07) | (0.079) | (0.05) | (0.243) | (0.02) | (0.352) | (0.084) | (6) | (1) | (5) |
| Cytosol | 0.76 | 0.222 | 0.19 | 1.073 | 0.06 | 3.258 | 0.500 | 30 | 36 | 34 |
| | (0.16) | (0.134) | (0.12) | (0.718) | (0.04) | (0.745) | (0.066) | (23) | (3) | (19) |

The different decays found in punctate and elongated mitochondria can be interpreted on the basis of the findings of DASPMI emission in mitochondria exposed to membrane potential manipulating conditions (Table 3.9) and in the light of the intracellular differences described. Accordingly, punctate ones exhibit fluorescence decays typical for mitochondria with high membrane potential. In comparison to elongated mitochondria, the fractional intensity of punctated mitochondria pertaining to LE state ($f_1$) has decreased by 10 % and fractional intensity ($f_3$) of TICT state has increased by 11 %. The decay parameters for elongated and punctated mitochondria were calculated from the fluorescence decays obtained from 20 and 4 different cells, respectively.

### 3.3.4.2 Cells in Different Physiological Conditions

Table 3.9 shows mean values of fluorescence decay kinetics of several DASPMI stained mitochondrial regions in 20 living XTH-2 cells and when exposed to poisons (4 cells) manipulating the energy status of a cell as are cyanide (KCN) to inhibit respiration by blocking complex IV function, nigericin which is known to increase inner mitochondrial membrane potential by electroneutral $K^+/H^+$ exchange, and CCCP a powerful uncoupler of respiratory chain activity from oxidative phosphorylation due to its protonophore character. In addition, average lifetime parameters of DASPMI over several mitochondrial regions under conditions increasing the membrane potential, i.e. after treatment with ATP and/or substrate (glutamate & malate) from 4 permeabilized XTH-2 cells are as well summarized.

Control values are in the range of those shown in Table 3.6 and 3.7. In KCN treated cells $\tau_1$ is in the range of control mitochondria with locally lower membrane potential (e.g. cell periphery), but $a_3$ is higher than in control. In the presence of nigericin, mitochondria membrane potential can be considered to be close to its maximum. This is represented by almost exclusive emission at very short $\tau_1$ and almost no contribution of $\tau_3$, indicative of a polar environment, also $\tau_2$ contribution to decay is only one third that in the control condition. Under the influence of ATP and/or substrate (glutamate & malate), in addition to similar shortening of $\tau_1$ as in the case of nigericin, increase of $\tau_2$ and $\tau_3$ with increasing membrane potential are evident. When treated with CCCP, DASPMI was promptly released in to cytosol with diffuse background. The lifetime values for CCCP treated cells predominantly arise from diffuse cytosol fluorescence, also evident from very high contribution (8 %) of $\tau_3$.

Control cells differ from nigericin treated cells by 5 % higher $f_1$ and 10 % less $f_3$. In the presence of KCN or CCCP, $f_3$ is higher than in control conditions. The $f_1$ and $f_2$ values of KCN treated cells are nearly equal, as is the case for peripheral mitochondria shown in Figure 3.26. The $f_1$ values of control and cells in the presence of ATP and/or substrate are

**Table 3.9 Influence of lifetime parameters of DASPMI in living XTH2 cells under conditions manipulating membrane potential.** Analysis was performed over several mitochondrial regions of interest from 20 control cells and 4 cells each under the influence of drug. The high standard deviations (shown below the decay parameters in parenthesis) result from biological variations occurring if measured on single cell or single mitochondrion level (compare values in <u>Table 3.6</u> and <u>3.7</u>).

| Condition | $a_1$ | $\tau_1$ (ns) | $a_2$ | $\tau_2$ (ns) | $a_3$ | $\tau_3$ (ns) | $<\tau>$ (ns) | $f_1$ (%) | $f_2$ (%) | $f_3$ (%) |
|---|---|---|---|---|---|---|---|---|---|---|
| Control | 0.74 | 0.159 | 0.23 | 0.701 | 0.03 | 2.540 | 0.357 | 33 | 45 | 22 |
| | (0.05) | (0.051) | (0.04) | (0.115) | (0.01) | (0.227) | (0.078) | (6) | (4) | (5) |
| Nigericin | 0.91 | 0.038 | 0.07 | 0.699 | 0.01 | 2.868 | 0.118 | 27 | 41 | 32 |
| | (0.06) | (0.028) | (0.05) | (0.063) | (0.01) | (0.259) | (0.064) | (9) | (3) | (8) |
| ATP | 0.86 | 0.093 | 0.13 | 0.762 | 0.02 | 3.160 | 0.229 | 31 | 45 | 24 |
| | (0.06) | (0.058) | (0.05) | (0.104) | (0.01) | (0.134) | (0.113) | (7) | (4) | (4) |
| Glutamate & malate | 0.90 | 0.080 | 0.09 | 0.812 | 0.01 | 3.343 | 0.185 | 32 | 43 | 25 |
| | (0.06) | (0.070) | (0.05) | (0.141) | (0.01) | (0.430) | (0.132) | (9) | (1) | (8) |
| KCN | 0.73 | 0.210 | 0.21 | 0.767 | 0.05 | 2.465 | 0.445 | 35 | 36 | 29 |
| | (0.05) | (0.027) | (0.04) | (0.110) | (0.01) | (0.308) | (0.030) | (5) | (6) | (4) |
| CCCP | 0.73 | 0.171 | 0.20 | 0.849 | 0.08 | 2.969 | 0.512 | 24 | 33 | 43 |
| | (0.03) | (0.038) | (0.03) | (0.205) | (0.03) | (0.213) | (0.110) | (3) | (6) | (7) |

about the same. This is due to the increase of inner membrane rigidity in very few cases of low membrane potential peripheral mitochondria of ATP treated cells. This behaviour in the presence of ATP was in addition to the increase of membrane rigidity with increasing potential. The increase of membrane rigidity with increasing membrane

potential is apparent from increase of $\tau_3$ for high membrane potential punctate mitochondria or in the presence of nigericin. In isolated mitochondria and vesicles, lipid fluidity changes and the membrane potential were found not to be kinetically coupled (O'Shea et al., 1984).

### 3.3.4.3 Interpretation of Fluorescence Decay Data

In Table 3.6 decrease in lifetime with increasing intensity is in accordance with our previous studies in solvents where quenching of lifetime with increasing solvent polarity was shown. While an increase in lifetime can be due either to an increase of viscosity or decrease of polarity. The reduction in lifetime and quantum efficiency is primarily due to the polarity of the medium. To further understand its viscosity dependent behavior in living cell, lifetime of DASPMI in nucleus, cytosol and nucleoli have been compared with mitochondria of different morphology (Table 3.8). An increased contribution of longer lifetime in nucleus and nucleoli was evident, with the longest lifetimes in nucleoli. This is consistent with the increased red fluorescence found in emission fingerprint of nucleus and nucleoli typical for dye immobilization by high viscosity of its environment typical for the highly packed nucleoproteins in nucleoli (Figure 3.24). Previously, groove binding of DASPMI with the nucleic acids (Kumar et al., 1993) was reported, which also would result in increased lifetime.

In comparison to elongated mitochondria, the shortening of $\tau_1$ in punctate mitochondria (Table 3.8) signifies the high local mitochondrial membrane potential. The low contribution of $f_1$ in spherical mitochondria, as in the cases of ROI 1, 2 and 4 of Table 3.6 wherein the mitochondria have higher membrane potential is notable. This is in accordance to solvent photophysics, wherein the charge-transfer state becomes the low-energy state in solvents of higher polarity and consequently emission from locally excited state diminishes. In comparison to the elongated, higher transmembrane potential in punctate mitochondria is accompanied with an increase in compactness of the mitochondrial inner membrane as suggested from the increase of $f_3$ by 10 %.

In slightly photodamaged mitochondria the average decay time is higher than in morphologically "healthy" mitochondria (comp. values in Table 3.6 and 3.7). In this photo-impaired cell average lifetime increases with increasing proximity to the nucleus (Figure 3.26, Table 3.7). This corresponds to our previous ethanol/glycerol mixture study, wherein significant lifetime changes without significant changes in relative contributions of the three states were measured at 560 – 580 nm (Ramadass & Bereiter-Hahn, 2007). Also, the increase of all the three lifetimes simultaneously suggests a viscosity dependent phenomenon. Hence, the increase of lifetime as we proceed towards the nucleus might be due to the increased packing of lipids in the inner-mitochondrial membrane of photo-injured mitochondria. Decreased membrane fluidity would then become manifest as an increase in DASPMI lifetime (in particular $\tau_3$), with small changes in contributions at the wavelength band measured.

Further substantiation of the above interpretation came from the influence of ionophores and uncouplers on mitochondrial membrane potential (Table 3.9). Conditions enhancing mitochondrial membrane potential, cause considerable shortening of $\tau_1$ (159 ps to 38 ps), with simultaneous increase in its contribution. DASPMI in energized mitochondria exhibits a behaviour similar to mono-exponential decay ($\tau = 6$ ps) in the polar solvent water (Ramadass & Bereiter-Hahn, 2007) but still with much longer decay and thus quantum yield. In comparison to control conditions, they are as well associated with decreased contribution ($a_2$ and $a_3$) and no considerable changes in lifetimes - $\tau_2$ and $\tau_3$. In contrast, the decrease of membrane potential by addition of KCN changes $\tau_1$ from 159 ps to 210 ps (in XTH-2 cells cyanide does not fully abolish membrane potential). This shows the direct influence of membrane potential on lifetime ($\tau_1$) associated with locally excited state and not significantly on charge transfer states ($\tau_2$ and $\tau_3$), which can be interpreted by dye molecules orienting themselves with the positive pyridinium in the proximity of proton rich inter-membrane space and the aniline moiety being located in the hydrophobic regions of the inner membrane.

The ground state dipole moment of DASPMI is largely stabilized by the local electric field and polar environment surrounding the positively charged methyl pyridinium ring. Upon excitation, DASPMI first reaches LE state that is confined to the positively charged methyl pyridinium ring. Further relaxation of the excited state by emission from charge transfer states, is largely confined now to the aniline ring located in the hydrophobic regions of the inner membrane. The TICT state lifetime $\tau_3$ is then expected to depend on the compactness of inner membrane aswell. The increased lifetimes in comparison to solvents are due to the absence of solvation dynamics. Lifetime analysis of red edge fluorescence (using LP 590 nm) from DASPMI stained XTH2 cells exhibited a higher contribution of $\tau_3$ up to 18 %, with a consequently decreased contribution of the shorter lifetime ($\tau_1$). This is typical of formation of consecutive excited states from initial excited molecule, such as LE→ICT→TICT.

### 3.3.5 Steady-State Fluorescence Anisotropy

Fluorescence polarization measurements provide useful information on the flexibility of molecules. A high anisotropy means that the probe does not change its molecular configuration and orientation while being in the excited state. Hence, emission anisotropy of DASPMI stained mitochondria in living cells of various types was determined using an inverted epi-fluorescence microscope with polarizer and dual-view system attached. Considering the range of fluorescence decay time of several tens of picoseconds to a few nanoseconds (Table 3.6 – 3.7), anisotropy of DASPMI will reveal intramolecular kinetics (i.e. twist) rather than molecule motions within the membrane.

Representative images of the distribution of polarization resolved fluorescence of DASPMI in mitochondria of living XTH2 cells are shown in Figure 3.27. Apart from regions of higher intensity near the nucleus, sub-mitochondrial zones of higher membrane potential revealed from higher DASPMI intensity were found to have higher anisotropy as well (arrowheads in inserts in Figure 3.27). Anisotropy values varied from 0.05 to 0.4 (Figure 3.27), indicating a wide range of torsional motions about the flexible single bonds
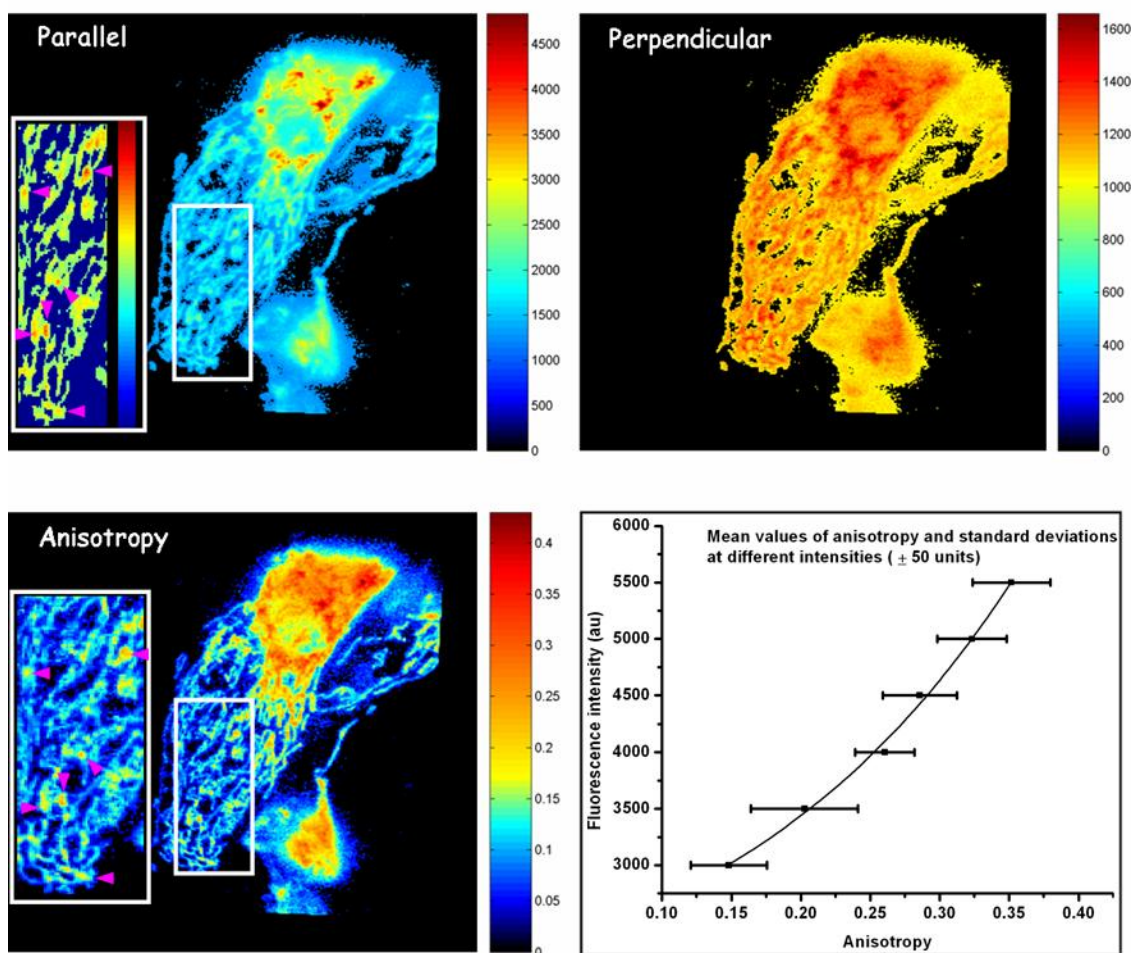
**Figure 3.27** *Distribution of polarization resolved fluorescence intensities and corresponding anisotropy values of DASPMI stained XTH2 cells. The very distinct high anisotropy at high intensity regions (inserts) inside several individual mitochondria is apparent. Such sub-mitochondrial zones of higher membrane potential are known to exist from previous studies in XTH2 cells. The plot of mean anisotropy values and corresponding pixel fluorescence intensities (± 50 units) were fitted to an exponential function of the form:* $y = y_0 + Ae^{(x/t)}$. *(Bar 5µm)*

adjoining the olefinic double bond. The twists about the single bonds may well be modulated by the local electric field and membrane fluidity. These two effects are indiscernible by steady-state anisotropy measurements. The increase of anisotropy with membrane potential has been demonstrated by plotting the mean values of anisotropy and
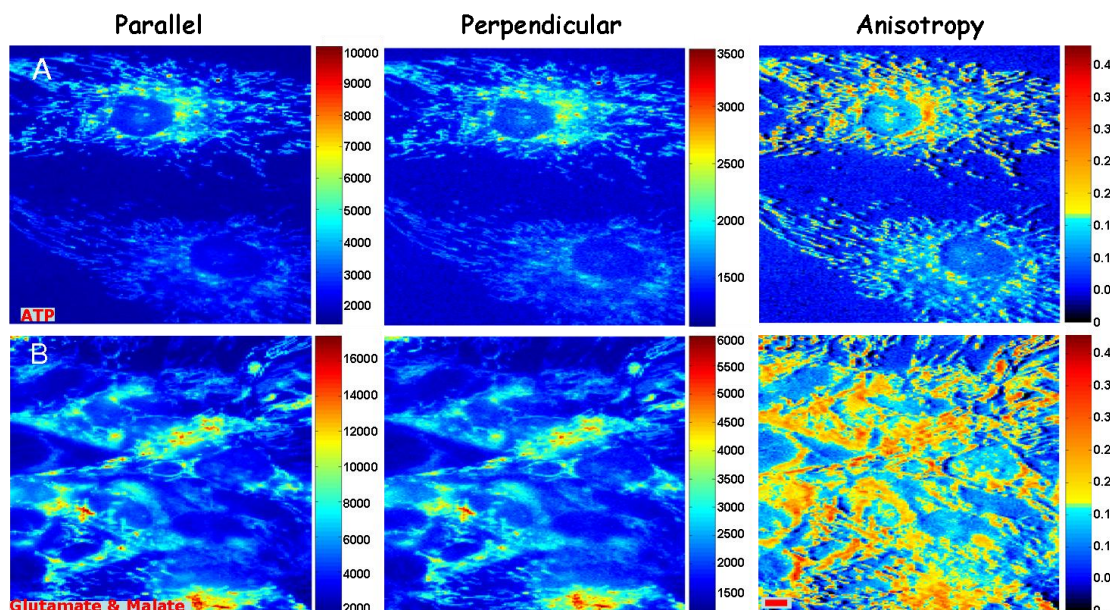
**Figure 3.28** *Anisotropy and polarization resolved fluorescence intensity distribution of DASPMI stained XTH2 cells after saponin permeabilisation in the presence of ATP or substrate (glutamate & malate).* *Higher anisotropy values under increasing membrane potential conditions are evident.*

standard deviations at different pixel intensities ($\pm$ 50 au) corresponding to total steady-state fluorescence (Figure 3.27). Anisotropy values were found to increase exponentially with increasing fluorescence intensity (Figure 3.27).

A previous study on distribution of DASPMI in isolated mitochondria showed a log-normal dependence of DASPMI concentration in mitochondria and membrane potential mediated changes caused by valinomycin-mediated potassium uptake (Mewes & Rafael, 1981). Accordingly the exponential correlation of DASPMI fluorescence and its emission anisotropy (Figure 3.27) implies the linear dependence of DASPMI emission anisotropy on mitochondrial membrane potential.

To understand the response of DASPMI to the influence of the local electric field, cells were permeabilized to allow for external control of mitochondrial energy status. Mitochondrial membrane potential was increased by the addition of ATP and substrates
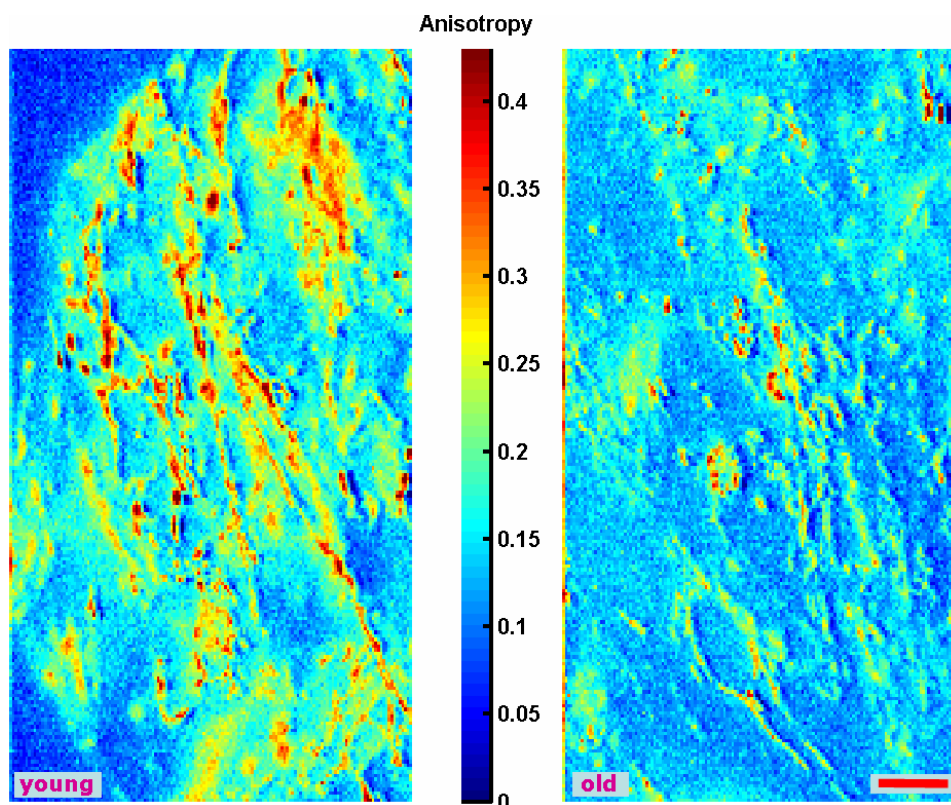
**Figure 3.29** *Emission anisotropy of DASPMI in young (passage 6) and old (passage 28) chicken embryo fibroblasts. Lower anisotropy values of aged CEF cells are due to their lower mitochondrial membrane potential. (Bar 5µm)*

(glutamate and malate). Polarized emission intensities and anisotropy distribution of representative XTH2 cells are shown in Figure 3.28. Fluorescence intensities as well as anisotropy values of DASPMI in mitochondria increased on addition of ATP and/or substrates to saponin-permeabilized cells (Figure 3.28).

Because of severe loss of dye molecules from the mitochondria in the presence of uncouplers, another physiological condition has been used to demonstrate differences of mitochondrial membrane potential by anisotropy. Decrease of mitochondrial membrane potential is a widely found property in senescent cells. Therefore DASPMI fluorescence anisotropy has been compared in young and old chick embryo fibroblasts (CEF) (Figure 3.29). The anisotropy in mitochondria of young cells (passage 6) was found to be uniform

and higher, in comparison to the old (passage 28) CEF cells. This correlates to the reduced uptake of DASPMI in old CEF cells. Mean values of anisotropy and standard deviations at different total pixel fluorescence intensities ($\pm$ 50 units) in young and old cells are shown in Figure 3.30. The initial, nearly linear increase of anisotropy in response to mitochondrial membrane potential (as visualized by increased fluorescence intensity) in old cells subsequently coincides at 5000 au intensity with young cells. The higher membrane potential in young CEF apparent from its higher intensity values exhibits sharp increase of anisotropy thereafter. The mean anisotropy values and corresponding fluorescence intensities from young and old CEF cells were exponentially correlated (Figure 3.30). Hence, membrane-potential-dependent anisotropy in DASPMI has the advantage of giving comparable measure of membrane potential from different cell types stained with different concentrations due to their independence from absolute intensity.
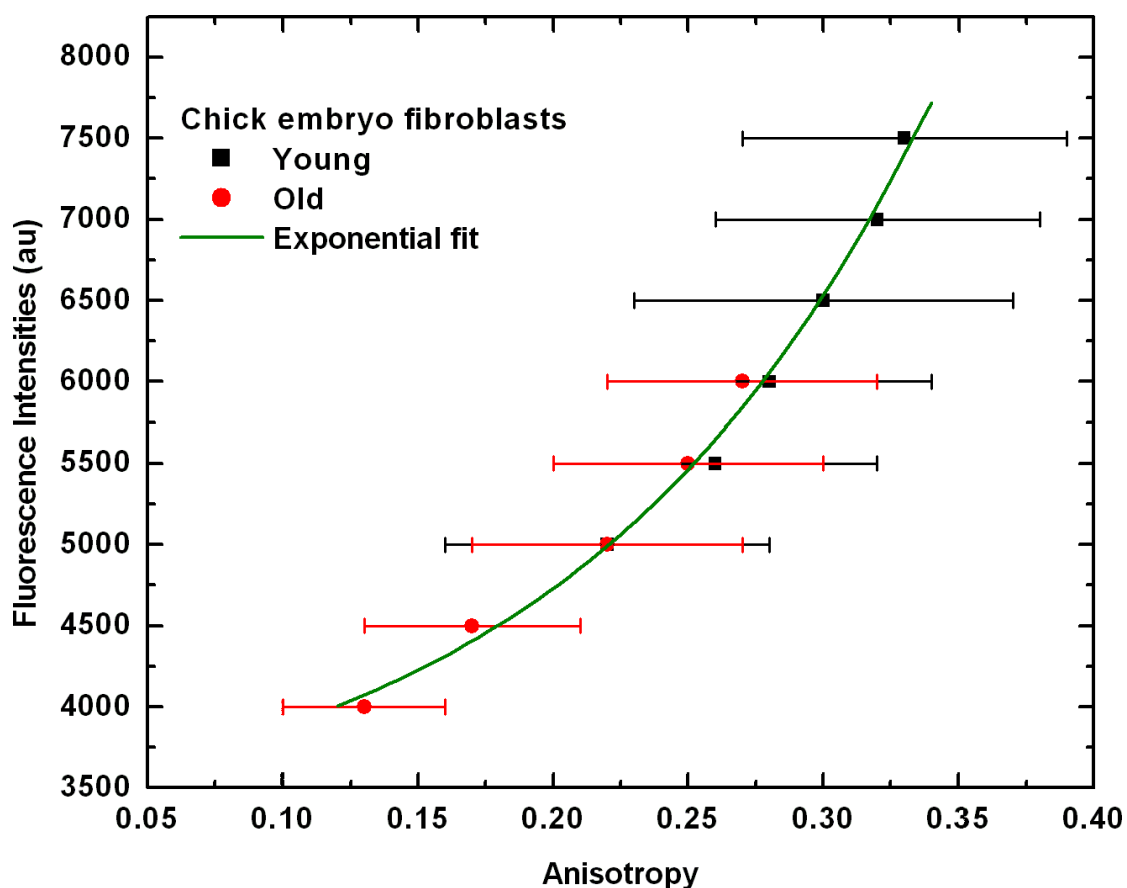
**Figure 3.30** *Mean values of anisotropy and standard deviations at different intensities (± 50 units) in senescent chick embryo fibroblasts (CEF). Mean pixel fluorescence intensities (± 50 units) from the summation of horizontally and vertically polarized steady-state intensity images of senescent CEF shown in* Figure 3.29 *have been plotted against mean anisotropy. The plot was fitted to an exponential function of the form:* $y = y_0 + Ae^{(x/t)}$ *. The consistent increase of anisotropy with fluorescence intensity and the loss of membrane potential apparent from low values of anisotropy in senescent CEF are evident.*

### 3.3.6 Discussion

The styryl dye DASPMI has a de-localised $\pi$ electron system with hydrophobic and hydrophilic regions. Because of its positively charged methylpyridinium moiety and hydrophobic aniline moiety the dye is able to diffuse easily between the various compartments of the cell (Figure 3.31). The electrophoretic force generated by the interaction of DASPMI with the membrane potential across the plasma membrane (-70 mV) and mitochondrial inner membrane (-150 mV) guides the dye into mitochondria. This was confirmed by uptake kinetics in saponin permeabilized XTH2 cells, which took longer time for saturation in mitochondria because of lack of pre-accumulation in the cytoplasm. From time course steady-state intensity measurements of DASPMI stained XTH2 cells, it was found that DASPMI localizes in the following order of preference – polarized mitochondria, nucleoli and cytosol. When CCCP was added to the stained XTH2 cells, DASPMI was promptly released from the mitochondria into the cytosol followed by an accumulation in the nucleoli.

The three-exponential decay kinetics of DASPMI in living cells (as found in glycerol) with lifetimes of $159 \pm 51$ ps ($74 \pm 5$ %), $701 \pm 115$ ps ($23 \pm 4$ %) and $2540 \pm 227$ ps ($3 \pm 1$ %) advocates for a viscous microenvironment. The three-exponential decay kinetics in living cells, representative of LE, ICT and TICT state are as well obvious from the emission finger print (Figure 3.24 A). Previously, investigation of time-resolved emission spectra of DASPMI in chloroform revealed a shoulder at shorter wavelengths pertaining to the locally excited state. The absence of green shoulder in the emission spectra of nucleoli is in accord with the more polar environment in ribonucleoprotein assemblies. The high sensitivity of DASPMI to mitochondrial membrane potential is evident from its prompt release from mitochondria on the addition of CCCP. The presence of hydrophilic and lipophilic domains, green shoulder in mitochondrial emission fingerprint and an absorption maximum between 460 – 470 nm in mitochondria ascertain the localisation of DASPMI in the inner mitochondrial membrane.
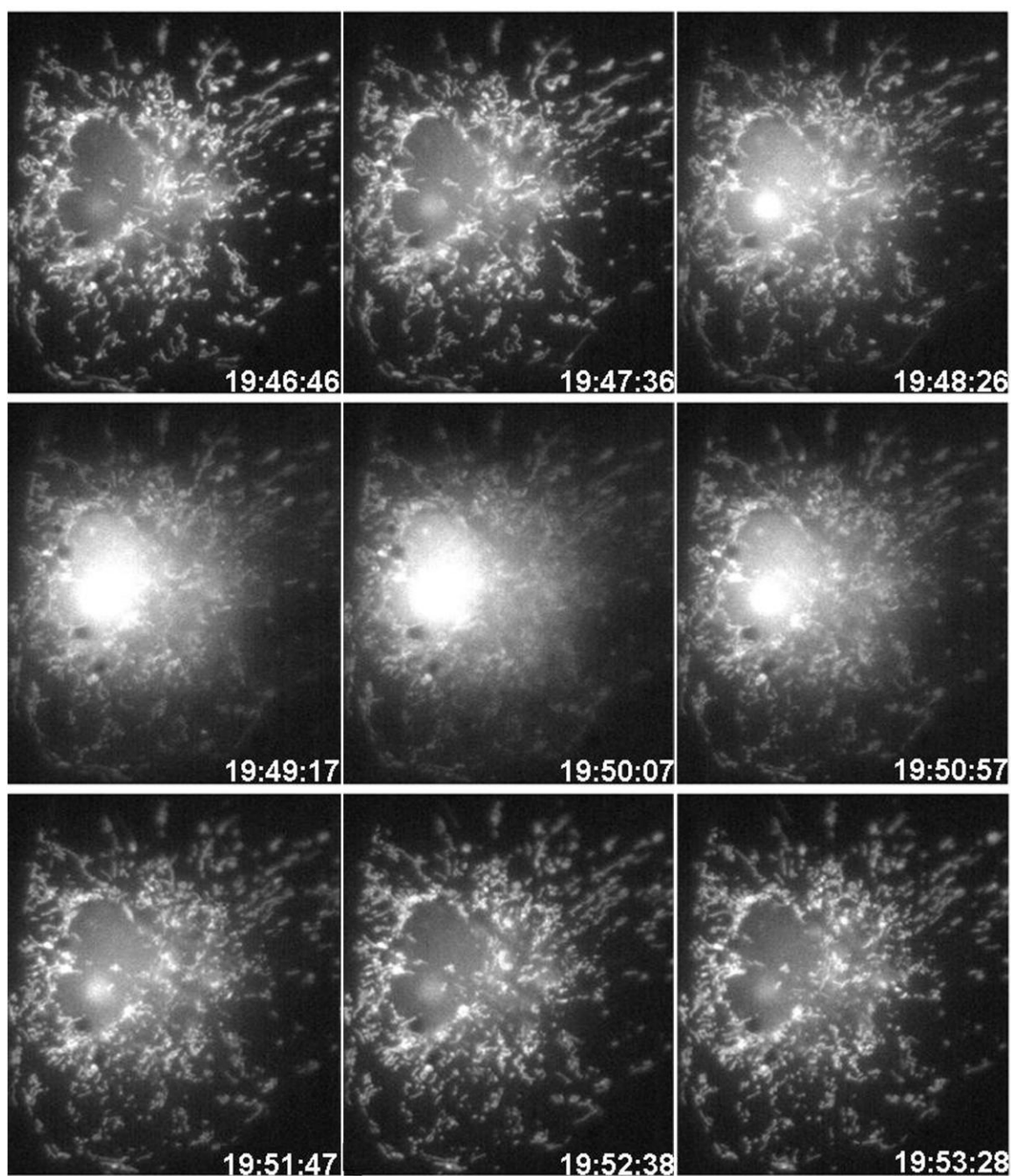
**Figure 3.31** *Diffusion of DASPMI between various compartments of the cell. DASPMI stained XTH2 cells were treated with nigericin and immediately imaged. Above raw* Sensi-Cam *images are part of a time sequence acquired over every 10 seconds. The cells remained in focus during the acquisition and the DASPMI was found to diffuse freely between different compartment of the cells including nucleus and nucleoli, before the return of fluorescence distribution to one before niegricin addition.*
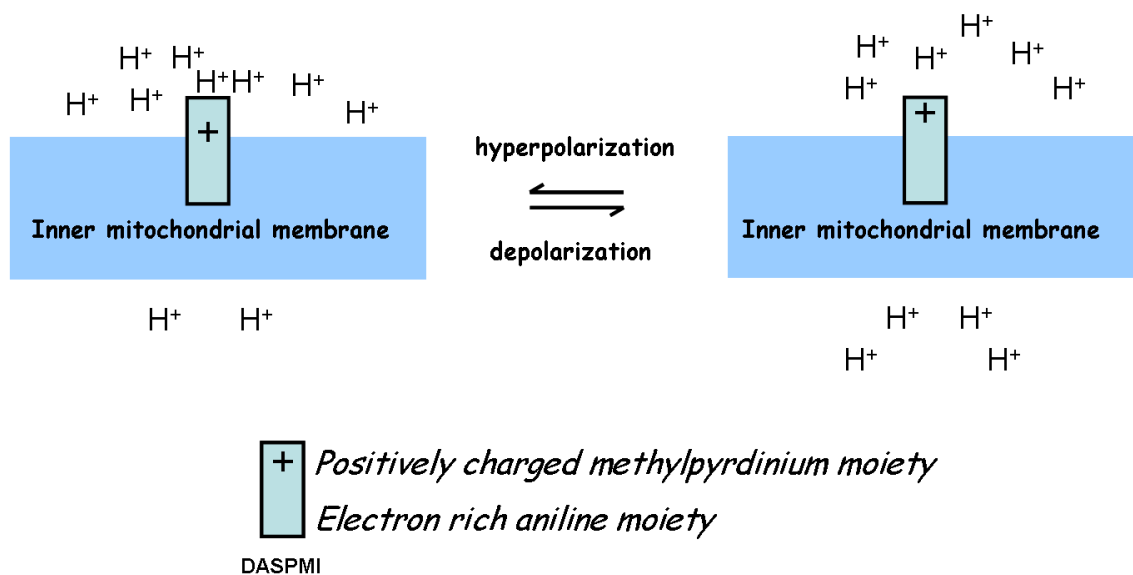
**Figure 3.32** *Location and orientation of DASPMI in the inner membrane. DASPMI preferentially locates its positively charged methyl pyridinium ring in the aqueous interface facing the outer mitochondrial membrane and its hydrophobic moiety along the hydrocarbon chain. As for orientation, it aligns itself along the local electric field for a maximum electrochromic response. Under high membrane potential conditions, the delocalization of π-electrons leads to a less polar structure imposing steric constraints about the single bonds neighboring the olefinic double bond.*

Considering the direct influence of mitochondrial membrane potential only on the shortest lifetime ($\tau_1$) of DASPMI and its remarkable shortening in energized mitochondria advocates the partial insertion of DASPMI in the outer-leaflet of inner mitochondrial membrane (Figure 3.32). This proposition is confirmed by the occurrence of disparate changes between lifetimes pertaining to locally excited state ($\tau_1$) and charge-shift states of DASPMI stained energized mitochondria. Furthermore, the occurrence of difference of more than 30 times between $\tau_1$ and $\tau_3$ (in energized mitochondria), excitation maxima of 470 nm in XTH cells (between DMSO and chloroform) and emission maxima of 565 nm (same as chloroform) support our deduction. A blue shift in both excitation and emission spectra is expected for molecules only partially inserted into the lipid environment (Loew et al., 1978; Loew et al., 1979; Loew & Simpson, 1981; Loew, 1996). The partial insertion of DASPMI in the outer-leaflet of inner mitochondrial
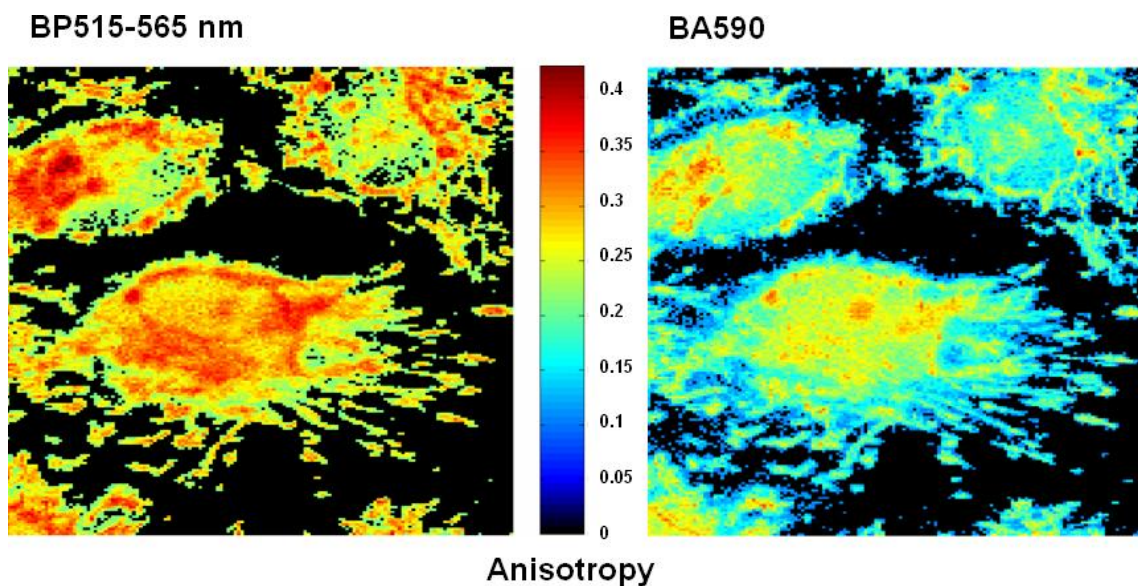
**Figure 3.33** *Emission wavelength dependent anisotropy of DASPMI. In response to high membrane potential condition, electrons are withdrawn from the electron rich aniline moiety leading to less polar DASPMI structure. Consequently, increase in rigidity about single bonds (i.e. double bond like character) neighboring olefinic double bond leads to an increase in anisotropy at the shorter wavelengths.*

membrane ensures the favorable polar environment for the positively charged methylpyridinium moiety and hydrophobic aniline moiety along the non-polar hydrocarbon chains of lipids. Under this scenario, photoabsorption largely confined to the positively charged methylpyridinium moiety can be expected to have absorption maxima of 470 nm and emission predominantly confined to aniline moiety to have emission maxima of 565 nm as is observed in living cells. This differential solvation has been previously been described for other styryl dyes and has as well been observed by us in phospholipids vesicles wherein absorption maxima was 430 nm and emission maxima 545 nm. In comparison to phospholipids vesicles, the red-shift of absorption maxima in mitochondria could be due to partial de-localization of pi-electrons under the influence of a local electric field. This assumption of only partial de-localization of pi-electrons and not a complete one is confirmed by the decrease of steady-state anisotropy at longer emission wavelengths (Figure 3.33). A complete shift of positive charge to the dimethyl

amino group would shift the absorption maxima and anisotropy to higher values, as has been shown to be the case in chloroform (Ramadass & Bereiter-Hahn, 2007).

The excited state dynamics of DASPMI depends on the influence exerted by the local electric field on DASPMI charge distribution and its local environment. $\tau_1$ attributed to fluorescence from initially excited state is largely localized in the positively charged methyl pyridinium moiety. $\tau_2$ and $\tau_3$ are the excited state lifetimes due to de-excitation from ICT and TICT state pertaining to the aniline moiety in the lipid environment. The shortening of $\tau_1$ in energized mitochondria is due to the increase in concentration of protons in the intracristael space and hence quenching of fluorescence from the methyl pyridinium moiety. Previous electron micrograph studies of DASPMI stained mitochondria in XTH2 cells allowed the proposition that selective accumulation in cristae would render photodamage of inner mitochondrial membrane (Bereiter-Hahn & Vöth, 1998). Quenching of DASPMI fluorescence by energy transfer to cytochromes can almost be excluded because of the prolonged decay times in the presence of cyanide when all the cytochromes should be in the reduced state with strong absorption bands.

The accumulation of DASPMI in mitochondria is a membrane potential driven process (Mewes & Rafael, 1981) accompanied by a strong change in quantum efficiency while changing environment from the aqueous solution to the mitochondrial membrane. Although much higher than in saline, quantum efficiency at mitochondrial inner membrane is largely determined by the quenching of fluorescence from locally excited state due to higher proton concentrations. Upon addition of CCCP, equal number of protons exists across the inner mitochondrial membrane destroying the membrane potential. Under such conditions, the charge of positively charged methyl pyridinium moiety increases leading to a more polar structure of DASPMI at the inner membrane, less quenching of $\tau_1$, but now the molecules are able to diffuse freely to other compartments of the cell. When higher concentrations of DASPMI are used to measure mitochondrial membrane potential, other possible localisations and less specific staining will decrease its sensitivity to mitochondrial membrane potential.

The influence of membrane potential on the torsional motions of the probe molecule is expected when considering the partial insertion of DASPMI in the inner mitochondrial membrane, partial de-localization of π-electron system and lipid fluidity changes evident from variation of $\tau_3$ by as much as 20 %. The fluorescence from locally excited state corresponds essentially to an electronic configuration found immediately upon excitation. Any changes in inner-membrane fluidity should have negligible effect on the fluorescence characteristics from locally excited state. Under high membrane potential condition, decrease of fractional fluorescence contribution from locally excited state leads to an increase in fluorescence from charge transfer states. Depolarization of fluorescence emission of DASPMI is essentially due to an increase in the fraction from TICT state which is associated with fluorescence from a twisted conformation of DASPMI. Consequently, the changes in anisotropy are due to modulation of TICT state fluorescence by changes in inner membrane fluidity or by changes in rigidity of single bonds neighbouring the olefinic double bond. Since the local electric field changes and membrane fluidity are not kinetically coupled, the fluorescence lifetime distribution of DASPMI is obscured. However, as the membrane rigidity increases with increasing membrane potential, mean fluorescence anisotropy of DASPMI (within the standard deviation, Figure 3.27 and Figure 3.30) may still correspond linearly to changes in average mitochondrial membrane potential.

# 4. CONCLUSIONS

## 4.1 TRPV4-Microfilament Interactions

Time- and space-correlated single photon counting (TSCSPC) has been used to show the spatial coupling of TRPV4 and actin in living cells. Addition of the spectral dimension to fluorescence decay data in FLIM have clearly elucidated the close association of TRPV4 and actin by a simultaneous decrease in donor lifetime (TRPV4-CFP) and increase in acceptor fluorescence (actin-YFP). The simultaneous measurement is necessary to be sure that the variations in lifetime are not due to other photophysical mechanisms or background fluorescence. This sensitive technique requires very low excitation light, in contrast to intensity based FRET measurements, where photobleaching and photoconversion (Valentin, 2005) might occur.

As an alternative donor fluorescent protein, an improved variant cerulean (Rizzo et al., 2004), showed an encouraging improvement in its photophysical parameters (quantum yield and extinction coefficient) and was suggested to be a better substitute to CFP. While recent investigations (Koushik et al., 2006) have revealed that cerulean could change its lifetime significantly when tagged to different proteins. Hence, the choice of FRET pair is crucial. Therefore, careful observation of fluorescence with temporal, spectral and spatial resolution has been approached to elucidate the mechanism of fluorescence quenching and prove spatial proximity.

As shown previously, TRPV4 is directly involved in regulatory volume decrease (Becker et al., 2005). However, the important question what endows TRPV4 channels with mechanosensitivity (or osmosensitivity) still remains to be answered. One hypothesis is that microfilaments interacting with the channel (directly or via binding proteins) act as mechanotransducers rendering TRPV4 mechanosensitive. The impairment of RVD by the disruption of actin cytoskeleton (Downey et al., 1995; Foskett & Spring, 1985; Khalbuss & Wondergem, 1991; Linshaw et al., 1992) and RVD related changes in cell elasticity

([Bereiter-Hahn et al., 1995](#)) are in favour of such an interpretation. The presence of high F-actin content at the interaction sites (microspikes, microvilli and lamellipodia; [Figure 3.1](#)), which are osmotically highly exposed areas further supports this theory. By studying living cells using TSCPSC, for the first time, we were able to prove the very close proximity (< 8 nm) between F-actin and the channel protein. This intimate arrangement may form a structural framework for transduction of mechanical forces to the TRPV4 channel via F-actin.

## 4.2 Photophysical Properties of DASPMI

Spectrally resolved decays of DASPMI at room temperature in different solvents have demonstrated the complex mechanism of DASPMI fluorescence. The added spectral dimension was necessary to simultaneously acquire lifetimes that globally describe its behaviour and the construction of emission profiles of different lifetime components. The occurrence of resonance structures, benzenoid and the quinoid form, obscures the lifetime dependence on polarity and viscosity. The delocalisation of the pi-electron system in the quinoid form increases the stiffness of single bonds neighbouring the olefinic double bond. This scenario is similar to the presence of benzenoid form in viscous solvents. In low viscous polar solvents like water, an increased quenching of fluorescence due to strong solvation and consequent effective non-radiative decay in TICT state leads to a lower quantum yield. While in high viscous glycerol, apart from solvation of the primary excited state, the non-radiative decay by the twist of flexible single bonds of the styryl group is restricted. The different rise times of secondary fluorescence found for various glycerol/ethanol mixtures ([Figure 3.21](#)) suggest an ultrafast rise time in ethanol. Hence the rise times or the formation of secondary state is dependent on solvent viscosity. The shifts of resonance balance to quinoid form in chloroform, decreases the positive charge at the pyridinium ring and flexibility of single bonds. Hence an increased rise time in chloroform, in comparison to more polar and viscous solvent ethanol.

In the non-polar solvent chloroform, a blue-emitting species corresponding to locally excited state was noticeable. In solvents of higher polarity, the locally excited state could be non-emissive or convoluted with other emissive states. Asymmetrical and structureless fluorescence emission spectra have been assigned to the existence of a locally excited state and two-state spectral relaxation of polar species ICT and TICT states.

In conclusion, based on DAS, steady-state emission anisotropy and time-resolved emission spectra a three-state model has been described quantitatively. The knowledge of DASPMI photophysics in a variety of solvents now provides the means of deducing complex physiological parameters of mitochondria, from its behaviour in living cells.

## 4.3 Fluorescence Dynamics of DASPMI in Living Cells

DASPMI was the first fluorochrome described to reveal mitochondrial membrane potential in living cells. The relationship between membrane potential and fluorescence intensity is given by a Nernst-type uptake and further modulated by changes in quantum yield. The change in quantum yield improves the ratio between cytoplasmic (aqueous) and mitochondria bound DASPMI fluorescence and allows to follow potential differences between mitochondria and even along a single mitochondrion with high speed, not possible with dyes which have to equilibrate between the mitochondrial matrix and the cytoplasm. The increase in quantum yield corresponds to the increase in fluorescence decay time which is about 6 ps in water and (on average) several hundreds of picoseconds in mitochondria. The underlying mechanisms are complicated: three different decay states have been identified, which correspond to three different conformational and charge distribution states of the styryl-dye molecule. A detailed analysis of the contributions of these states to DASPMI fluorescence enables us now to understand the interaction of this fluorochrome with mitochondrial membranes under different physiological conditions.

Spatially resolved fluorescence decays and steady-state measurements have elucidated the complex behaviour of DASPMI in living cells. The complexity of its behaviour arises from the presence of hydrophilic (electron-accepting methylpyridinium moiety) and hydrophobic domains (electron-donating aniline moiety) in its structure. The selective staining of mitochondria at low DASPMI concentration is due to the preferential localisation of the methyl pyrdinium moiety in the polar environment and hydrophobic aniline moiety along the hydrocarbon chains of the inner membrane. Under the influence of membrane potential, partial de-localisation of pi-electrons of DASPMI leads to a decrease in positive charge at the methylpyridinium moiety and thus formation of a less polar structure. The loss of mitochondrial membrane potential, as in the presence of CCCP results in the re-formation of the polar structure of DASPMI and its prompt release into the hydrophilic cytosol.

The increase in intensity of DASPMI with increasing mitochondrial membrane potential is primarily because of larger uptake of DASPMI in to mitochondria. Quantum efficiency of DASPMI decreases with increasing membrane potential and polarity of the environment, however it still is many times higher than in aqueous solution. In another mitochondria specific dye rhodamine 123, equilibrium exists between the concentration gradient of intra- and extra-mitochondria space. When these cells are brought into dye free medium, the concentration gradient induces the release of rhodamine 123 into the medium within minutes or hours (Nadakavukaren et al., 1985). When DASPMI stained cells are placed in a probe free medium, the dye remains for hours because the cell membrane is not easily penetrated and thus the electromotive equilibrium of the probe is retained inside the cell.

The variation of spectral and decay parameters of mitochondrial DASPMI, substantiate and confirm the intracellular heterogeneity of mitochondrial membrane potential. Shortest lifetime $\tau_1$ of DASPMI is a direct indicator of mitochondrial membrane potential. The influence exerted by the mitochondrial membrane potential on the

positively charged methylpyridinium moiety and the inner membrane fluidity manifest as linear changes of mean anisotropy with membrane potential.

Fluorescence anisotropy distribution of DASPMI stained XTH2 cells illustrated a wide range of anisotropy values $(0.05 - 0.4)$. Membrane-potential-dependent anisotropy of DASPMI was demonstrated in an ageing CEF cell model. The reduction of anisotropy in an aged CEF cell is in concurrence with well known supposition of decrease in mitochondrial membrane potential in aged cell cultures. In XTH2 cells, previously known sub-mitochondrial zones of higher membrane potential were apparent from higher DASPMI intensity and were found to have higher anisotropy values. Membrane potential dependent hierarchical anisotropy exemplifies the increase in rigidity of the single bonds neighbouring the olefinic bond with increasing mitochondrial potential.

Using the very complex response of DASPMI in living mitochondria to photon absorbtion, information can be derived on the energy status as well on membrane fluidity, i.e. lower membrane fluidity in spherical mitochondria than in the elongated ones has been shown for the first time by analysis of fluorescence decay parameters. This is a parameter important for inner mitochondrial protein exchange following mitochondrial fusion, an event supposed to represent a rescue mechanism in case of protein impairment.

Further studies may involve the calibration of anisotropy of DASPMI as a potentiometric probe devoid of discrepancies arising due to variances in dye uptake and the uneven staining in single cell studies using a fluorescence microscope. This can be approached by the external control of mitochondrial energy status in permeabilized cells using valinomycin mediated control of potassium ion diffusion potential. The localization of DASPMI at the mitochondrial inner membrane allows determination of inner membrane viscosity in various morphologically different mitochondrial populations and in the perspective of cellular ageing.

APPENDIX

## Time- and Space-Correlated Single Photon Counting

Time-resolved fluorescence spectroscopy and microscopy provide very useful and accurate information on various dynamic processes by the measurable response imposed by the environment on the photophysical characteristics of the fluorophore. Good quality data acquisitions are prerequisites in obtaining reliable parameter estimates. Distortions of the fluorescence response due to artifacts may lead to erroneous conclusions. Here a brief overview of the optical layout and the potential difficulties encountered at different stages of establishment of the setup and as well under daily laboratory circumstances, including the practical remedies are discussed. A variety of artifacts resulting from optical and electronic pitfalls are as well presented.

## Optical Layout

The core of a time- and space-correlated single photon counting spectroscope (Figure I) is a fast micro-channel plate detector which resolves space either along a line of measurement (DL-detector) or over a two-dimensional light sensitive area (QA-detector). The image of a fluorescence microscope is optically coupled to the photocathode of such a detector. The photocathode reacts by a burst of electrons when hit by a photon; the resulting current is amplified via two multi-channel plates (MCP) and finally reaches a delay-line or a quadrant anode (Figure 2.2). This provides an electric signal which is time correlated to the fluorescence excitation pulse and space correlated to the position the photon impinged onto the photocathode. Thus for each point of measurement a fluorescence decay curve can be generated.

In DL-detector, the fluorescence signal from microscope are collected and focused onto the entrance slit of a spectrograph wherein it is spectrally resolved. The short laser pulses
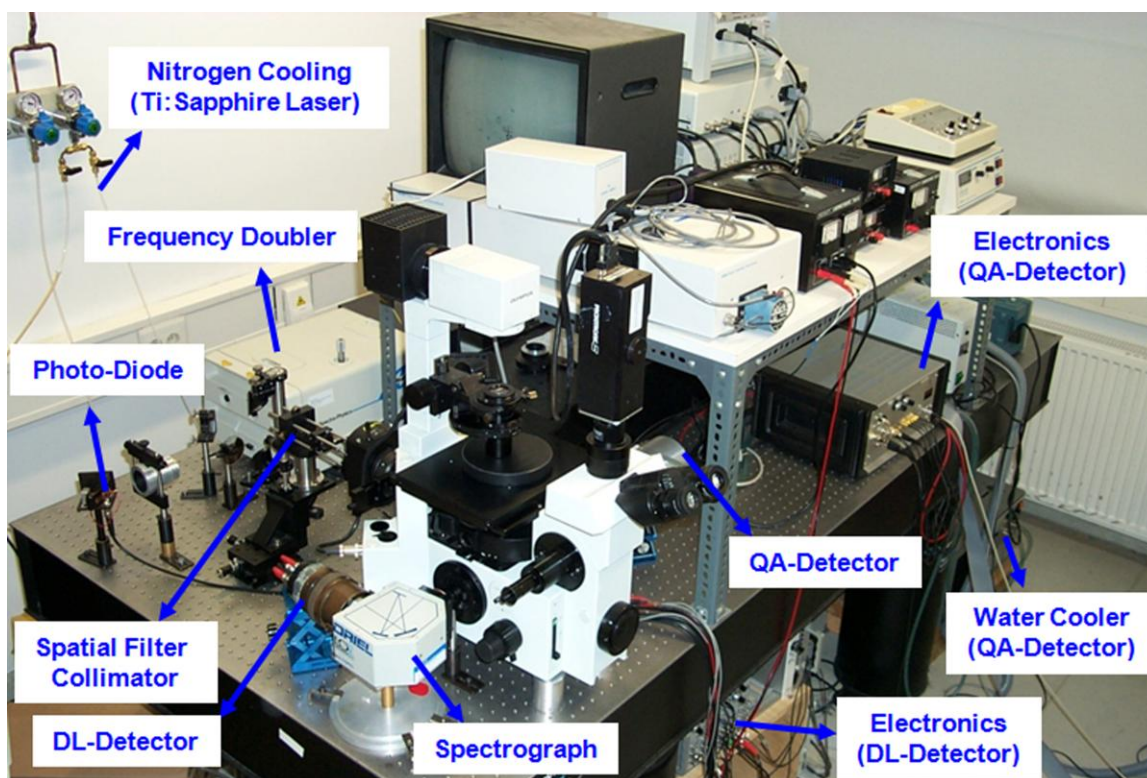
**Figure I** *Photograph of time- and space-correlated single photon counting spectroscope setup.*

(pulse duration in the range of femtoseconds or a few picoseconds) used to excite the fluorophore, also trigger a photo-diode thus allowing determination of the temporal relation between excitation pulse and the emission of fluorescence. Photon emission, its spatial coordinate in relation to wavelength and temporal information are read in to a PC via an A/D converter and a transputer (MCA). The acquisition program (SPCView) displays the temporal and spectral information as a two dimensional histogram (Figure II). The DL-detector has a maximum gain of about $1 \times 10^{6}$ at -2000 V.

In QA-detector, the incident photon produces a cone-shaped cloud of electrons at the end of second MCP, as in the case of DL-MCP-PMT above, whose centre hits the quadrant-anode at a spatial position identical to that of the photon. The charges from various quadrants are amplified, discriminated, and fed to an analog circuit for calculation of
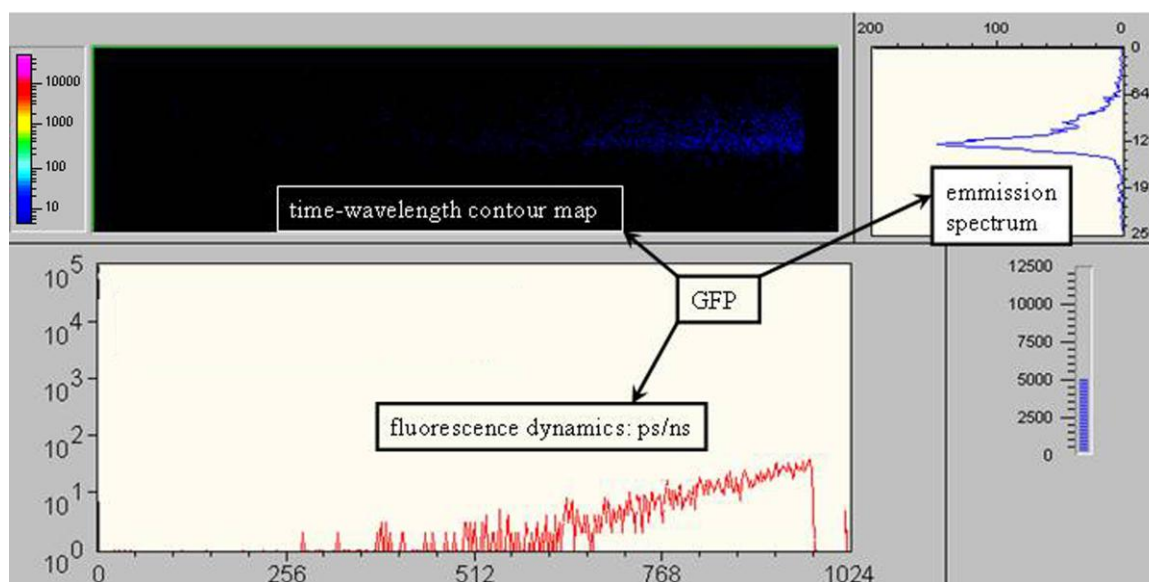
**Figure II** *DL-detector acquisition software (SPCView) displaying the GFP fluorescence decay, its emission spectra and the two-dimensional pseudo color histogram, containing temporal and spectral information.*

spatial coordinates. The timing information is derived from the auxiliary pulse from second MCP and the stop signal from the photo-diode. For a better spatial resolution, the QA-detector and microscope was optically coupled through a beam expander. Due to the travel time difference between the various incident photons, the IRF obtained from different regions of interest IRF are different and slightly shifted in time. Hence, de-convolution of IRF from fluorescence decay has to be done from the respective regions-of-interest. The QA acquisition program records the relative time of arrival of each photon and hence sequential intensity images over time may as well be obtained.


**Optical Artifacts**


**Pulsed Excitation Light Source.** Femtosecond mode-locked titanium: sapphire (Ti-Sapphire) laser was tuned between 690 and 1000 nm to obtain excitation wavelengths of 345 – 500 nm after frequency doubling. To bring the 82 MHz Ti-Sapphire optical pulse

train repetition rate down, a pulse selector module was introduced before the frequency doubling. The Ti-Sapphire was water cooled to $18^0$C and when tuned for long wavelengths (900 – 1000 nm) Tsunami head was purged with the highest purity (99.99 %) nitrogen, to prevent tuning discontinuities. It has been observed that at times during experiments a sudden drop in average laser power may occur due to long term drift in laser cavity length. Retuning resets the laser to previous intensity levels and pulse shape. A remarkable drop in laser intensity and concomitant pulse shape changes during the collection of the fluorescence decay leads to unacceptable fits of the acquired fluorescence decays. The weighted residuals and the autocorrelation function are a clear indication for a bad fit.

In addition to the monitoring of the pulse output characteristics from Ti-Sapphire laser, the output pulse characteristics from photo-diode are to be checked for any unstable operation of pulse picker. Pulse picker radiofrequency warm-up effects may create side pulses leading to different harmonic content of the excitation.

**Optical Alignment.** The frequency doubled laser pulses were optically aligned to an inverted fluorescence microscope in the epi-fluorescence mode. The frequency doubled laser pulses were spatially filtered, expanded and optically aligned to the condenser of an inverted fluorescence microscope (epi-illumination, Olympus IX70) to obtain uniform illumination over the sample area. A good IRF is a pre-requisite to obtain a higher time resolution. The instrument response function (IRF) cannot be properly determined with loosely positioned or inclined and slipping optical units. Small drifts in beam position on the diode create undesirable distortion in acquired data and increase in FWHM of IRF. The best remedy is to reduce the distance between the optical components so beam drift is less of a problem. In this work, IRF was usually obtained at the excitation wavelength using a scatterer or mirror as sample.

One of the prominent problems encountered during the establishment of the setup were prepulses in the instrument response function recorded (Figure III). The pre-pulses were
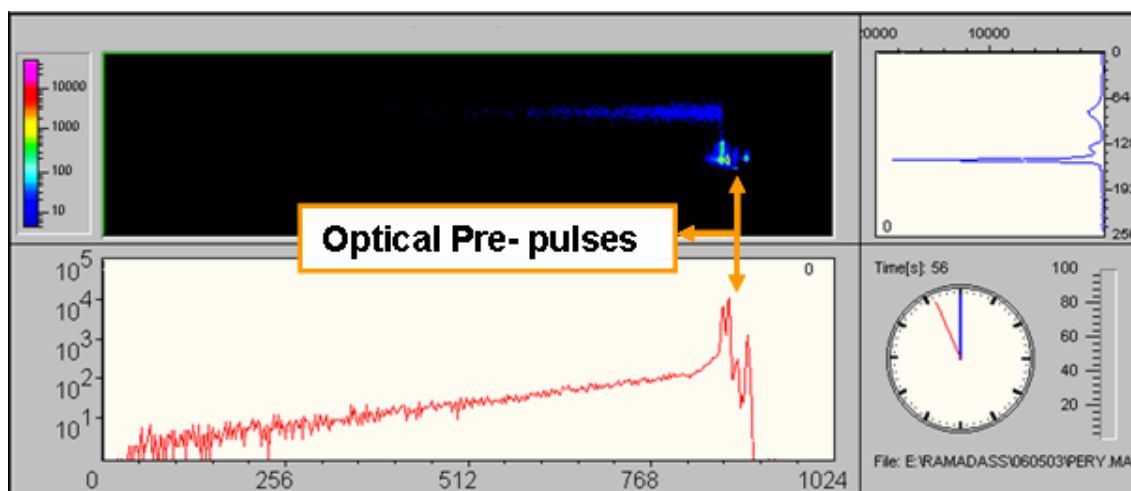
**Figure III** *Optical pre-pulses due to improper optical alignment of the system*. *The weak pre-pulses seen are due to shorter optical path taken by the excitation pulse due to direct refraction from the dichroic mirror and the bottom of the objective. Also evident is a stronger pre-pulse resulting from the DL-detector not in the focal field of spectrograph and their oblique alignment.*

attributed to direct refraction of part of the laser light by the dichroic mirror and the bottom of the objective. They were eliminated by reducing the distance between the optical components and by using a spatially filtered collimated laser source as illumination.

For the acquisition of spectrally-resolved fluorescence decays, the fluorescence collected was collected using a plano-convex lens from one of the exit port of microscope. The collected fluorescence was collimated and was further focused on the entrance slit of spectrograph. The focal field of the spectrograph should ideally be parallel to the exit face of the spectrograph and as well retain the same numerical aperture from one edge to the other.

**Electronic Artifacts**

**Pulse Pile-Up Effect.** It is important to keep the number of detected fluorescence photons ("stop") small compared to the number of excitation pulses ("start"). The pulse pile-up at Time-to-Amplitude-Converter results in distortion of counting statistics and appearance of shorter fluorescence decay.

**Linearity of Time Response of the TAC.** The linear time response of the TAC is critical for acquisition of accurate fluorescence decays. The response is nearly linear when the duration in which the TAC is in operation and unable to respond to any more signal i.e. dead time is minimized. Hence the data collection was done in reverse configuration; the detected fluorescence signal (MCP2 signal from QA- or DL-detector) was used as "start" pulse and the detected excitation pulse (photodiode signal delayed by an appropriate delay line) as the "stop" pulse.

**Constant Fraction Discriminator (CFD).** The heart of the timing circuit is the CFD. Its purpose is to detect an input analog pulse and generate a fast logic pulse with a constant fixed offset in time with respect to the pulse. Pulses from each side of the anode are amplified and then sent to a Constant Fraction Discriminator (CFD). The CFDs produce the ECL logic pulses to start and stop a Time to Amplitude Converter (TAC) which outputs an analog voltage pulse whose amplitude is proportional to the time difference of the start and stop signals. This pulse is then digitized and represents the pixel location of the input pulse. Since the delay line anode are symmetric, the start and stop designations are arbitrary until an extra delay is added on the stop side to ensure that start always comes before stop for a given pulse.

The added delay on the stop side can either be before or after the CFD. I usually add the delay before the CFD with a compact lumped-delay circuit. The lumped delay can degrade the pulse shape; however this is not much of a concern for a large ECL pulse. The alternative is to add an extra length of low dispersion cable to the input to the stop

CFD, but this is a very bulky implementation when the delays of the anode are on the order of a hundred nanoseconds.

## DL-Electronic Schemes
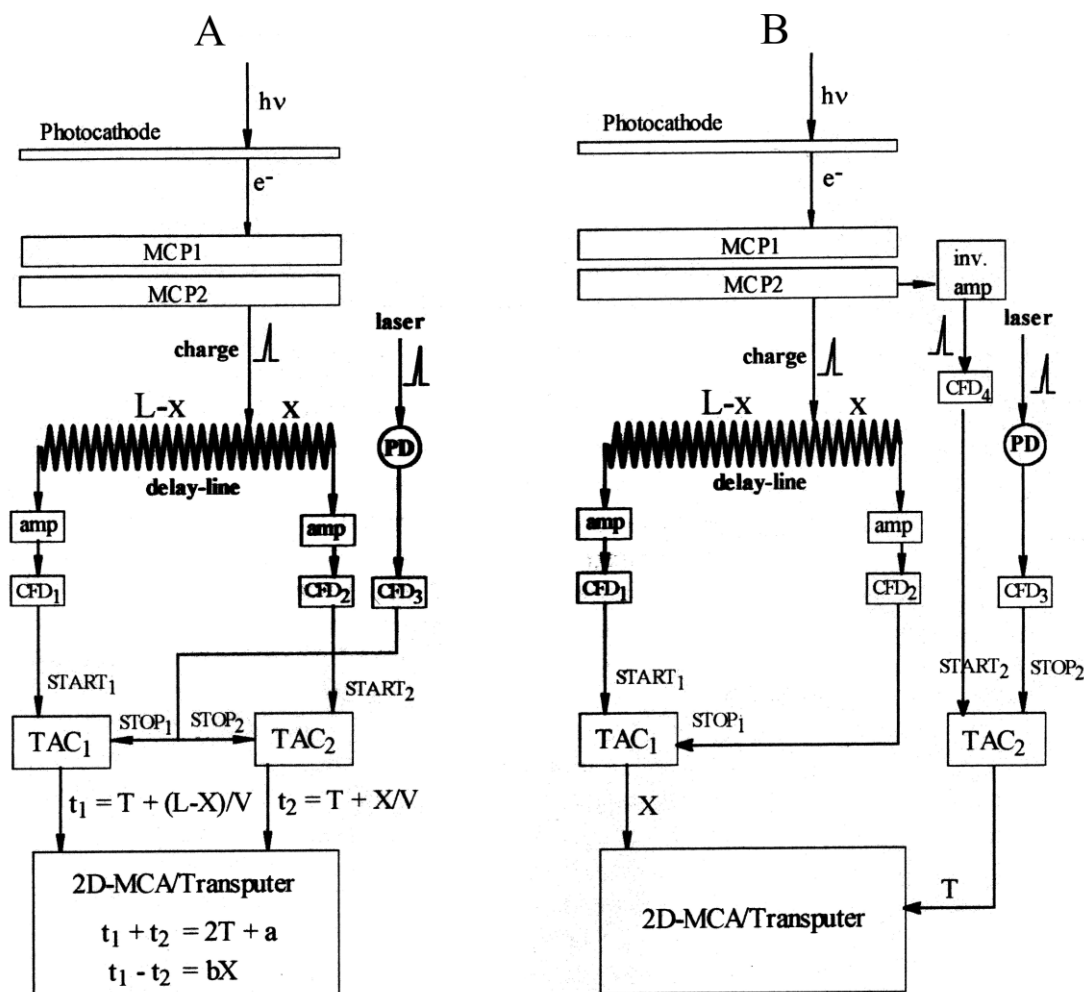


**Figure IV** *Block diagram of the symmetric (A) and asymmetric scheme (B) of operation of DL-system.* *MCP – microchannel plate photomultiplier, TAC – time-to-amplitude converter, CFD – constant fraction discriminator, MCA – multi-channel analyzer, amp – amplifiers.*
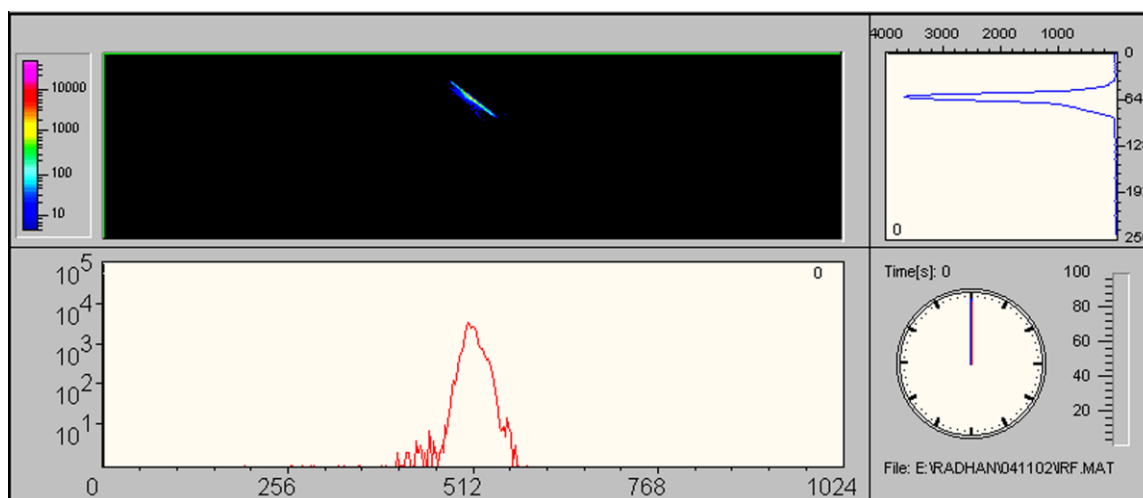
**Figure V** *Skewing of the two-dimensional histogram due to mismatch in arrival of the temporal and spectral information to 2D multi-channel analyzer.*

The delay-line splits the electric pulse, emanating from the 2<sup>nd</sup> MCP, and the difference in propagation time of both the parts yields the space-coordinate. A 2D multi-channel analyzer (MCA), equipped with transputer and local memory, calculates time- and spatial coordinate from the sum and difference (Figure IV A), respectively, of the outputs of both time-to-amplitude converters (TAC). An alternative scheme (Figure IV B) utilizes an auxillary timing signal from the 2<sup>nd</sup> MCP, resulting in independent TACs and sum/difference calculation are obsolete. The challenge encountered with the scheme 1 was that improper electronic settings may lead to skewing of the two-dimensional matrix (Figure V).

**QA-Electronic Scheme**

The electronic scheme which was used to obtain the spatially-resolved fluorescence decays using QA-detector is shown in Figure VI. The stop signal obtained from the photo-diode was amplified, delayed and was then sent to CFD. The logic pulses from CFD were then sent to QA-electronics as a stop signal.
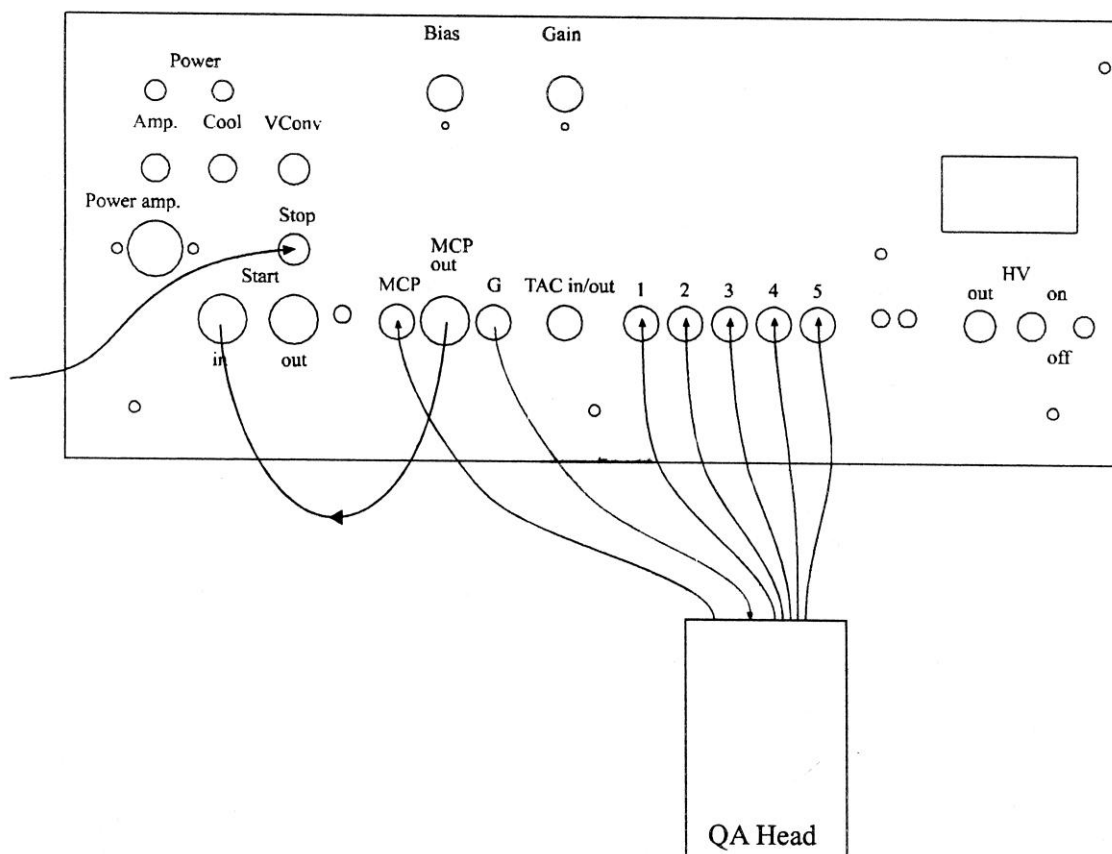
**Figure VI Block diagram of the QA-detector electronic scheme.** *The "STOP" signal in the electronic scheme is given from an external constant fraction discriminator.*

When the QA-detector head is charged, improper operation of the system such as discontinuous operation in the time domain may occur. For this reason, the QA-detector and its electronics need to be checked in test mode before any data acquisition. In test mode, all the electronics excluding the high voltage unit is checked for normal operation of the system.

## ABBREVIATIONS

| | |
|---|---|
| $\overset{0}{A}$ | Angstrom |
| ADC | analogue-digital converter |
| ATP | adenosine 5'-triphosphate |
| BA | barrier filter |
| BBO | beta barium borate |
| BP | band-pass |
| $^{0}C$ | degree Celsius |
| $Ca^{2+}$ | calcium |
| CCCP | carbonylcyanide-m-chlorophenylhydrazone |
| CCD | charge coupled device |
| CEF | Chick embryo fibroblast |
| CFD | constant-fraction discriminator |
| CFP | cyan fluorescent protein |
| CHO | Chinese Hamster ovary |
| cm | centimeter |
| $CO_2$ | carbon dioxide |
| DAS | decay associated spectra |
| DASPMI | 2-(4-(dimethylamino)styryl)-1-methylpyridinium iodide |
| DCLP | dichroic long band-pass |
| DL-detector | delay-line detector |
| DMSO | dimethyl sulfoxide |
| F-actin | filamentous actin |
| FCS | foetal calf serum |
| FIFO | first-in-first-out |
| FLIM | fluorescence lifetime imaging microscopy |
| FRET | Förster resonance energy transfer |
| fs | femtosecond |
| FWHM | full width half maximum |

| | |
|---|---|
| G | grating factor |
| GFP | green fluorescent protein |
| h | hours |
| HaCaT | human keratinocyte cell line |
| HBSS | Hank's balanced salt solution |
| ICT | intramolecular charge transfer |
| IRF | instrument response function |
| JC1 | 5,5',6,6'-tetrachloro-1,1',3,3'-tetraethylbenzimidazolylcarbocyanine iodide |
| K | Kelvin |
| KCN | potassium cyanide |
| LE | locally excited state |
| LP | long-pass |
| M | molar |
| MCP | micro-channel plate |
| MHz | megahertz |
| min | minutes |
| mM | millimolar |
| mm | millimeter |
| mV | milliVolt |
| NA | numerical aperture |
| nm | nanometer |
| ns | nanosecond |
| PBS | phosphate buffer saline |
| PMT | photomultiplier tube |
| ps | picosecond |
| QA-detector | quadrant-anode detector |
| ROI | regions of interest |
| RT | room temperature |
| RVD | regulatory volume decrease |

| | |
|---|---|
| RVI | regulatory volume increase |
| TAC | time-to-amplitude converter |
| TCSPC | time-correlated single-photon counting |
| TICT | twisted intramolecular charge transfer |
| TRES | time-resolved emission spectra |
| TRITC | tetramethyl rhodamine isothiocyanate |
| TRPV4 | transient receptor potential vanilloid 4 |
| TSCSPC | time- and space-correlated single photon counting |
| UV | ultraviolet |
| XTH | Xenopus laevis tadpole heart |
| YFP | yellow fluorescent protein |
| <r> | anisotropy |
| μM | micromolar |
| τ | lifetime |
| $\chi^2$ | reduced goodness-of-fit parameter |

# REFERENCES

**Arniges**, M.; Vazquez, E.; Fernandez-Fernandez, J. M.; Valverde, M. A. 2004. Swelling-activated $Ca^{2+}$ entry via TRPV4 channel is defective in cystic fibrosis airway epithelia**.** *J. Biol. Chem.* 279, 54062–54068.

**Axelrod**, D. 2001. Total internal reflection fluorescence microscopy in cell biology. *Traffic* 2, 764–774.

**Balaban**, R. S.; Nemoto, S.; Finkel, T. 2005. Mitochondria, oxidants, and aging. *Cell* 120, 483–495.

**Becker**, D.; Blase, C.; Bereiter-Hahn, J.; Jendrach, M. 2005. TRPV4 exhibits a functional role in cell-volume regulation. *J. Cell Sci.* 118, 2435–2440.

**Bereiter-Hahn**, J. 1976. *D*imethylaminostyrylmethylpyridiniumiodine (DASPMI) as a fluorescent probe for mitochondria in situ. *Biochim. Biophys. Acta* 423, 1–14.

**Bereiter-Hahn**, J.; Seipel, K. H.; Vöth, M.; Ploem J. S. 1983. Fluorometry of mitochondria in cells vitally stained with DASPMI or rhodamine 6 GO. *Cell Biochem. Funct.* 1, 147–155.

**Bereiter-Hahn**, J. 1990. Behavior of mitochondria in the living cell. *Int. Rev. Cytol.* 122, 1–63.

**Bereiter-Hahn**, J.; Yastas, S.; Litniewski, J. 1995. Mechanical basis of cell morphogenesis and volume control, part of Mechanics of Swelling. *Appl. Mech. Rev.* 48, 674–680.

**Bereiter-Hahn**, J.; Vöth, M. 1998. Do single mitochondria contain zones with different membrane potential? *Exp. Biol. Online* 3, 1–13.

**Boudreault**, F.; Grygorczyk, R. 2004. Cell swelling-induced ATP release is tightly dependent on intracellular calcium elevations**.** *J. Physiol.* 2, 499–513.

**Bringmann**, D.; Ernsting, N. P. 1995. Femtosecond solvation dynamics determining the band shape of stimulated emission from a polar styryl dye. *J. Chem. Phys.* 102, 2691–2700.

**Cappello**, G.; Badoual, M.; Ott, A.; Prost, J.; Busoni, L. 2003. Kinesin motion in the absence of external forces characterized by interference total internal reflection microscopy. *Phys. Rev. E Stat. Nonlin. Soft Matter Phys.* 68, 021907–021917.

**Chen**, L. B. 1988. Mitochondrial membrane potential in living cells. *Ann.Rev.Cell Biol.* 4, 155–181.

**Collins**, J. M., Foster, K. A. 1983. Differentiation of promyelocytic (HL-60) cells into mature granulocytes: mitochondrial-specific rhodamine 123 fluorescence. *J. Cell Biol.* 96, 94–99.

**Darzynkiewicz,** Z., Traganos, F., Staiano-Coico, L., Kapuscinski, J., Melamed, M. R. 1982. Interactions of rhodamine 123 with living cells studied by flow cytometry**.** *Cancer Res.* 42, 799–806.

**Diaz**, G.; Setzu, M. D.; Zucca, A.; Isola, R.;Diana, A.; Murru, R.; Sogos V.; Gremo, F. J. 1999. Subcellular heterogeneity of mitochondrial membrane potential: relationship with organelle distribution and intercellular contacts in normal, hypoxic and apoptotic cells. *J. Cell Sci.* 112, 1077–1084.

**Dowling**, K.; Dayel, M. J.; Lever, M. J.; French, P. M. W.; Hares, J. D.; Dymoke-Bradshaw, A. K. L. 1998. Fluorescence lifetime imaging with picosecond resolution for biomedical applications. *Opt. Lett.* 23, 810–812.

**Downey**, G. P.; Grinstein, S.; Sue-A-Quan, A.; Czaban, B.; Chan, C. K. 1995. Volume regulation in leukocytes: requirement for an intact cytoskeleton**.** *J. Cell. Physiol.* 163, 96–104.

**Ebner**, H. L.; Cordas, A.; Pafundo, D. E.; Schwarzbaum, P. J.; Pelster, B.; Krumschnabel, G. 2005. Importance of cytoskeletal elements in volume regulatory responses of trout hepatocytes. *Am. J. Physiol. Regul. Integr. Comp. Physiol.* 289, 877–890.

**Egner**, A.; Hell, S. W. 2005. Fluorescence microscopy with super-resolved optical sections. *Trends Cell Biol.* 15, 207–215.

**Elangovan**, M.; Day, R. N.; Periasamy, A. 2002. Nanosecond fluorescence resonance energy transfer-fluorescence lifetime imaging microscopy to localize the protein interactions in a single living cell. *J. Microsc.* 205, 3–14.

**Eng**, J.; Lynch, R. M.; Balaban, R. S. 1989. Nicotinamide adenine dinucleotide fluorescence spectroscopy and imaging of isolated cardiac myocytes. *Biophys. J.* 55, 621–630.

**Ephardt**, H.; Fromherz, P. 1991. Anilinopyridinium: solvent-dependent fluorescence by intramolecular charge transfer. *J. Phys. Chem.* 95, 6792–6797.

**Förster**, T. 1948. Zwischenmolekulare Energiewanderung und fluoreszenz. *Ann. Phys.* 6, 55–75.

**Foskett**, J. K.; Spring, K. R. 1985. Involvement of calcium and cytoskeleton in gallbladder epithelial cell volume regulation. *Am. J. Physiol. Cell Physiol.* 248, C27–C36.

**Fromherz**, P.; Heilemann, A. 1992. Twisted internal charge transfer in (aminophenyl) pyridinium. *J. Phys. Chem.* 96, 6864–6866.

**Fuchs**, J.; Zimmer, G.; Bereiter-Hahn, J. 1987. A multiparameter analysis of the perfused rat heart: responses to ischemia, uncouplers and drugs. *Cell Struct. Funct.* 5, 245–253.

**Gadella**, T. W. J. JR.; Jovin, T. M.; Clegg, R. M. 1993. Fluorescence lifetime imaging microscopy (FLIM) – spatial resolution of microstructures on the nanosecond time-scale. *Biophys. Chem.* 48, 221–239.

**Grailhe**, R.; Merola, F.; Ridard, J.; Couvignou, S.; Le Poupon, C.; Changeux, J.-P.; Laguitton-Pasquier, H. 2006. Monitoring protein interactions in the living cell through the fluorescence decays of the cyan fluorescent protein. *ChemPhysChem* 7, 1442–1454.

**Haughland**, R. P. Handbook of Fluorescent Probes and Research Products. Molecular Probes. Eugene, 2002, pp.74–76, 86–96, 830–837, 867.

**Hellwig**, N.; Albrecht, N.; Harteneck, C.; Schultz, G.; Schaefer, M. 2004. Homo- and heteromeric assembly of TRPV channel subunits. *J. Cell Sci.* 118, 917–928.

**Irion**, G.; Ochsfeld, L.; Naujok, A.; Zimmermann, H. W. 1993. The concentration jump method. Kinetics of vital staining of mitochondria in HeLa cells. *Histochemistry* 99, 75–83.

**Jacob**, M. C.; Favre, M.; Bensa, J.-C. 1991. Membrane cell permeabilisation with saponin and multiparametric analysis by flow cytometry. *Cytometry* 12, 550–558.

**James**, T.; Bohman, R. 1981. Proliferation of mitochondria during the cell cycle of the human cell line (HL-60). *J. CellBiol.* 89, 256–260.

**Johannes**, H. 1941. Beitrage zur Vitalfärbung von Pilzmyzelien. II. Die Inturbanz der Färbungen mit Rhodaminen. *Protoplasma* 36, 181–194.

**Johnson**, L. V., Walsh, M. L., Boekus, B. J., Chen, L. B. 1980. Localization of mitochondria in living cells with Rhodamine 123. *Proc. Natl. Acad. Sci. U.S.A.* 77, 990–994.

**Johnson**, L. V., Walsh, M. L., Boekus, B. J., Chen, L. B. 1981. Monitoring of relative mitochondrial membrane potential in living cells by fluorescence microscopy. *J. Cell Biol.* 88, 526–535.

**Jonkman**, A. M.;**V**an der Meulen, P.; Zhang, H.**;** Glasbeek, M. 1996. Subpicosecond solvation relaxation of DASPI in polar liquids. *Chem. Phys. Lett.* 256, 21–26.

**Kemnitz**, K.; Pfeifer, L.; Paul, R.; Fink, F.; Bergmann, A. 1995. Time- and space-correlated single photon counting spectroscopy. *Proc. SPIE* 2628, 2–11.

**Kemnitz**, K.; Paul, R.; Coppey, J.; Coppey-Moisan, M. 1996. Fluorescence lifetime imaging of cells on the picosecond timescale. *Proc. SPIE*, 2926, 177–187.

**Khalbuss**, W. E.; Wondergem, R. 1991. Involvement of cell calcium and transmembrane potential in control of hepatocyte volume. *Hepatology* 13, 962–969.

**Kim**, J.; Lee, M. 1999. Excited-state photophysics and dynamics of a hemicyanine dye in AOT reverse micelles. *J. Phys. Chem. A* 103, 3378–3382.

**Klar**, T. A.; Engel, E.; Hell, S. W. 2001. Breaking Abbe's diffraction resolution limit in fluorescence microscopy with stimulated emission depletion beams of various shapes. *Phys. Rev. E* 64, 066613-1–066613-9.

**Knutson**, J. R.; Beechem, J. M.; Brand, L. 1983. Simultaneous analysis of multiple fluorescence decay curves: A global approach. *Chem. Phys. Lett.* 102, 501–507.

**Koushik**, S. V.; Chen, H.; Thaler, C.; Puhl III, H. L.; Vogel, S. S. 2006. Cerulean, venus, and venus$_{Y67C}$ FRET reference standards. *Biophys. J.* 91, L99–L101.

**Kumar**, C. V.; Turner, R. S.; Asuncion, E. H. 1993. Groove binding of a styrylcyanine dye to the DNA double helix: the salt effect. *J. Photochem. Photobiol. A: Chem.* 74, 231–238.

**Lakowicz**, J. R. *Principles of Fluorescence Spectroscopy*; Plenum: New York, 1983.

**Lakowicz**, J. R.; Berndt, K. 1991. Lifetime-selective fluorescence imaging using an rf phase-sensitive camera. *Rev. Sci. Instrum.* 62, 1727–1734.

**Lakowicz**, J. R. Principles of Fluorescence Spectroscopy, 2nd edn. Plenum Press, New York, 1999.

**Lambert**, A. J.; Brand, M. D. 2007. Research on mitochondria and ageing. *Aging Cell.* 6, 417–420.

**Leip**, O.; Breipohl, W.; Wegener, A.; Augustin, A. J. 1994. Distribution pattern of viable mitochondria in bovine lens epithelial cells. *Dev. Ophthalmol.* 26, 90–96.

**Lewis**, A.; Taha, H.; Strinkovski, A.; Manevitch, A.; Khatchatouriants A.; Dekhter R.; Ammann E. 2003. Near-field optics: From subwavelength illumination to nanometric shadowing. *Nat. Biotech.* 21, 1378–1386.

**Lichtman**, J. W.; Conchello J.-A. 2005. Fluorescence microscopy. *Nat. Methods* 2, 910–919.

**Liedtke**, W.; Choe, Y.; Marti-Renom, M. A.; Bell, A. M.; Denis, C. S.; Ali, A. S.; Hudspeth, A. J.; Friedman, J. M.; Heller**,** S. 2000. Vanilloid receptor–related osmotically activated channel (VR-OAC), a candidate vertebrate osmoreceptor. *Cell* 103, 525–535.

**Liedtke**, W.; Friedman, J. M. 2003. Abnormal osmotic regulation in trpv4_/_ mice. *Proc. Natl. Acad. Sci. U. S. A.* 100, 13698–13703.

**Liedtke**, W.; Tobin, D. M.; Bargmann, C. I.; Friedman, J. M. 2003. Mammalian TRPV4 (VR-OAC) directs behavioral responses to osmotic and mechanical stimuli in Caenorhabditis elegans. *Proc. Natl. Acad. Sci. U. S. A.* 100, 14531–14536.

**Light**, D. B.; Attwood, A. J.; Siegel, C.; Baumann, N. L. 2003. Cell swelling increases intracellular calcium in Necturus erythrocytes. *J. Cell Sci.* 116, 101–109.

**Linshaw**, M. A.; Fogel, C. A.; Downey, G. P.; Koo, E. W.; Gotlieb, A. I. 1992. Role of cytoskeleton in volume regulation of rabbit proximal tubule in dilute medium. *Am. J. Physiol. Renal Physiol.* 262, F144–F150.

**Loew**, L. M.; Bonneville, G. W.; Surow, J. 1978. Charge shift optical probes of membrane potential. Theory. *Biochemistry* 17, 4065–4071.

**Loew**, L. M.; Scully, S.; Simpson, L.; Waggoner, A. S. 1979. Evidence for a charge-shift electrochromic mechanism in a probe of membrane potential. *Nature*. 281, 497–499.

**Loew**, L. M.; Simpson, L. L. 1981. Charge-shift probes of membrane potential. A probable electrochromic mechanism fro p-aminostyrylpyridinium probes on a hemispherical lipid bilayer. *Biophys. J.* 34, 353–365.

**Loew**, L. M. 1996. Potentiometric dyes: imaging electrical activity of cell membranes. *Pure &Appl. Chem.* 68, 1405–1409.

**Maroncelli**, M.; Fleming, G. R. 1987. Picosecond solvation dynamics of coumarin 153: The importance of molecular aspects of solvation. *J. Chem. Phys.* 86, 6221–6239.

**McCormick**, S. 1990. Fluorescent labelling of $Na^+$ ,$K^+$ -ATPase in intact cells by use of a fluorescent derivative of ouabain: salinity and teleost chloride cells. *Cell Tissue Res.* 260, 529–533.

**Mewes**, W.-H.; Rafael, J. 1981. The 2-(dimethylaminostyryl)-l-methylpyridinium cation as indicator of the mitochondrial membrane potential. *FEBS Lett.* 131, 1–10.

**Mittal**, A. K.; Bereiter-Hahn, J. 1985. Ionic control of locomotion and shape of epithelial cells: I. Role of calcium influx. *Cell Motil.* 5, 123–136.

**Nadakavukaren**, K. K.; Nadakavukaren, J.; Chen, L. B. 1985. Increased rhodamine 123 uptake by carcinoma cells. *Cancer Res.* 45, 6093–6099.

**Nilius**, B.; Vriens, J.; Prenen, J.; Droogmans, G.; Voets, T. 2004. TRPV4 calcium entry channel: a paradigm for gating diversity. *Am. J. Physiol. Cell Physiol.* 286, C195–C205.

**O'Connor**, D. V.; Phillips, D. *Time-correlated Single Photon Counting*; Academic Press: London, 1984.

**O´Connor**, E. R.; Kimelberg, H. K. 1993. Role of calcium in astrocyte volume regulation and in the release of ions and amino acids. *J. Neurosci.* 13, 2638–2650.

**O´Neil**, R. G.; Heller, S. 2005. The mechanosensitive nature of TRPV channels. *Pflugers Arch. Eur. J. Physiol.* 451, 193–203.

**Okada**, Y.; Maeno, E.; Shimizu, T.; Dezaki, K.; Wang, J.; Morishima, S. 2001. Receptor-mediated control of regulatory volume decrease (RVD) and apoptotic volume decrease (AVD). *J. Physiol.* 532, 3–16.

**Orrenius**, S. 2007. Reactive Oxygen Species in mitochondria mediated cell death. *Drug Matab. Rev.* 39, 443–455.

**O'Shea**, S. P.; Feuerstein-Thelen, S.; Azzi, A. 1984. Membrane-potential-dependent changes of the lipid microviscosity of mitochondria and phospholipid vesicles. *Biochem. J.* 220, 795–801.

**Pedersen**, S. F.; Owsianik, G.; Nilius, B. 2005. TRP channels: An overview. *Cell Calcium* 38, 233–252.

**Pepperkok**, R.; Squire, A.; Geley, S.; Bastiaens, P. I. 1999. Simultaneous detection of multiple green fluorescent proteins in live cells by fluorescence lifetime imaging microscopy. *Curr. Biol.* 9, 269–272.

**Petty**, H. R. 2007. Fluorescence Microscopy: Established and emerging methods, experimental strategies, and applications in immunology. *Microsc. Res. Tech.* 70, 687–709.

**Pritchard**, S.; Guilak, F. 2004. The Role of F-Actin in Hypo-osmotically induced cell volume change and calcium signaling in anulus fibrosus cells. *Ann. Biomedical Eng.* 32, 103–111.

**Ramadass**, R.; Becker, D.; Jendrach, M.; Bereiter-Hahn, J. 2007. Spectrally and spatially resolved fluorescence lifetime imaging in living cells: TRPV4 − microfilament interactions. *Arch. Biochem. Biophys.* 463, 27–36.

**Ramadass**, R. ; Bereiter-Hahn, J. 2007. Photophysical properties of DASPMI as revealed by spectrally resolved fluorescence decays. *J.Phys.Chem*. *B* 111*,* 7681–7690.

**Rizzo**, M. A.; Springer, G. H.; Granada, B.; Piston, D. W. 2004. An improved cyan fluorescent protein variant useful for FRET. *Nat. Biotechnol.* 22, 445–449.

**Röcker**, C.; Heilemann, A.; Fromherz, P. J. 1996. Time-resolved fluorescence of a hemicyanine dye: Dynamics of rotamerism and resolvation. *J. Phys. Chem.* 100, 12172–12177.

**Saks**, V. A.; Velsler, V. I.; Kuznetsov, A. V.; Kay, L.; Sikk, P.; Tiivel, T.; Tranqui, L.; Olivares, J.; Winkler, K.; Wiedemann, F.; Kunz, W. S. 1998. Permeabilized cell and skinned fiber techniques in studies of mitochondrial function in vivo. *Mol. Cell. Biochem.* 184, 81–100.

**Schlage**, W.; Kuhn, C.; Bereiter-Hahn, J. 1981. Established *Xenopus* tadpole heart endothelium (XTH) cells exhibiting selected properties of primary cells. *Eur. J. Cell Biol.* 24, 342.

**Selvin**, P. R. 2000. The renaissance of fluorescence resonance energy transfer. *Nat. Struct. Biol.* 7, 730–734.

**Shen**, M. R.; Chou, C. Y.; Browning, J. A.; Wilkins, R. J.; Ellory, J. C. 2001. Human cervical cancer cells use $Ca^{2+}$ signalling, protein tyrosine phosphorylation and MAP kinase in regulatory volume decrease. *J. Physiol.* 537, 347–362.

**Shibasaki**, K.; Itoh, K. 1991. Surface-enhanced resonance Raman scattering study on the hemicyanine dye 4- [2-(4-Dimethylaminophenyl)ethenyl]-lmethylpyridinium iodide adsorbed on a silver electrode surface. *J. Raman Spectrosc.* 22, 753–758.

**Siano**, D. B.; Metzler, D. E. 1969. Band shapes of the electronic spectra of complex molecules. *J. Chem. Phys.* 51, 1856–1861.

**Spooner**, S. P.; Whitten, D. G. *Photochemistry in Organized & Constrained Media*; Ramamurthy, V., Ed. Wiley-VCH: Weinheim, 1991; pp 691–739.

**Strehmel**, B.; Rettig, W. 1996. Photophysical properties of fluorescence probes I: dialkylamino stilbazolium dyes. *J. Biomed. Opt.* 1, 98–109.

**Strehmel**, B.; Seifert, H.; Rettig, W. 1997. Photophysical properties of fluorescence probes. 2. A model of multiple fluorescence for stilbazolium dyes studied by global analysis and quantum chemical calculations. *J.Phys.Chem.B* 101, 2232–2243.

**Strotmann**, R.; Harteneck, C.; Nunnenmacher, K.; Schultz, G.; Plant, T. D. 2000. TRPC4, a nonselective cation channel that confers sensitivity to extracellular osmolarity. *Nat. Cell Biol.* 2, 695–702.

**Stubbs**, C. D.; Botchway, S. W.; Slater, S. J.; Parker, A. W. 2005. The use of time-resolved fluorescence imaging in the study of protein kinase C localisation in cells. *BMC Cell Biol.* 6, 22–33.

**Suhling**, K.; French, P. M.; Phillips, D. 2005. Time-resolved fluorescence microscopy. *Photochem Photobiol Sci.* 4, 13–22.

**Suzuki**, M.; Hirao, A.; Mizuno, A. 2003. Microfilament-associated Protein 7 Increases the membrane expression of transient receptor potential vanilloid 4 (TRPV4). *J. Biol. Chem.* 278, 51448–51453.

**Tony**. Ng, A. Squire; Hansra, G.; Bornancin, F.; Prevostel, C.; Hanby, A.; Harris, W.; Barnes, D.; Schmidt, S.; Mellor, H.; Bastiaens, P. I. H.; Parker, P. J. 1999. Imaging protein kinase C-alpha activation in cells. *Science* 283, 2085–2089.

**Tramier**, M.; Gautier, I.; Piolot, T.; Ravalet, S.; Kemnitz, K.; Coppey, J.; Durieux, C.; Mignotte, V.; Coppey-Moisan, M. 2002. Picosecond-hetero-FRET microscopy to probe protein-protein interactions in live cells. *Biophys. J.* 83, 3570–3577.

**Tsukada**, M.; Mineo, Y.; Itoh, K. 1989. Resonance Raman and surface-enhanced resonance Raman scattering study on the structure of a merocyanine dye, 4-(2-(4-hydroxyphenyl)ethenyl)-l-methylpyrldinium. *J. Phys. Chem.* 93, 7989–7992.

**Ulmann**, A. *An Introduction to Ultrathin Organic Films:From Langmuir-- Blodgett to Self--Assembly*; Academic Press: San Diego, CA, 1991; Chapters 3 and 5.

**Valentin**, G.; Verheggen, C.; Piolot, T.; Neel, H.; Coopey-Moisan, M.; Bertrand, E. 2005. Photoconversion of YFP into a CFP – like species during acceptor photobleaching FRET experiments. *Nat. Methods* 2, 801–801.

**Vriens**, J.; Watanabe, H.; Janssens, A.; Droogmans, G.; Voets, T.; Nilius, B. 2004. Cell swelling, heat, and chemical agonists use distinct pathways for the activation of the cation channel TRPV4. *Proc. Natl. Acad. Sci. U. S. A.* 101, 396–401.

**Wallrabe**, H.; Periasamy, A. 2005. Imaging protein molecules using FRET and FLIM microscopy. *Curr. Opin. Biotechnol.* 16, 19–27.

**Wang**, Y. L.; Dembo, M. 2004. Regulation of mechanical interactions between fibroblasts and the substratum by stretch activated calcium channels. *J. Cell Sci.* 117, 85–92.

**Watanabe**, H.; Vriens, J.; Prenen, J.; Droogmans, G.; Voets, T.; Nilius, B. 2003. Anandamide and arachidonic acid use epoxyeicosatrienoic acids to activate TRPV4 channels. *Nature* 424, 434–438.

**Wouters**, F. S.; Verveer, P. J.; Bastiaens, P. I. 2001. Imaging biochemistry inside cells. *Trends in Cell Biology*. 11, 203–211.

## ACKNOWLEDGEMENTS

*I would like to acknowledge the contributions of all the people who have helped me bring my PhD to fruition.*

*A special thanks to my supervisor, Prof. Dr. Jürgen Bereiter-Hahn, for giving me the opportunity to join the department of Kinematic Cell Research Group, Institute for Cell Biology and Neuroscience at Johann Wolfgang Goethe University. I deeply appreciate his support, his profound interest in the project, and for his extremely incisive discussions, crucial advices and generous nature.*

*This work would not have been possible without fruitful discussions, always a helping hand and a great working atmosphere at Kinematic Cell Research Group. At this point, I want to thank David Luttorp and Christopher Blase for their interesting scientific discussions and for their kindness and generosity. Special thanks to Monika Vöth for her helpful discussions in my early days of work. I want to thank Heinz Schewe, Valerii Sukhorukov, Sören Mai and Dr. Karin Busch for their useful scientific discussions during the KIZEFO-seminars.*

*I am very thankful to Christopher Blase for helping me in translating German version of my PhD thesis summary (Zusammenfassung).*

*I would like to thank the entire Max Planck research school members for providing excellent teaching and practical courses.*

*My gratitude goes to Dr. Zdenek Petrášek, Biophysics - Schwille Lab, TU Dresden for his precious knowledge, discussions, and grateful suggestions regarding custom made analysis software.*

*I am especially thankful to my project collaborators Dr. Daniel Becker and Dr. Marina Jendrach for there helpful thoughts and discussions, in realizing the project of "TRPV4-microfilament interaction". In particular, I am grateful to Dr. Marina Jendrach for her*

**125**

*part in cloning various constructs; Dr. Daniel Becker for transfection and co-localization studies.*

*I am thankful to my project collaborators Prof. Dr. Bernd Ludwig and Dr. Mohd Khalid Siddiqui for their academic discussions and contribution to my work on interaction studies of DASPMI in vesicles.*

*I would like to thank my project collaborator PD Dr. Andreas Dreuw for simulation studies on excited-state dynamics of DASPMI.*

*I am grateful to Prof. Dr. Robert Tampe, Prof. Dr. Jacob Piehler and Dr. Rupert Abele (JW Goethe University) for providing facilities for steady-state anisotropy and steady-state spectral measurements.*

*I am thankful to Prof. Dr. Josef Wachtveitl for critical reading of my work on "Photophysical properties of DASPMI in solvents".*

*I would like to thank Valentina Strecker for providing ageing CEF cells.*

*My special gratitude goes to Jitendra Kumar, Sridhar Sreeramulu, Vijayalaxmi Manoharan, Umar Rashid, Dr. Jessica Bidinger, Dr. Sachin Surade, Dr. Sanjeev Baniwal and Dr. Raja K. Muruga Poopathi for being an extremely diverse crowd of people and at the same time being helpful and exciting friends.*

*For motivation and support during the last years and always being in reach of my thoughts, I want to thank Zofia Zegan.*

*My greatest thanks are to my family. Thanks to my wonderful parents and brothers for there love and support.*

*In the end, I acknowledge International Max Planck research school 'structure and function of biological membrane', Deutsche Forschungsgemeinschaft (Be 423/22) and European Commission (project no. 35150407, MIMAGE) for there financial support.*

**Ehrenwörtliche Erklärung**

## Erklärung

Ich erkläre hiermit, dass ich mich bisher keiner Promotionsprüfung unterzogen habe.

Frankfurt am Main / Gründau, den 28.05.2008

Radhan Ramadass

## Eidesstattliche Versicherung

Ich erkläre hiermit an Eides Statt, dass ich die im Fachbereich Biochemie, Chemie und Pharmazie der Johann Wolfgang Goethe-Universität eingereichte Dissertation über

**The Behavior of DASPMI in Living Cells:**
**Spectrally and Spatially Resolved Fluorescence Lifetime Imaging**

selbständig angefertigt und mich anderer Hilfsmittel als der in ihr angegebenen nicht bedient habe, insbesondere, dass aus Schriften Entlehnungen, soweit sie in der Dissertation nicht ausdrücklich als solche mit Angabe der betreffenden Schrift bezeichnet sind, nicht stattgefunden haben.

Frankfurt am Main, den 28.05.2008

Radhan Ramadass

# CURRICULUM VITAE

## PERSONAL



**Name:** Radhan Ramadass
**Age:** 29 years
**Place of birth:** Chingleputt, India
**Marital status:** single

## EDUCATION

| | |
|---|---|
| April 2002- | **Ph.D., Biophysics, Johann Wolfgang Goethe University, Frankfurt/Main.** |

Dissertation:  The Behavior of DASPMI in Living Cells: Spectrally and Spatially Resolved Fluorescence Lifetime Imaging

Advisor:  Prof. Dr. Jürgen Bereiter-Hahn

| | |
|---|---|
| 1999-2001 | **Master of Science**, **Physics**, **Indian Institute of Technology**, Madras |

Dissertation:  Theoretical Simulations on Femtosecond Pulse Generation by a Fibre Laser.

Advisor:  Prof. Dr. Prem B. Bisht

| | |
|---|---|
| 1996-1999 | **Bachelor of Science** - Mathematics, Physics and Computer Science as Major, **Osmania University**, Hyderabad, India. |

## RESEARCH INTEREST

Advanced light microscopy techniques to study and monitor various biological systems ranging from single cells to single molecules in living cells and tissues, including molecular photophysics and dynamics.

## RESEARCH EXPERIENCE

**Doctoral Research**, Frankfurt University, Germany, Since April 2002.

An advanced picosecond fluorescence decay microscope, based on time- and space-correlated single photon counting technique was established to understand the behaviour of an mitochondria selective potentiometric probe 2-(4-(dimethylamino)styryl)-1-methylpyridinium iodide (DASPMI). A comprehensive three-state photophysical model was proposed to explain its emission-wavelength dependent decay parameters, fluorescence anisotropy and time-resolved emission spectra in a variety of solvents. Further, acquisition of spatially-resolved fluorescence decays and steady-state emission anisotropy from DASPMI stained mitochondria in living cells revealed its localisation, mechanism of voltage sensitive fluorescence and its membrane-potential-dependent anisotropy in living cells. Using the very complex response of DASPMI in living mitochondria to photon absorption, it was shown that information can be derived on the energy status as well on membrane fluidity, i.e. lower membrane fluidity in spherical mitochondria than in the elongated ones has been shown for the first time by analysis of fluorescence decay parameters. Also, its importance in the scenario of investigation of cellular ageing and dynamic processes such as mitochondrial fission-fusion events has been highlighted.

**Masters Research,** Chennai, India, April 2001

Figure eight laser is a passively mode locked fiber laser source capable of producing soliton pulses of picosecond or femtosecond duration. Theoretical simulations on ultra-fast pulse generation due to the dispersion and non-linear effects of fiber were studied. The best parameters for this fiber laser with erbium as the gain medium to produce a stable and ultra-fast pulse of 600 fs duration was found.

## PUBLICATIONS

- **Radhan Ramadass\*** and Jürgen Bereiter-Hahn. How DASPMI Reveals Mitochondrial Membrane Potential: Fluorescence Decay Kinetics and Steady-State Anisotropy in Living Cells. **Biophysical Journal**, **Accepted**.

- **Radhan Ramadass\*** and Jürgen Bereiter-Hahn. Photophysical Properties of DASPMI as Revealed by Spectrally Resolved Fluorescence Decays. **Journal of Physical chemistry B**, **2007**, 111, 7681-90.

- **Radhan Ramadass\***, Daniel Becker, Marina Jendrach and Jürgen Bereiter-Hahn. Spectrally and Spatially Resolved Fluorescence Lifetime Imaging in Living Cells: TRPV4 – Microfilament Interactions. **Archives of Biochemistry and Biophysics**, **2007**, 463, 27-36. (This issue carried a photo on its front cover from this paper)

- R. J. Rajesh, **R. Radhan** and P. B. Bisht. Simulation of best fit parameters for femtosecond pulse generation in Figure of Eight Laser. **Femtochemistry and Femtobiology:** Ultrafast Dynamics in Molecular Science, (World scientific, **2002**), 583-586.

## PROFESSIONAL AFFILIATIONS

- American Biophysical society (since 2007)

- American Society of Cell Biology (2006)

- ProComDoc, Frankfurt/Main, European Union Project - Structuring the European Research Area Human resources and mobility (2005)

## ABSTRACTS AND PRESENTATIONS

- **Radhan Ramadass** and Jürgen Bereiter-Hahn. Mechanism of Voltage Sensitive Fluorescence of DASPMI. **Annual meeting of German Society of Cell Biology**, Marburg, March **2008** (*Eur. J. Cell Biol.* 87S1, Suppl. 58).

- **Radhan Ramadass** and Jürgen Bereiter-Hahn. Fluorescence Lifetime Imaging of Mitochondria Probed with Fluorescent Dye DASPMI. **Annual meeting of German Society of Cell Biology**, Frankfurt/Main, March **2007** (*Eur. J. Cell Biol.* 86: 8-8 Suppl. 57).

- Becker D, Blase C, Morciano M, **Ramadass R**, Mueller M, Jendrach M, Bereiter-Hahn J. TRPV4: through thick and thin,. **Annual meeting of German Society of Cell Biology**, Frankfurt/Main, March **2007** (*Eur. J. Cell Biol.* 86: 30-30 Suppl. 57).

- **Radhan Ramadass** and Jürgen Bereiter-Hahn. Excited State Photophysical Properties of DASPMI in Solvents and Living Cells. **Annual Biophysical meeting**, Baltimore, March **2007** (*Biophys. J.* : 326A-326A Suppl. S, JAN 2007).

- **R. Ramadass** and J. Bereiter-Hahn. Photophysics of DASPMI Stained Mitochondria in Living Cells, **Annual Meeting of American Society of Cell Biology**, San Francisco, December **2005**.

- D. Becker, **R. Ramadass**, C. Blase, M. Jendrach, J. Bereiter-Hahn.Interaction of Cation Channel TRPV4 and Actin Cytoskeleton **Annual Meeting of American Society of Cell Biology**, San Francisco, December **2005**.

- **Radhan Ramadass** and Jürgen Bereiter-Hahn.Picosecond Fluorescence Decay Microscopy of DASPMI Stained Mitochondria in Living Cells, **Annual Meeting of German Society of Cell Biology**, Hidelberg, March **2005** (*Eur. J. Cell Biol.* 84 Suppl. 55).

- **Radhan Ramadass**, Daniel Becker, Chris Blase, Marina Jendrach, Jürgen Bereiter-Hahn. Imaging Protein-Protein Interactions in Living Cells Using Time-Resolved Spectroscopy, **Annual Meeting of German Society of Cell Biology**, Hidelberg, March **2005**, (*Eur. J. Cell Biol.*, 84 Suppl. 55).

- **R. Radhan**, R. J. Rajesh and P. B. Bisht. Effect of Coupler ratio and NALM length on Figure of Eight Laser, **OPTONICS 2001: Second International Conference on Optics and XXVII Annual Convention of the Optical Society of India**, Trivandrum, India, August **2001**, Presentation.

## SCHOLARSHIPS

- International Max-Planck-Research School PhD fellowship program (April 2002 – September 2005).

- European Union Project "MiMage" (October 2005 - ).

## LECTURES AND WORKSHOPS

- "Scientific Presentation skills", Prof.Dr.Ulrike Kaunzner (Bologna University, Germany). Max-Planck Institute for Computer Science, Saarbrucken , November - 2004.

- Granada Doctoral School, Spain, September - 2005

Intercultural Communication, Project Elaboration and Management Tools, English as an International Language, Acquisition and Development of Skills through Research Training.

- Courses Organized by International Max-Planck Research School on Structure and Function of Biological Membranes, Electron Paramagnetic Resonance (Practical course) and Cryo-Electron Microscopy (Practical course).

## LANGUAGES

Near native: English

Native: Tamil, Hindi and Telugu

Basic: German